UNIVERSITÀ degli STUDI di CATANIA

**Department of Biological, Geological and Environmental Sciences**

# UNIVERSITÀ DEGLI STUDI DI CATANIA

## Dottorato di ricerca in Scienze della Terra e dell'Ambiente

**Dottorati innovativi con caratterizzazione industriale**

**XXXV Cycle**

---

# SICILY AS A PILOT REGION FOR MICRO-ZONATION OF THE LOW-ENTHALPY GEOTHERMAL POTENTIAL

**Ph.D. candidate:**
**Giovanni Floridia**

---

**Advisor:**
**Prof. Marco Viccaro**

**Coordinator:**
**Prof.ssa Agata Di Stefano**

**Ph. D. attended during 2019/23**

# Contents

List of Tables ..... 3
List of Figures ..... 4
Graphical abstract and Research highlights ..... 10
Premessa ..... 11
Preface ..... 13
Riassunto ..... 15
Abstract ..... 17
1 Chapter 1 – Overview and research objectives ..... 19
1.1 Overview ..... 19
1.2 Research objectives ..... 20
1.3 Geothermal state of play in Sicily ..... 22
1.4 Geological and geodynamic background ..... 25
2 Chapter 2 – Methodology and Workflow ..... 28
2.1 Modelling approach ..... 28
2.2 Initial 3D geological models ..... 31
2.3 Gravity modelling ..... 34
2.4 Thermal modelling ..... 37
3 Chapter 3 –Regional thermal modelling ..... 39
3.1 Gravity-based geological model ..... 39
3.1.1 Lower boundary constraints: Density and Temperature distributions in the upper mantle ..... 43
3.2 Thermal modelling ..... 49
3.2.1 Crustal Model. ..... 51
3.2.2 CSEM Mantle Model. ..... 53
3.2.3 EU60 Mantle Model. ..... 53
3.3 Calibration against shallow temperature measurements (1-7 km depth b.g.l) ..... 56
3.4 Regional Geodynamic implications ..... 63
3.5 Regional Geothermal implications ..... 66
4 Chapter 4 – Thermal modelling: a case study from South-Eastern Sicily ..... 68
4.1 Hyblean Foreland ..... 68
4.1.1 Elements of geology ..... 68
4.1.2 Hydrogeological setting ..... 71
4.2 Case study ..... 75

4.2.1 3D gravity-based model ..... 75
4.2.2 Hydrogeological setting ..... 81
4.3 Thermal modelling ..... 83
4.3.1 Steady-state thermal model simulation ..... 84
4.3.2 Observed versus modelled temperature: validation against 1-2-3-4 Km depth (b.g.l) 88
4.4 Numerical simulations of a low-enthalpy open-loop system ..... 90
4.5 Sustainability over time ..... 93
5 Chapter 5 – Products ..... 97
5.1 Project conceptualization ..... 97
5.2 Database ..... 98
5.3 Methods ..... 100
5.4 Web Portal ..... 103
5.5 Distribution ..... 106
6 Chapter 6 – Industrial Application ..... 107
6.1 State of play ..... 107
6.2 Carbon Fiber Powder: an innovative additive for hybrid geothermal systems compounds ..... 109
6.3 Methods ..... 111
6.3.1 Development and testing of Innovative Probes ..... 111
6.3.2 Developing and testing of hybrid grout ..... 117
6.4 Results ..... 120
6.4.1 Innovative probes (I50-I80) ..... 120
6.4.2 I50 prototype system ..... 123
6.4.3 Additivate grouts ..... 124
6.4.4 The implications of using innovative compounds ..... 127
6.5 End of Waste and economic implication on Geothermal Applications ..... 130
Conclusions and future perspectives ..... 133
Appendix ..... 136
References ..... 149

# List of Tables

Table 3.1- Density values used for gravimetric regional modelling workflow. ..... 40
Table 3.2- Average major element concentrations (wt.%) for the lithospheric mantle used for the Vs conversion..... 45
Table 3.3 - Thermal modelling parameters used for the workflow. ..... 50
Table 4.1 - Density values used for gravimetric local modelling workflow. ..... 80
Table 4.2 - Hydrogeological and thermal properties ..... 91
Table 4.3 – Doublet Simulation (case studies) ..... 91
Table 6.1- Experimental data resulting from tests on the geo-exchange prototype system. ..... 114
Table 6.2- Components used for the preparation of the bentonitic grout mixtures with CFP as additive (ST% no CF powder; CFP5% mixture with 5% of CFP). ..... 117
Table 6.3- Compressive strengths (Rc) at the fracture point obtained on the starting pure material and doped bentonitic grout (+5 % of carbon fiber). Ff is the strength applied at the center of prismatic samples. ..... 119
Table 6.4- Thermal conductivity obtained from measures on the starting and doped (+5% of CF) bentonitic grouts..... 119
Table 6.5 - Calculated thermal resistance (Rb) for a 250 m borehole filled with standard and innovative grout. ..... 129
Table 6.6- Parameters for the geothermal field model following the ASHRAE approach. ..... 130
Table 6.7- Dimensioning of the geothermal field (probes of 100 m length). ..... 130
Table 6.8- Global economy impact by using CFP composite materials in geothermal systems. ..... 132

# List of Figures

Figure 1.1– a) Simplified tectonic map of Sicily and central Mediterranean b) Location of the studied area. c) Heat flow map of Sicily (from Della Vedova et al., 2001). Figure from Montanari et al., 2017. ..... 26
Figure 2.1- Workflow of the research..... 29
Figure 2.2- Datasets integrated for the reconstruction of the regional geo-lithological configuration. Red dots display the location of the updated Italian National Geothermal Database well bores. Yellow solid lines show the traces of reflection and refraction seismic profiles of the offshore CROP project (CNR, ENI, ENEL) and the onshore SI.RI.PRO project. Yellow dashed line illustrates the trace of the geological interpretation of the Nebrodi-Iblei profile. Coordinates are in EPSG:32633 – WGS84/UTM zone 33N. ..... 33
Figure 2.3 - Thickness (m) of: a) Metamorphic Unit of the European plate, b) Volcanics domain, c) Paleogene-Quaternary deformed deposits (Paleogene-Quaternary), d) consolidated Meso-Cenozoic units (mostly carbonates). Top (depth in km) of e) the Crystalline Basement, f) the Moho depth. Coordinates are in EPSG:32633 – WGS84/UTM zone 33N. ..... 35
Figure 2.4 – (a) the Bouguer anomaly (based on a Bouguer slab correction density of 2670 kg/m³) from ISPRA (the Italian National Institute for Environmental Protection and Research - Land Protection and Georesources Department). (b) residual gravity field obtained with IGMAS+ for initial model, (c) residual gravity field after Harvester module inversion applied to obtain the density configuration of the crystalline crust. Coordinates are in EPSG:32633 – WGS84/UTM zone 33N..... 36
Figure 3.1 - Upper (a) and lower crust (b) thickness from Fatiando inversion using Harvester module. Coordinates are in EPSG:32633 – WGS84/UTM zone 33N. ... 42
Figure 3.2 - Xenolith data available for the region ( Bianchini et al., 2010; Ciliberto et al., 2009; Correale et al., 2012; Scribano et al., 2009; Tonarini et al., 1996). ..... 43
Figure 3.3 - a) Average mineralogical composition used for the Vs conversion; b) depleted samples (tonarini, 1996)..... 45
Figure 3.4 –Temperature (b) and density (c) maps computed from the conversion of Vs (a) (CSEM mantle Tomography); slices from 50 Km (1) to 250 Km (5) depth b.s.l. (steps: 50 Km). ..... 47

Figure 3.5– Temperature (b) and density (c) maps computed from the conversion of Vs (a) (EU mantle Tomography); slices from 50 Km (1) to 250 Km (5) depth b.s.l. (steps: 50 Km). ..... 48
Figure 3.6 – Temperature at depth of 50 km (below mean sea level) as derived from (a) the "CSEM Europe" mantle tomographic model (Fichtner et al., 2018) and (b) the "EU60" tomographic model (Zhu et al., 2015), both being imposed as alternative lower boundary conditions for the thermal modelling process. Note the different scales of the temperature intervals shown in the maps. Coordinates are in EPSG:32633 – WGS84/UTM zone 33N. ..... 51
Figure 3.7- Temperature maps at different selected depths below ground level (a: 1 km, b: 2 km, c: 3 km, d: 4 km, e: 5 km, and f: 10 km) derived from the Crustal Model, assuming a constant heat flow of 30 mW/m2 at the crust-mantle boundary. Coordinates are in EPSG:32633 – WGS84/UTM zone 33N..... 52
Figure 3.8- Temperature maps through the thermal model implementing the mantle temperatures derived from the CSEM Mantle Model at depths below ground level of a: 1 km, b: 2 km, c: 3 km, d: 4 km, e: 5 km, f: 10 km, g: 20 km, and h: 30 km. Coordinates are in EPSG:32633 – WGS84/UTM zone 33N..... 54
Figure 3.9 - Temperature maps through the thermal model implementing the mantle temperatures derived from the EU60 Mantle Model at depths below ground level a: 1 km, b: 2 km, c: 3 km, d: 4 km, e: 5 km, f: 10 km, g: 20 km, and h: 30 km. Coordinates are in EPSG:32633 – WGS84/UTM zone 33N..... 55
Figure 3.10 - Dataset of wellbore temperatures from the updated Italian National Geothermal Database used for the comparison (red dots) and subdomain partitioning of the region. Red boxes display the subdomains used for the comparison between modelled and measured temperatures. In detail: a) Entire investigated area; b) Hyblean foreland domain; c) north-eastern domain; d) western domain. The isolines display the topography (DEM 2m) and Bathimetry (Emodnet project). ..... 57
Figure 3.11 - Temperatures modelled (black points) vs. measured (red points) for the Crustal Model. (a) Comparison between modelling results and available measurements for the entire domain. b) Model validation for the region of the Hyblean promontory; c) Model validation for the north-eastern domain; d) Model validation for the Western domain. The temperature comparisons are associated with the graph showing the Root Mean Square Error expressed in (°C) for different depth

ranges expressed in meter (1 = [1000 - 0]; 2 = [0 - -1000]; 3 = [-1000 - - 2000]; 4 = [-2000 - -3000]; 5 = [-3000 - -4000]; 6 = [-4000 - -5000]; 7 = [-5000 - -6000]. .... 59
Figure 3.12- Temperature modeled (black points) vs. measured (red points) for the CESM Mantle Model. a) Comparison between modelling results and available measurements for the entire domain; b) Model validation for the region of the Hyblean promontory; c) Model validation for the north-eastern domain; d) Model validation for the Western domain. The temperature comparisons are associated with the graph showing the Root Mean Square Error expressed in (°C) for different depth ranges expressed in meter (1 = [1000 - 0]; 2 = [0 - -1000]; 3 = [-1000 - - 2000]; 4 = [-2000 - -3000]; 5 = [-3000 - -4000]; 6 = [-4000 - -5000]; 7 = [-5000 - -6000]. .... 60
Figure 3.13 - Temperature modeled (black points) vs. measured (red points) for the alternative interpretation of the CESM Mantle Model. a) Comparison between modelling results and available measurements for the entire domain; b) Model validation for the region of the Hyblean promontory; c) Model validation for the north-eastern domain; d) Model validation for the Western domain. The temperature comparisons are associated with the graph showing the Root Mean Square Error expressed in (°C) for different depth ranges expressed in meter (1 = [1000 - 0]; 2 = [0 - -1000]; 3 = [-1000 - - 2000]; 4 = [-2000 - -3000]; 5 = [-3000 - -4000]; 6 = [-4000 - -5000]; 7 = [-5000 - -6000]. ..... 61
Figure 3.14 - Temperature modeled (black points) vs. measured (red points) for the EU60 Mantle Model. (a) Comparison between modelling results and available measurements for the entire domain; b) Model validation for the region of the Hyblean promontory; c) Model validation for the north-eastern domain; d) Model validation for the Western domain. The temperature comparisons are associated with the graph showing the Root Mean Square Error expressed in (°C) for different depth ranges expressed in meter (1 = [1000 - 0]; 2 = [0 - -1000]; 3 = [-1000 - - 2000]; 4 = [-2000 - -3000]; 5 = [-3000 - -4000]; 6 = [-4000 - -5000]; 7 = [-5000 - -6000]. .... 62
Figure 3.15- Temperature (a) and Heat flow distribution (b) at Moho depth for the EU60 Mantle Model. ..... 65
Figure 4.1 - Geological map of southeastern Sicily (Lentini, 1987); the red box illustrates the area of local high-resolution modelling phase..... 71
Figure 4.2 – Hydrogeological basins distribution in Sicily (Arpa, Regione Sicilia)..... 73
Figure 4.3- Hydrogeological basin of the Hybean area (IGV, Arpa, Regione Sicilia)... 74

Figure 4.4- Hydrogeological dataset (ISPRA, Genio civile Siracusa, Ragusa). Red dots illustrate the springs; Blue dots show the distribution of hydric wells..... 74
Figure 4.5 - a) Geological configuration of the local model domain. b) development of the 3D geological model; c) section of the reconstructed mesh. ..... 76
Figure 4.6 - Location of the measure station for the new gravimetric survey (Maurel&Prom). Black dots display the location of the available well logs in the area. ..... 77
Figure 4.7– Bouger anomaly (mGal) maps of the local domain. a) measured Bouger anomaly values; b) calculated Bouger anomaly (IGMAS+); c) residuals (IGMAS+) d) Gravimetric analysis of model sections (Bouger anomaly). Red line measured, red dotted line calculated, blue line residuals.. ..... 78
Figure 4.8 - Free -air (mGal) maps of the local domain. a) measured Free -air anomaly values; b) calculated Free -air (IGMAS+); c) residuals (IGMAS+); d) Gravimetric analysis of model sections (free-air anomaly). Red line measured, red dotted line calculated, blue line residuals. ..... 79
Figure 4.9 - Potentiometric surface derived from the linear interpolation of dynamic water state (data from Genio Civile Siracusa)..... 82
Figure 4.10- Temperature maps at different selected depths below ground level (a: 1 km, b: 2 km, c: 3 km, d: 4 km) assuming an average thermal conductivity value of 1.7 W/mK. Coordinates are in EPSG:32633 – WGS84/UTM zone 33N..... 85
Figure 4.11- Temperature maps at different selected depths below ground level (a: 1 km, b: 2 km, c: 3 km, d: 4 km) assuming thermal conductivity values for each lithology. Coordinates are in EPSG:32633 – WGS84/UTM zone 33N..... 86
Figure 4.12- Temperature maps at different selected depths below ground level (a: 1 km, b: 2 km, c: 3 km, d: 4 km) assuming an average thermal conductivity value of 2.5 W/mK. Coordinates are in EPSG:32633 – WGS84/UTM zone 33N..... 87
Figure 4.13- Temperature maps at different selected depths below ground level (a: 1 km, b: 2 km, c: 3 km, d: 4 km) assuming an average of thermal conductivity values of 3.7 W/mK. Coordinates are in EPSG:32633 – WGS84/UTM zone 33N..... 87
Figure 4.14- Temperature maps at different selected depths below ground level (a: 1 km, b: 2 km, c: 3 km, d: 4 km) assuming an average thermal conductivity per each unit. The major tectonics features are included in the modelling phase and superimposed on the thermal maps. Coordinates are in EPSG:32633 – WGS84/UTM zone 33N. 88

Figure 4.15- Temperatures modelled (black points) vs. measured (red points) for the local Model (thermal cond. 2.5 W/mK) a) simulation without tectonics; b) simulation with tectonics. The temperature comparisons are associated with the graph showing the Root Mean Square Error expressed in (°C) for different depth ranges expressed in meter (1 = [1000 - 0]; 2 = [0 - -1000]; 3 = [-1000 - - 2000]; 4 = [-2000 - -3000]; 5 = [-3000 - -4000]; 6 = [-4000 - -5000]; 7 = [-5000 - -6000]. ..... 89
Figure 4.16 - a) location of the modelled area; b) schematic representation of the main geometry of the modelled area. Blue lines represent the location of the injection wells, while red lines show the location of the extraction wells. ..... 92
Figure 4.17 – Micro domain simulation slice at 240 m above sea level (time 0). ..... 92
Figure 4.18 - Reservoir temperature distribution in case study 1 a) example of the reservoir top temperature perturbation in the last step of the simulation (summer); b) example of the reservoir bottom temperature perturbation in the last step of the simulation (summer). ..... 94
Figure 4.19 – Temperature variation for doublet in case study_1 over time for production (a) and injection (b) well. ..... 95
Figure 4.20– Temperature variation for doublet in case study_2 over time for production (a) and injection (b) well. ..... 96
Figure 5.1– Visual identity of the STORAGE project. ..... 99
Figure 5.2 – Client-server workflow for STORAGE project. ..... 100
Figure 5.3 – Example of the PHP code used in Storage project. ..... 102
Figure 5.4 – Nodes interpolation according to a weighted average between the four closest values to the selected point in the area. a) example of regional data interpolation (lateral resolution of 5 km); b) example of local domain interpolation (geothermal microzonation area with lateral resolution of 200 m). ..... 104
Figure 5.5 – Web portal page. a) bullet interactive menu; b) research by municipalities tool; c) research by coordinates; d) interactive maps (blue polygon: regional modelling area, re polygon: local domain area). ..... 104
Figure 5.6 – Outputs of the research. a) location of the selected point in terms of referred database; b) location of the selected point (coordinates in WGS84); c) tables with numerical results; d) interactive maps (blue polygon: regional modelling area, re polygon: local domain area). ..... 105
Figure 5.7– On-line repository: visualization and downloading of the regional and local dataset obtained from the thermal modelling stage. ..... 105

Figure 6.1- a) Setup of the thermal test for the hybrid polyethylene probe and (b) detail of the temperature detection system S3 and heating cable component. ..... 112
Figure 6.2- Production of the innovative probes with radial carbon fibre (CF) rings and (b) finishing of the radial CF rings. ..... 113
Figure 6.3 - (a) Preparation of the standard system for the thermal response test; (b) preparation of the innovative system for the thermal response test; and (c) heating cable configuration. ..... 115
Figure 6.4- Geo-exchange prototype configuration: (**a**) no-water and static initial condition; (**b**) dynamic regime test; (**c**) primary and secondary circuit configuration; and (**d**) details of the supplementary double circuit device. ..... 116
Figure 6.5 - Results of the thermal test in standard (ST) and innovative probes (I50–I80): heating step, cooling step, heating-cooling step. ..... 121
Figure 6.6- Results of thermal test in standard (ST) and innovative geo-heat exchanger prototype (I50): standard initial condition, static condition, dynamic condition. Values were recorded every 5 min, although graphs show values at 30, 60, 120, 180, and 240 min for convenience. ..... 122
Figure 6.7- S1, S2 and S3 measurements in standard and innovative configuration during the primary-secondary circuits tests. ..... 123
Figure 6.8 - Standard (ST) and innovative (I) systems during the initial, static, dynamic and primary-secondary circuits tests. ..... 124
Figure 6.9- (a) Diagram reporting the uniaxial (Rc) and (b) flexural compressive (Rf) strengths at the fracture point for the starting and doped (+ 5% of graphite powder) bentonitic grouts as a function of the load applied to the sample (Ff and Fc). Symbols are as follows: triangles for the starting grout; circles for the grout + 5% of CFP. Open symbols are for tests at 14 days, filled symbols for those at 28 days. ..... 126

# Graphical abstract and Research highlights

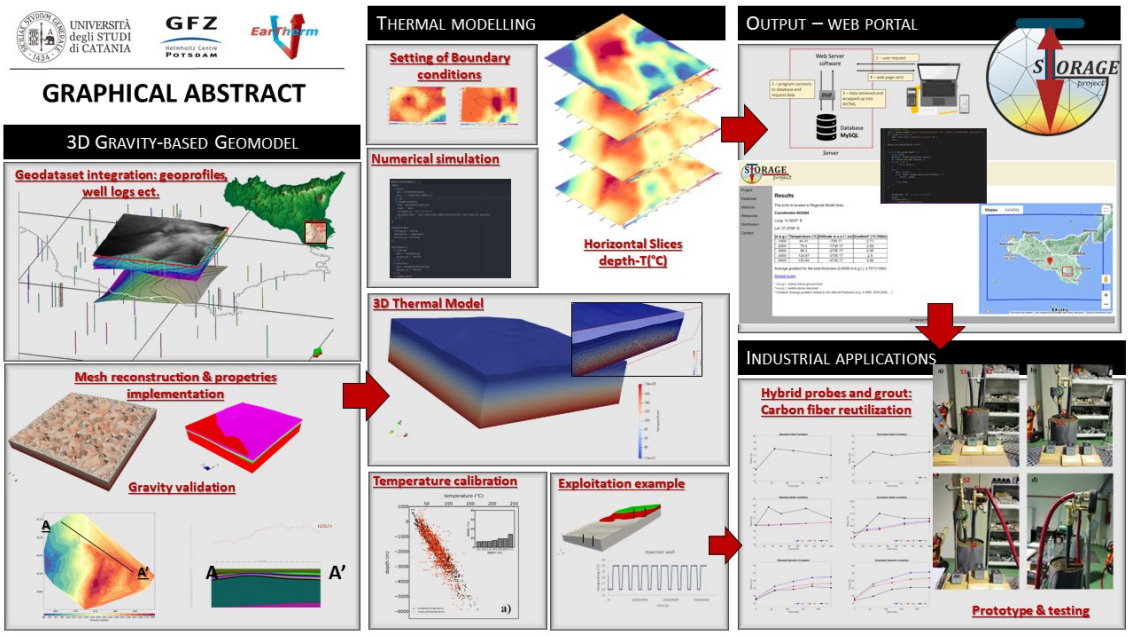


- Innovative workflow for the characterization of geothermal steady-state condition of Sicily;
- New perspectives for the geothermal resources' exploration in Sicily;
- Lithospheric present state of Sicily derived from a gravity modelling approach;
- Conductive thermal field obtained from a steady-state thermal simulation for regional context;
- Quantification of the subsurface thermal field of a local high-resolution domain;
- Validation of the models against a shallow temperature dataset;
- New interactive web portal for the assessment of geothermal resources;
- Optimization of low enthalpy geothermal systems;
- Reuse of industrial carbon fibre waste materials in a geothermal context.

# Premessa

La collaborazione tra la Sezione di Scienze della Terra del Dipartimento di Scienze Biologiche, Geologiche e Ambientali dell'Università degli Studi di Catania, l'azienda EarTherm s.r.l e l'Ente di Ricerca estero GFZ (GeoForschungsZentrum) si inserisce in un contesto di ricerca scientifica d'avanguardia che ha consentito di espletare gli obiettivi prefissati dal piano di ricerca dottorale finanziato nell'ambito del Programma Operativo Nazionale Ricerca e Innovazione 2014-2020 (PON-RI). Si tratta di uno strumento gestito dal Ministero dell'Università e della Ricerca (MUR), attraverso cui le regioni cosiddette "in transizione" hanno la possibilità di sviluppare l'alta formazione, in coerenza con i fabbisogni del sistema produttivo nazionale e in linea con gli obiettivi della politica di coesione dell'Unione europea a favore delle proprie aree territoriali più svantaggiate. La ricerca è stata definita nell'ambito dell'azione l.1 -Dottorati di ricerca innovativi dell'Asse di intervento denominata "Interventi in Capitale Umano" e finanziata dall'Unione europea attraverso il Fondo Europeo di Sviluppo Regionale (FESR), il Fondo Sociale Europeo (FSE) e il cofinanziamento nazionale. In linea con i programmi precedenti (PON "Ricerca Scientifica, Sviluppo Tecnologico, Alta Formazione" 2000-2006, PON "Ricerca e Competitività" 2007-2013) e con lo scopo di fornire continuità all'innovazione, il progetto contribuisce alla creazione di mutamenti di valenza strutturale e allo sviluppo intelligente, sostenibile e inclusivo. A tal proposito, sono molteplici le tematiche incentivate da questi strumenti; tra queste, l'individuazione di nuovi campi di applicazione, lo sviluppo di competenze e l'interazione con le comunità locali garantiscono uno sviluppo territoriale, basato sulla definizione di modelli di innovazione che favoriscono la connessione tra imprese e università o enti di ricerca. In un periodo storico con una spiccata e crescente sensibilità su tematiche in particolare energetico-ambientali, il piano di ricerca triennale si è sviluppato secondo la logica di innovazione e sviluppo tecnologico sostenibile, di gestione efficiente di energie a basso contenuto di CO2, nonché di efficientamento energetico, secondo i principi di "energy saving" e "end of waste". Con l'obiettivo di ottimizzare sistemi energetici a bassissimo impatto ambientale lo studio si pone come base per l'individuazione e l'analisi di forme rinnovabili e sostenibili di approvvigionamento energetico, nonché come strumento necessario nell'ottica di ottimizzazione di sistemi che sfruttano l'energia stoccata sotto forma di calore nelle porzioni più superficiali della crosta terrestre, la cosiddetta "risorsa geotermica". Le indagini promosse costituiscono, quindi, uno strumento essenziale per

l'innovazione tecnologica in ambito energetico e soprattutto per le politiche di sviluppo sociale ed economico nella Regione Siciliana, rendendola un laboratorio di innovazione per l'esplorazione geotermica. Inoltre, esse permetterebbero il contestuale instaurarsi di nuove competenze professionali e all'avanguardia richieste dall'attuale mercato del lavoro.

Le finalità industriali del progetto di ricerca implicano lo sviluppo di un contenuto altamente applicativo che permette di fornire strumenti utili a tecnici ed esperti di settore che potranno comprendere meglio le potenzialità della risorsa, generando un notevole interesse da parte di imprenditori e aziende di settore. Non bisogna trascurare, infine, come l'interazione tra realtà sia del mondo accademico sia di quello più specificatamente applicativo permettano un'intensa attività formativa e divulgativa, molto importante per lo sviluppo di una coscienza comunitaria sempre più incentrata sulle risorse rinnovabili. Ne consegue un particolare riferimento alla geotermia di bassa temperatura, intesa come strumento efficace nell'attuale fase di transizione energetica.

# Preface

The collaboration between the Earth Sciences Section of the Department of Biological, Geological and Environmental Sciences of the University of Catania, the EarTherm s.r.l company, and the GeoForSchungsZentrum research centre (GFZ) is part of an innovative scientific research programme funded by the National Operational Program for Research and Innovation 2014-2020 (PON-RI). It is a tool managed by the Ministry of Universities and Research (MUR) through which the so-called "transition" regions have the opportunity to develop higher education programmes in line with the needs of the national production system and with the aims of the European Union's policy on behalf of its most disadvantaged areas. The research has been defined in the framework of action l.1 - Dottorati di ricerca innovativi dell'Asse di intervento denominata "Interventi nel Capitale Umano" financed by the European Union via the European Regional Development Fund (ERDF), the European Social Fund (ESF) and national co-financing. In line with previous European programs (PON "Scientific Research, Technological Development, Higher Education" 2000-2006, PON "Research and Competitiveness" 2007-2013) and with the aim of providing continuity to innovation, the project contributes to the creation of structural changes, as well as intelligent, sustainable, and inclusive growth. In this regard, there are many areas of discussion that have arisen from these tools; among these, the identification of new fields of application, the development of existing and new skills, and the interaction with local communities ensure territorial development, based on the definition of innovation models that promote the connection between companies, research institutions and universities. At present, marked and growing sensitivity on energy-environmental issues clearly emerges more and more often; in this context, this three-year research programme has been developed according to the logic of innovation and sustainable technological development, as well as the efficient management of low CO2 content energy and distributed energy efficiency, according to the principles of "energy saving" and "end of waste". With the aim of optimizing energy systems with a very low environmental impact, the study relies on the identification and analysis of renewable and sustainable forms of energy supply, as well as the development of a necessary tool for the optimization of systems that exploit the heat energy stored in the most superficial portions of the earth's crust, the so-called "Geothermal Resource". The promoted investigations represent an essential tool for technological innovation in the thermal energy sector in Sicily and it also provides the basis for the local social and economic development

policies (establishment of new cutting-edge professional skills required by the existing job market), making the Sicilian Region an innovation laboratory for low-temperature geothermal exploration. The industrial implications of the research project suggest the development of highly applicative content that allows technicians and sector experts to better understand the potential of geothermal resources and exploit its principles for cutting-edge engineering, generating considerable interest from business owners and companies in the energy sector. Finally, it should be not overlooked how the interaction between both the academic entity and the industrial application allows an intense training and dissemination activity useful for the development of a community awareness increasingly focused on renewable resources with reference to Geothermal Energy as an effective tool in the current energy transition phase.

# Riassunto

La quantificazione del potenziale geotermico del sottosuolo si basa principalmente sulla valutazione della condizione termica e meccanica della litosfera. Tali indagini sui regimi termici richiedono una conoscenza dettagliata delle caratteristiche geologiche e dei loro meccanismi di funzionamento. Questo approccio diventa ancora più rilevante in contesti geodinamici complessi e attivi. A questo proposito, la regione Sicilia, che si trova nel Mediterraneo centro-occidentale, rappresenta un caso studio eccezionale per il suo potenziale geotermico quasi inesplorato. In questo lavoro di tesi si tenta di ricostruire lo stato litosferico della Sicilia per quantificarne il regime termico di bassa e media profondità. Partendo da una modellazione che coinvolge tutto il territorio siciliano, attraverso una modellazione gravimetrica, sono state definite le principali unità geologiche e le loro proprietà dipendenti dalla litologia, al fine di definire un modello geologico 3D coerente con i dataset geofisici disponibili. Il modello geologico così ottenuto è stato quindi oggetto di una fase relativa alla computazione dell'attuale campo termico conduttivo in stato stazionario. Attraverso l'implementazione delle proprietà fisiche quali conducibilità termica e produzione di calore radiogenico per singole unità litologiche, è stato possibile modellare e ottenere la temperatura in ogni punto del dominio di studio. Inoltre, al fine di individuare le migliori soluzioni è stato possibile analizzare parallelamente 3 modelli che assumono differenti condizioni al contorno. Infine, i risultati ottenuti dalla modellazione termica sono stati validati attraverso il confronto con un set di dati misurati di temperatura, derivato da set di dati pubblici ricavati nell'ambito dall'esplorazione di idrocarburi in Sicilia. In secondo luogo, utilizzando le condizioni termiche estrapolate dalla fase di preventiva modellazione su scala regionale, lo stesso flusso di lavoro è stato applicato per una specifica area della Sicilia sud-orientale. In particolare, un nuovo dataset gravimetrico acquisito ha consentito di dettagliare maggiormente il modello geologico di partenza e di calcolare il campo termico ad esso associato a più alta risoluzione. I risultati ottenuti indicano che il campo regionale termico a profondità inferiori a 10 km è in gran parte controllato dalla variabilità dello spessore delle coperture sedimentarie dell'avanpaese e dell'orogene, mentre le condizioni di temperatura al di sotto dei 10 km sembrano essere controllate principalmente dal contributo mantellico e dal contributo radiogeno delle rocce di basamento cristallino. Dall'analisi degli outputs della modellazione termica viene registrato un flusso di calore alla Moho piuttosto eterogeneo; è infatti possibile constatare localmente un flusso di

calore superiore a 80 $mW/m^2$, rivelando un particolare contesto geodinamico con aree specifiche caratterizzate da un potenziale geotermico di medio-alta entalpia. Il modello termico della Sicilia consente quindi di vincolare aree con importanti anomalie geotermiche, come le zone vulcaniche dell'Arco delle Isole Eolie, l'area etnea e la Rift Zone del Canale di Sicilia, aree che risultano quindi idonee allo sfruttamento risorse geotermiche di medio-alta entalpia. La modellazione termica sia su scala locale suggerisce anche che risorse geotermiche a bassa entalpia sono disponibili su diverse aree del dominio di studio, avvalorando l'ipotesi che vuole le unità carbonatiche il maggiore reservoir geotermico della regione. Tutti questi aspetti fanno della Sicilia una regione pilota in Italia, per gli studi che riguardano l'esplorazione e lo sfruttamento della risorsa geotermica. Applicato ad un complesso contesto geologico come quello della Sicilia, lo studio fornisce un solido flusso di lavoro che può essere trasferito ad altre zone d'Italia, incentivando così studi volti alla quantificazione delle potenziali risorse geotermiche e al loro sfruttamento. A tal proposito, attraverso lo sviluppo di un portale web dedicato, è stato possibile implementare i valori di temperatura, che riproducono lo stato termico della regione, fornendo uno strumento interattivo utile alla valutazione della condizione geotermica regionale e locale, nonché essenziale nella pianificazione dello sfruttamento della risorsa. La vocazione industriale del progetto di ricerca ha permesso, inoltre, di indagare gli aspetti più applicativi dello sfruttamento dell'energia geotermica, tra questi il miglioramento dell'efficientamento energetico degli impianti e la distribuzione di strumenti utili per l'incentivazione dello sfruttamento delle temperature di sottosuolo. A tal proposito, mediante un caso studio relativo allo sfruttamento delle risorse geotermiche superficiali è stato possibile verificare e ottimizzare il funzionamento di un impianto che sfrutta, attraverso diverse configurazioni, le condizioni termiche studiate. Inoltre, è stato possibile individuare e sviluppare alcune configurazioni nuove per le sonde e le malte di riempimento di un impianto geotermico. Migliorando, attraverso l'aggiunta di materiali non convenzionali, le caratteristiche di scambio termico e l'ottimizzazione della resa dell'intero sistema. Infine, l'intero progetto si pone di attenzionare la risorsa geotermica e indicare un workflow innovativo per la caratterizzazione di essa, nonché uno strumento essenziale nella gestione e sfruttamento della risorsa rinnovabile, come richiesto dalla sempre più attuale transizione energetica.

# Abstract

The evaluation of the thermal and mechanical nature of the lithosphere is the primary factor used to quantify the subsurface geothermal potential. Such studies call for a thorough understanding of the geological and tectonic forces acting on the local thermal, tension, and hydraulic regimes as well as associated counter-feedback mechanisms. In dynamic and complex tectonic settings, this strategy becomes even more relevant. In this sense, Sicily is an interesting case study due to its untapped geothermal potential trapped in a complicated geodynamic environment. The present-day geological configuration resulted from the collision between the African and European plates, which led to the coexistence of compressional phases, beginning with the Oligocene-Miocene clockwise rotation of Corsica-Sardinia and alternated extensional phases in the Tyrrhenian basin due to the southward progression of the Sicilian-Maghrebian chain towards areas of the internal foreland (Hyblean domain). In this thesis, a reconstruction of the present-day lithospheric state of Sicily to quantify its shallow and intermediate depth thermal regime has been firstly attempted. Starting from 3D lithospheric-scale gravity modelling the main geological units and their lithology-dependent rock properties, which we integrate into a 3D geological model consistent with available borehole and seismic datasets, have been defined. Then the constructed geological model with its lithology-dependent density, thermal conductivity and radiogenic heat production has been used to obtain the present-day conductive thermal field as a whole and for individual tectonic or geological units, thereby considering different boundary conditions. Finally, the modelling results have been validated against a shallow temperature dataset derived from hydrocarbon exploration wells. Secondly, using the extrapolated thermal conditions of the regional modelling step, the same workflow has been applied for a specific area of the south-eastern part of Sicily. In particular, a new gravimetric dataset allowed to reconstruct a 3D density model of the local domain and to develop the local high-resolution thermal field. The results indicate that the thermal regional field at depths shallower than 10 km is largely controlled by variability in sedimentary thickness in the foreland and the orogen, while deeper temperatures are primarily controlled by the distribution of the heat transferred from the mantle together with the radiogenic contribution of the shallow crystalline basement rocks and deeper crustal layers. The thermal modelling portrays a rather heterogeneous Moho heat flow, locally higher than 80 mW/m2, revealing a particular geodynamic setting with specific areas characterized by high-to-medium

enthalpy geothermal potential. The proposed 3D model of Sicily thereby allows to constrain areas with important geothermal anomalies, such as the volcanic zones of the Aeolian Island Arc, the Etna area and the Sicily Channel Rift Zone, which could be suitable areas for the exploitation of medium-to-high enthalpy resources. The model also suggests that low-enthalpy resources are available over extended areas of the region, especially in the carbonate layers. Being the first effort in a complex Geological setting, the research provides a solid workflow that can be transferred to other areas of Italy, thereby fostering studies aimed at the quantification of potential geothermal resources. In order to make available the obtained thermal models, the implementation of interactive thematic maps reproducing the thermal steady-state field has been uploaded within a dedicated Web portal, providing a useful tool for the assessment of the geothermal condition of the investigated area. Although the efficiency of a shallow geothermal installation is chiefly based on geological properties, the total heat extracted from the subsoil also depends on the intrinsic thermal exchange characteristics of probes and grout materials. In this context, the industrial vocation of the research program has allowed to investigate applied aspects. Therefore, the development of Carbon Fiber mixed materials has improved the heat exchange and optimized the performance of an entire geothermal system. The project provides an innovative workflow usable in geothermal characterization, new interactive tools in the management of the geothermal resources, as well as more applied aspects such as the optimization of the components of geothermal systems exploiting low enthalpy.

All these aspects make Sicily a potential pilot region for geothermal exploration studies in southern Italy, and they provide a useful tool for the optimization of the exploitation of this renewable resource as required by the ongoing energy transition.

# 1 Chapter 1 – Overview and research objectives

## 1.1 Overview

The current energy crisis, due for multiple reasons (Doukas H. and Nikas A., 2022) as well as the constant increase of energy demand, requires a redefinition of the energy supply models currently based on the exploitation of coal, oil, natural gas, nuclear energy, or hydro-power (Eurostat, Energy Data – 2020), resources frequently imported from other countries. In recent years, the European Energy Policies have focused on several aspects for the energy transition with the objective of reducing gas emissions and improving the quality of life of citizens (i.e. REPowerEU Plan). Digital and interconnected development of the Energy Market would allow for a supply based mainly on Renewable Sources. In this regard, the European Commission has adopted a series of proposals to make Community policies on climate, energy, transport, and taxation capable of reducing net greenhouse gas emissions by at least 55% by 2030 compared to 1990 levels (European Green Deal). Considering the exploitation of renewable energies in the last 10 years, energy supply from renewable systems like solar, wind, and biomass have been significantly encouraged by several programs, having achieved remarkable cost reductions, while other types of unconventional forms of exploitation like Ocean, Tides and Geothermal Energy have been totally ignored. In such a context, in line with the necessity for a diversification in unconventional forms of exploitation, Geothermal Resources find their natural place. At present, although the European Energy Strategies encourage the Geothermal Resources exploitation (i.e. RePOwer EU plan, 2022), many countries still do not follow the existing guidelines. Different approaches in the management of geothermal heat exploitation have been used from different countries: Germany, Austria, and Sweden, for example, have been investing for decades in new technologies for the exploitation of geothermal heat (Lund, 2007; European Geothermal Energy Council 2019; 2020), while other countries (e.g., France) only more recently have started applying incisive supporting policies for geothermal energy (Lund, 2007; Sanner, 2017; Huttrer, 2020). Although the exploration of geothermal energy, applied to dry-steam power plants, took place for the first time in Larderello (Tuscany) in the 1920s (Ciardi, Cataldi, 2005; UGI, 2007), in Italy an insignificant percentage of the energy produced from renewable sources has a geothermal origin (European Geothermal Energy Council, 2020). The entire Italian peninsula shares a widespread low-to-high enthalpy

geothermal potential (Limberger et al., 2018) and it finds potential fields of application in many important social and economic sectors such as industry, tourism, and healthcare, with both small and big enterprises involved (Buonasorte et al., 2010, Manzella et al., 2018).

This project aims to evaluate and assess the subsurface geothermal condition to make Southern Italy, and Sicily in particular, a natural laboratory for the investigation of geothermal resources. In order to define an innovative workflow to characterize the thermal field of Sicily (Southern Italy), firstly a regional scale thermal field and later a high-resolution local condition have been investigated with the aim to develop useful web tools for the visualization and subsequent analysis of the geothermal resource. In addition, the collaboration with specialized companies in the geothermal systems sector, has made it possible to design new configurations and develop innovative compounds for the optimization of heat exchange.

## 1.2 Research objectives

The main objective of the study is to apply an innovative workflow to calculate and reconstruct the 3D steady-state thermal field of the Sicilian area and of a detailed local domain. The entire research activity therefore starts from the concept of the reconstruction of a 3D geological model based on gravity constraint and ends with the characterization of the thermal conditions of the subsoil in a steady state, as a dominant process in the transportation of heat on a regional scale. In addition, considering a pilot area in the south-eastern portion of the island, where a new high-resolution gravimetric survey was obtained, the 3D high resolution thermal field distribution was reconstructed with the aim of supporting the innovative concept of geothermal "micro-zonation" and the subsequent application and possible improvement of the resource exploitation. To achieve this goal, the project has been developed in two main phases. In the first step, a multidisciplinary approach, both on a regional and local scale, was applied in the following order:

i) development of a 3D gravity-based model;

ii) reconstruction and investigation of the steady-state 3D thermal field on a regional and local scale, as well as validation of the best-fit models against available measured temperatures;

iii) investigation of the transient-state 3D thermal field and exploitation case study of shallow geothermal resources for a pilot site area inside the local domain.

During the second phase of the program, in order to define its final industrial application, it was possible to:

iv) implement the temperature maps on an interactive web portal to support exploration and operating purposes;

v) explore innovative solutions for the improvement of geothermal heat exchange in low enthalpy systems.

The first phase was developed with the collaboration of the German Research Centre for Geosciences (GFZ - Helmholtz-Centre Potsdam) and involved the (i) definition of a starting dataset based mainly on geological and geophysical data to obtain the starting 3D geological model on a regional and local scale. During the second step (ii), through the implementation of thermal properties (such as thermal conductivity and radiogenic heat production) into numerical algorithm of specific software, as well as the identification and analysis of the boundary conditions of the geological model, it was possible to reconstruct and investigate the steady-state 3D thermal field. According to the different boundary conditions adopted for the regional modelling, three different models were analysed to individuate the best fit between modelled and measured shallow temperature. Thus, assuming the most suitable boundary conditions, the local high-resolution thermal field was also extrapolated. In the end (iii), the extrapolation of temperature maps at different depths was considered for both regional and local scales.

In comparison to the steady-state assumption of the regional modelling approach, the transient state was investigated in a case study of the local domain. In particular, the implementation of shallow geothermal systems (injection and extraction wells at depth < 500 m) for variable times was considered.

The second part of the project required industrial cooperation with the EarTherm company, which develops industrial applications; in this regard, (iv) the prototype of interactive web solutions for consultation and sharing of obtained maps to individuate the most suitable areas for geothermal purposes was developed and in the final stage of the project (v), different solutions for the optimization of the heat exchange in low enthalpy geothermal system was investigated.

## 1.3 Geothermal state of play in Sicily

Sicily, with its complex geological situation, represents a natural laboratory for the study of geothermal energy. The island offers a very favourable geological context since the region is characterized by a complex collisional setting with intense volcanic activity (Aeolian Island, Pantelleria, Etna); in addition, the presence of thermal anomalies linked to hydrothermal manifestations (Favara et al., 1998; Favara et al., 2001; Caracausi et al., 2005), as well as areas with anomalies in the geothermal gradient and in the heat flux, have been identified and analysed over time (Della Vedova et al., 2001; Caracausi et al., 2005) (Figure 1.1). In particular, western Sicily is a very interesting area characterized by the presence of several thermal manifestations, often used for balneotherapy (Alaimo et al., 1978; Caracausi et al.,2005; Favara et al., 1998; Favara et al., 2001), and high heat flow evidence (Della Vedova et al., 2001). In addition, several classical written works described the geothermal manifestations emerging in Sicily, emphasizing the functional and rational utilization of the geothermal manifestations since ancient times (Ciardi et al., 2005). Among these, the Imera, actual Termini Imerese or "Terme Segestane" in the western domain, to the Alì Terme or Terme Vigliatore in the eastern portion. Considering the most up-to-date aspects of geothermal energy exploration and characterization in Sicily, many measurements within oil and gas wells showed a positive heat flux and temperature anomalies at depth (Cataldiet al., 1995) useful for geothermal purpose. Although this positive validation, in the current state, the geothermal resources in Sicily have received little encouragement except for a few projects. In order to assess the geothermal potential, various research programs have been launched in the region. First, the geothermal exploration program on the island of Vulcano in the 1950s (VULCANO-Agip exploration program, Sommaruga, 1984) was the first attempt at the characterization of the recognized geothermal reservoir. Afterwards, the exploration program of the island of Pantelleria, promoted by the Sicilian Mining Authority (EMS) and sponsored by the European Union, took place in the 1960s. Subsequently, the project was re-launched by CESEN in 1990s with the collaboration of the International Institute of Geothermal Research (IIRG) of the Italian National Research Council (CNR) (Chierici et al., 1995) to investigate in detail the geothermal field. In addition to the geothermal characterization of the minor island of Pantelleria, mainly related to the exploitation of high-enthalpy resources, other projects were aimed at defining the medium-to-low temperature geothermal potential for the entire regional territory. Among these, the most important

was the VIGOR project (Evaluation of the geothermal potential of the convergence regions, Campania-Puglia-Calabria-Sicily), which proved to be useful to provide analytical information in order to start geothermal prospecting activities and to increase the share of energy consumed from renewable sources, as well as to improve energy efficiency and to promote local development activities. Currently, the strong geothermal vocation of the smaller islands in Sicily (i.e. Aeolian Island, Pantelleria) has generated multiple partnerships aiming at the development of regional projects and at the study of energy self-sufficiency, as well as the environmental and social sustainability of small island realities. Considering the results obtained from the comparison between the heat flux maps drawn up by the Institute of Geosciences and Georesources (IGG) and the results of the VIGOR project (Western Sicily) (Montanari, 2015), the potential of the geothermal resource seems to be highly exploitable, but still scarcely investigated. Several studies have discussed the geothermal potential of Sicily (Di Sipio et al., 2013; Abate et al., 2014; Trumpy et al., 2015; Montanari et al., 2015; 2017; Santilano et al., 2016), and agree in the identification of the local carbonate formations as the main geothermal reservoir (e.g. Fancelli et al., 1991, Montanari et al., 2015). The geothermal resource is still largely geologically undefined and requires to be properly assessed by adopting innovative exploration workflow strategies (e.g. integrative thermal modelling assisted by gravity and petrophysical constrains). The large number of exploration wells drilled during the exploration campaigns for hydrocarbons between the 50s and 60s covers a large part of the Sicilian territory and provides various well-log data (thermometric, sonic, gamma-ray data) and geochemical data useful for the study of regional geothermal conditions. Although the areal geothermal characterization is linked to site surveys (such as drilling and sampling), the use of numerical modelling is an excellent tool for the preliminary characterization of the resource. In this regard, there are few studies that take into consideration and develop numerical models to evaluate the heat exchange in the subsoil. In Italy a few studies have been recently carried out to map the geothermal potential of particular regions based on 3D analytical modelling approaches (Basilici et al., 2019; Basilici et al., 2020; Santini et al., 2020; Santini et al., 2021) whereas in Sicily, Abate et al., 2014 and Montanari et al., 2017 suggest similar approaches for the respectively restricted area of termini Imerese and Mazara del Vallo. Thus, understanding the 3D temperature distribution on a regional scale becomes an essential step to investigate the geothermal potential and stimulate interest towards its direct exploitation. This study is aimed at exploring a new workflow for the

characterization of the shallow-to-medium depth thermal configuration of the sediments (1-5 km) and crust (5-30 km) of the regional domain in order to help assessing the most suitable areas for geothermal exploitation in Sicily.

## 1.4 Geological and geodynamic background

Sicily is part of the western Mediterranean area, located above the geotectonic boundary between the African and the European lithospheric plates. It is a complex geodynamic setting, and its geological evolution has been affected by the ongoing, southward advance of the Sicilian-Maghrebian orogen towards its internal foreland areas (Catalano, 2002; Lentini and Carbone, 2014). This still active tectonic setting, related to the polyphasic evolution of a compressional regime, began with the Oligocene-Miocene clockwise rotation of Corsica-Sardinia, simultaneous with extensional tectonics in the Tyrrhenian basin (Catalano, 2002). As a result of its geodynamic evolution, Sicily is characterized by plate collision domains, subduction zones, and back-arc extensional basins resulting in a rheological and thermal configuration that is considered suitable for geothermal energy exploitation (Montanari et al., 2015, 2017; Santilano et al., 2016; Trumpy et al., 2015; 2016). The present-day geothermal potential of Sicily has usually been differentiated based on tectonic aspects and the homogeneity of distinct lithological domains (Gola et al., 2013; Santilano et al., 2016; Montanari et al., 2017). Catalano et al., 2002, for example, provided a simplified geological scheme of the collisional system characterized by three different domains: the Foreland, the Foredeep, and the Orogenic Domain (Figure 1, Milano et al., 2020). Areas of the Pelagian foreland Block represent the submerged foreland of an external undeformed structural domain consisting of a still debated thinned continental or oceanic crust (Catalano et al, 2000; Ciliberto et al., 2009; Scribano et al., 2009), which is covered by a thick Meso-Cenozoic carbonate succession (>5 km) with volcanic intercalations (Calcagnile et al., 1982). On the other hand, the Ionian Basin is considered the remnant of an oceanic crust (ca. 15 km thick) in the southern sector of the active subduction of the Calabrian Arc (Scarfì et al., 2018). The Pelagian Block is separated to the east from the Ionian basin by the Hyblean-Maltese Escarpment (ME), a system of active NNW-SSE oriented normal faults, which also involves the eastern slope of Mt. Etna volcano, playing therefore a fundamental role in the seismo-tectonic behaviour of the whole area (Cristofolini et al., 1985). The structural flexure of the Hyblean foreland towards NW produces NE-SW oriented faults associated to the fore-deep system of the Catania-Gela nappe system. At present, this nappe system is partially buried by allochthonous units of the Sicilian chain. It is a narrow, weakly deformed depression with a WNW-ESE strike direction, extending also off-shore of


*Figure 1.1– a) Simplified tectonic map of Sicily and central Mediterranean b) Location of the studied area. c) Heat flow map of Sicily (from Della Vedova et al., 2001). Figure from Montanari et al., 2017.*

Sicily. Plio-Pleistocene filling of the basin consists of pelagic marly limestones and sandy clays overlying the Messinian evaporites (Catalano, 2004). The orogenic domain is widely exposed in Sicily and consists of an external thrust system, the Apennine-Maghrebian Chain, the Calabridi units and the Neogene-Quaternary covers. It is a complex chain made up of an ESE trending fold and thrust belt representing allochthonous material derived from the innermost European elements of the orogenic domain (i.e., the crystalline units of the Peloritani and Kabilo-Calabride chains) and thrust over the sedimentary basin successions and the Maghrebian-Sicilian chain (Lentini and Carbone, 2014). The orogenic chain resulted from the deformation of different paleo-geographic domains since Late Oligocene times, and it is principally constituted by an 8-9 km thick wedge of Meso-Cenozoic imbricated carbonate platforms (Meso-Cenozoic Carbonates Units) overlain by a 2-3 km thick tectonic stack of basin carbonate thrust sheets, which derive from the detachment of the roofs of the Ionian paleo-basin. The latter, in turn, are overlain by Oligo-Miocene terrigenous deposits and by remnants of the Mesozoic-Tertiary basin deposits of the Gela nappe (Neogene-Quaternary deformed

deposits; Carbone et al., 1987; Lentini and Carbone, 2014). The higher structural position of the entire orogenic building consists of Variscan crystalline basement formations of the Peloritani-Calabrian units (Carbone et al., 1987; Lentini and Carbone, 2014), belonging to the European plate. This is the innermost element of the orogen with remains of the original Meso-Cenozoic roofs. This active tectonic context, as also evidenced by current and past seismicity (Lavecchia et al., 2007) (i.e. 5.9 magnitude destructive earthquake occurring in the Belice valley in 1968, Selinunte, Mazara del Vallo and Sciacca repeatedly destroyed), is often related to the geothermal favourability (Trumpy et al., 2015; Trumpy et al., 2016). The complex collisional context of Sicily is also characterized by the presence of important volcanic systems, such as the Mt. Etna volcano in the eastern part of the island, the Aeolian Island Arc (Tyrrhenian domain system) and Pantelleria (Sicily Channel rift zone). These are examples of variably active volcanic systems where surface heat flow can reach values higher than 100 mW/m2 (Della Vedova et al., 2001).

# 2 Chapter 2 – Methodology and Workflow

The general workflow followed for the definition of thermal models on a regional and local scale will be presented in this section with the intention of identifying key concepts for the characterization of geothermal resources. Starting from the geological modelling that integrates the available data, it was possible to constrain the lithological conditions through the gravimetric data. Finally, using implemented algorithms, the steady-state thermal model for low-resolution modelling on a regional scale, and a higher-resolution case study related to examples of transient-state focus, has been defined. The subsequent analysis of the final outputs allows the definition of user-friendly interactive tools.

## 2.1 Modelling approach

With the aim of investigating the thermal field of a region, an extensive vision of the crustal setting is essential. In this regard, thorough information on the lithology involved and the physical properties analysed are essential for the evaluation of the thermal state of a given area. Usually, geothermal potential assessments are often based on invasive methods (e.g. well drilling), legally authorized inspections and high costs (Moeck, 2014). Among the alternatives to accurately evaluate the geothermal resources of a specific area, the integration of large datasets becomes an interesting method, as it allows to facilitate the numerical modelling process. Although some attempts, based on modelling studies, have been conducted to map the geothermal potential of multiple regions in Italy (Basilici et al., 2019; Basilici et al., 2020; Santini et al., 2020; Santini et al., 2021), a programmatic modelling approach is still inadequately developed. Concerning the Sicilian area, regional studies aimed at integrating all the available information on the complexity of the subsurface of Sicily and to investigate its influence on the resulting thermal field are still lacking in the existing literature. In this thesis, a multidisciplinary workflow already tested in other geological settings ranging from sedimentary basins to collisional contexts (Scheck-Wenderoth et al., 2014; Sippel et al., 2017; Spooner et al, 2020; Rodriguez Piceda et al., 2022) attempts to bridge this gap of information. The workflow conceived in this study allows the analysis of temperature changes on a lithospheric scale and the identification of areas which are suitable for geothermal exploration on a regional scale, as well as the investigation of the thermal field of a high-resolution local domain. Starting from a regional 3D geological model that integrates all available geological and

geophysical information, the steady-state thermal field resulting from the geological model is calculated.

Our workflow consists of the following main stages (Figure 2.1) :

(1) integration of multiple geological and geophysical dataset into an initial 3D geological model (see chapter 3);
(2) development of a 3D density-based lithological model that fits the main features of the observed gravity field (bouguer anomaly, free-air anomaly) to constraint the lithological variations within the study area (see section 3.1);
(3) implementation of the relevant thermal properties of the considered geological units (see section 3.1);
(4) testing of different boundary conditions (see section 3.1.1) in order to find the best-fit thermal state between modelled and observed temperatures;
(5) definition of local condition and simulation of a transient state for a pilot area (see chapter 4);
(6) management of thematic maps in an on-line platform (chapter 5).

The available geological and geophysical dataset on a low-resolution regional scale have been integrated to generate an initial geometry. The interfaces between modelled lithospheric units are intended to represent abrupt changes in density configuration within the lithosphere, delineating bodies with homogeneous physical properties. To better constrain the regional model, we tested the effect of its geometric configuration on the

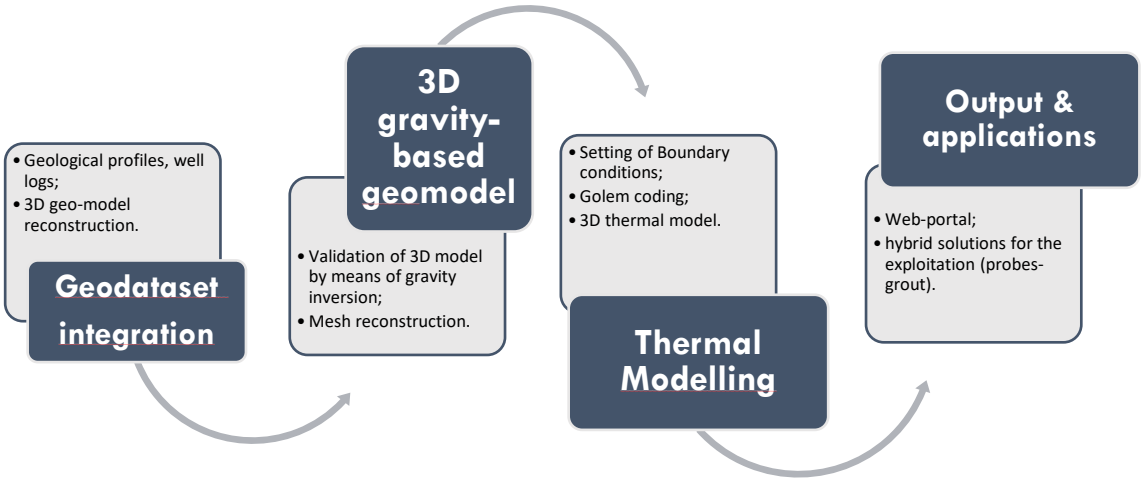


*Figure 2.1- Workflow of the research*

gravitational field (according to the Bouger anomaly), assuming that differences between observed and modelled Bouguer anomalies in the initial model reflect heterogeneities in the sub-sedimentary crustal density configuration, which have not been considered in the initial model. In this regard, a heterogeneous density configuration of the crustal thickness has been calculated by taking into account the contribution to the gravity field response from a heterogeneous mantle. The mantle conditions (bottom boundary of the model) have been produced from a direct conversion of available seismic tomography models by means of specific algorithms (Kumar, 2022). Subsequently, the final differentiation of the crystalline crust was computed (Uieda et al. 2016). Gravity analysis have been conducted by means of IGMAS+ software. Based on the 3D geological model, obtained from the gravimetric modelling phase, a subsequent step of the work involved the thermal modelling process. The latter was performed using numerical simulator of coupled Thermal-Hydraulic-Mechanical processes GOLEM (Cacace and Jacquey, 2017) to evaluate the steady-state conditions. As for the gravity modelling phase, in order to evaluate the mantle contribution to the resulting thermal field, the lower thermal boundary of the model has been constrained. In this regard, two seismo-tomographic models have been used to obtain the temperature distribution across the upper mantle domain. The fit of the resulting three models has been compared to the available surface and shallow temperature measurements and a sensitivity study has been conducted. The same methodologies (first gravity analysis and secondly thermal modelling) have been used for the definition of a high-resolution thermal modelling phase in a specific area of south-eastern Sicily. In this regard, a new gravity survey has been used for gravity computations. The resulting 3D geological model has been used for the implementation of thermal properties and the simulation of steady-state thermal fields. In addition, an exploitation case study has been performed in order to assess the transient state and the variations of the thermal field (operation time of a low enthalpy geothermal system for 10 years). Both the regional and local thermal field analysis allow the definition of the temperature condition at different depths, which have been extrapolated and used for the definition of temperature-depth maps that can be available on an interactive web platform.

## 2.2 Initial 3D geological models

The first phase of the workflow has provided the integration of all the available geological and geophysical datasets into a consistent 3D geological model of the regional area (Figure 2.2, Appendices). The dataset, which includes the most important interpreted seismic lines (Catalano, Sulli 2000; Lentini, Carbone, 2012; Finetti, 2005) and hydrocarbon exploration wells (data from the ViDEPI Project: http://unmig.sviluppoeconomico.gov.it/videpi/progetto.htm and Geothopica project, Trumpy et al., 2017), has been used to reconstruct a simplified geometry on a lithospheric scale. In particular, to constrain the basic geometry of the model, available information on the major layers has been integrated. In detail, the Sicilian Region DTM (https://www.sitr.regione.sicilia.it/geoportale/it/metadata/details/502, 2021) and bathymetric survey data from the EMODnet Digital Terrain Model (DTM) for the European sea regions (https://www.emodnet-bathymetry.eu, 2021) have been considered as the top elevation boundary of the model. Given the low data resolution, for the regional context, a homogeneous physical property (like density) for each and every one of the three-dimensional layers has been assumed. In particular, four major density contrasts, that can be traced throughout the entire study area, have been differentiated: (1) the crust-mantle boundary or Moho; (2) the top of the crystalline basement; (3) the top of a Meso-Cenozoic succession; (4) the top of a sequence of Oligo-Pleistocene deformed deposits (which delineates the Earth's surface and sea floor, respectively). Each surface has been defined through the use of convergent interpolation algorithms of scatter information implemented in the PETREL software (©Schlumberger). Although each three-dimensional layer is characterised by a heterogeneous geological condition, given the available data and the low resolution of the extended area, the simplification regarding the investigated units has been considered acceptable. The model resulting from the first stage of the data elaboration has a lateral resolution of 5 km and seven units have been differentiated in depth. From top to bottom have been distinguished: (1) seawater; (2) a Metamorphic Unit representing parts of the European plate; (3) Volcanic Domains; (4) the Paleogene-Quaternary deformed deposits; (5) the unit of Meso-Cenozoic Carbonates; (6) Crystalline Basement Rocks; (7) the Lithospheric mantle (down to 80 km depth below sea level). The density variability expressed in $kg/m^3$ for each geological unit considered in the model has been summarized in Table 1. Thicknesses and depth elaborated maps of each unit of the 3D model have been illustrated in Figure 2.3. Seawater represents the

uppermost layer in our model, while the Metamorphic Unit and Volcanic domains appear as isolated volumes in a regional context. In detail, the Metamorphic Unit is found in the north-eastern sector of the island within the Peloritani mountains and the Aspromonte Massif, where it reaches the maximum thickness of 1.5 km (Fig. 2.3a). The unit of the Volcanic Domains is limited to the Mt. Etna region, the volcanic parts of the Aeolian Island Arc and the Pantelleria island, with thicknesses ranging from 100 m in the Aeolian Arc and composing the upper 2 km above sea level in the Mt. Etna region (Fig. 2.3b). The Oligo-Pleistocene deformed deposits (mostly terrigenous) show variations in thickness from a few meters beneath the foreland domain (Hyblean Mts.) to approximately 6 km in the Caltanissetta Basin area (Figure 2.3c) (Lentini and Carbone, 2014). The top of the Meso-Cenozoic Carbonates has been produced from the corresponding depth map of Sicily based on a geophysical modelling study, using available Bouguer and free-air gravimetric data (Montanari et al., 2015), and integrated with geological interpretations from offshore and onshore seismic profiles (Montanari et al., 2015; 2017). Thicknesses of about 10 km were obtained in the western part of Sicily, decreasing down to 2 km in the Tyrrhenian and Ionian domains (Fig. 3d). The depth of the basement was constrained by the interpretations of Milano et al. (2020) and integrated with the main geological profiles of the area (SI.RI.PRO and Nebrodi Iblei, Figure 2.2). Accordingly, the resulting thickness of the unit of Crystalline Basement Rocks ranges between 14 km in the inland domain and up to 2 km offshore (depth map in Fig. 2.3e). To constrain the base of the crust, information on the Moho depth was reconstructed from different studies (Cassinis et al., 2003; Catalano et al., 2012; Di Stefano et al., 2011; Finetti, 2005; Milano et al., 2020). Figure 2.3f shows the Moho depth as varying across the different tectonic domains. The Caltanissetta Basin and the northern area of Sicily are characterized by a deep Moho interface, between 25 and 35 km (SI.RI.PRO project, Catalano et al. 2012), while the shallowest Moho depths are located in the Tyrrhenian domain and in the Sicily channel, with a total crustal thickness lower than 10 km (Morelli, 2007). With the aim of building the 3D high resolution geological model of a pilot area in the south-east portion of the Sicilian region (Hyblean domain), the same approach and workflow have been applied. In this case, an area of 935 $km^2$ located in the south-eastern domain of Sicily (Hyblean foreland, red box in Figure 4.1) was taken into account. Unlike the regional model, the resolution of the local model is greater and results in a later and vertical resolution of 500 m. The entire area consists of a Meso-Cenozoic succession above the crystalline basement. By means of consisting database of hydrocarbon

exploration wells (data from the ViDEPI Project: http://unmig.sviluppoeconomico.gov.it/videpi/progetto.htm and Geothopica project, Trumpy et al., 2017) and several geological profiles (see appendix A_2), the Meso-Cenozoic succession has been constrained. As for the regional context, through the implementation of these datasets in the specialized PETREL software (©Schlumberger), the respective surfaces of each geological unit have been obtained (convergent Interpolation algorithm). For the geological setting of the pilot area, it was possible to distinguish nine model lithological formations, well described in literature (Lentini, F. et al., 2012), from top to bottom: (1) Palazzolo F.ne; (2) Tellaro F.ne; (3) Ragusa F.ne; (4) Amerillo F.ne; (5) Hybla F.ne; (6) Buccheri F.ne and Chiaramonte F.ne (7) Modica F.ne; (8) Noto F.ne and Streppenosa F.ne; (9) Gela F.ne. Layers 6 and 8 have been combined, as taken individually they create issues in the subsequent thermal modelling phase. Furthermore, the simplified model takes into account the tectonic structures that could justify the multiple intersections for the investigated layers.

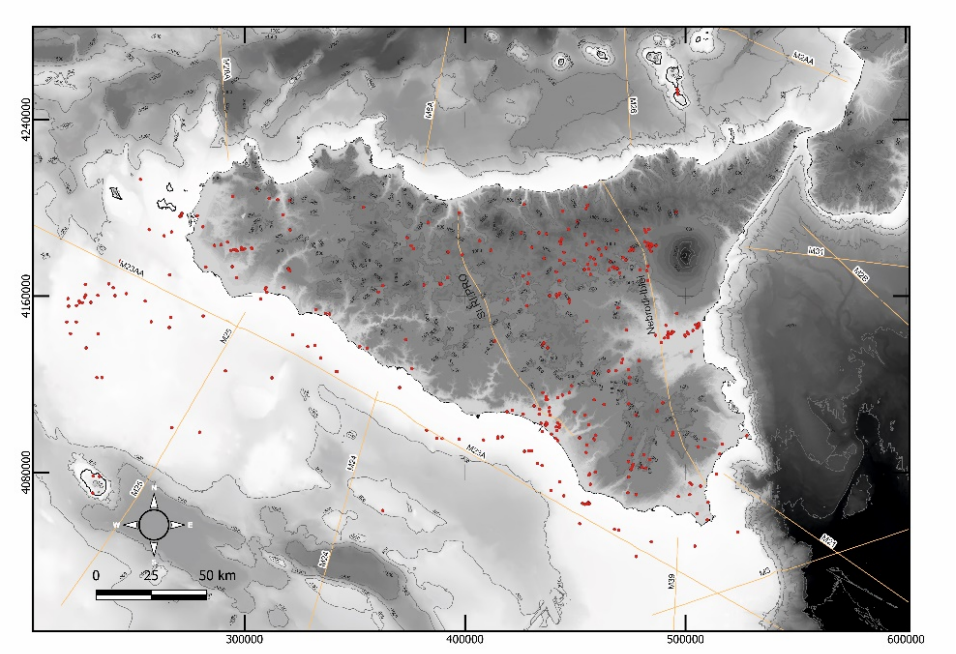


*Figure 2.2- Datasets integrated for the reconstruction of the regional geo-lithological configuration. Red dots display the location of the updated Italian National Geothermal Database well bores. Yellow solid lines show the traces of reflection and refraction seismic profiles of the offshore CROP project (CNR, ENI, ENEL) and the onshore SI.RI.PRO project. Yellow dashed line illustrates the trace of the geological interpretation of the Nebrodi-Iblei profile. Coordinates are in EPSG:32633 – WGS84/UTM zone 33N.*

## 2.3 Gravity modelling

One of the most important phases of the entire workflow is the gravity analysis, which is useful to map the density distribution of the different rock lithologies and quantify the gravitational response to the imposed density distribution. In fact, after having constrained the geometry of the significant geological layers, the analysis of residual gravity anomalies has been carried out. The Bouguer gravity anomaly derived from public dataset for the regional domain (Figure 2.4a "ISPRA, ENI, OGS (2009), Cartografia Gravimetrica Digitale d'Italia alla scala 1:250.000" 2009) and the new gravimetric survey for local domain, which includes Bouger and Free-air anomaly data, have been therefore considered (Figure 4.6). Subsequently the direct comparison between the anomaly described above and corresponding gravity response of the 3D geological model as calculated by the software IGMAS+ (Schmidt et al., 2020) was investigated. For the differentiation between regional and local modelling, different geological sceneries have been taken into consideration. While for the regional model homogeneous density values were attached for the five reconstructed thicknesses separated by the major density contrasts surfaces (moho, crystalline basement, carbonates unit, sedimentary cover, volcanic and metamorphic complex base), local carbonate sequence (up to 5 km depth) in the south-eastern portion of the regional domain was differentiated on the basis of a new gravimetric survey performed as part of the geological exploration. In this case, in the first attempt, it was assigned to eleven lithology-dependent density units (section 4.2.1).

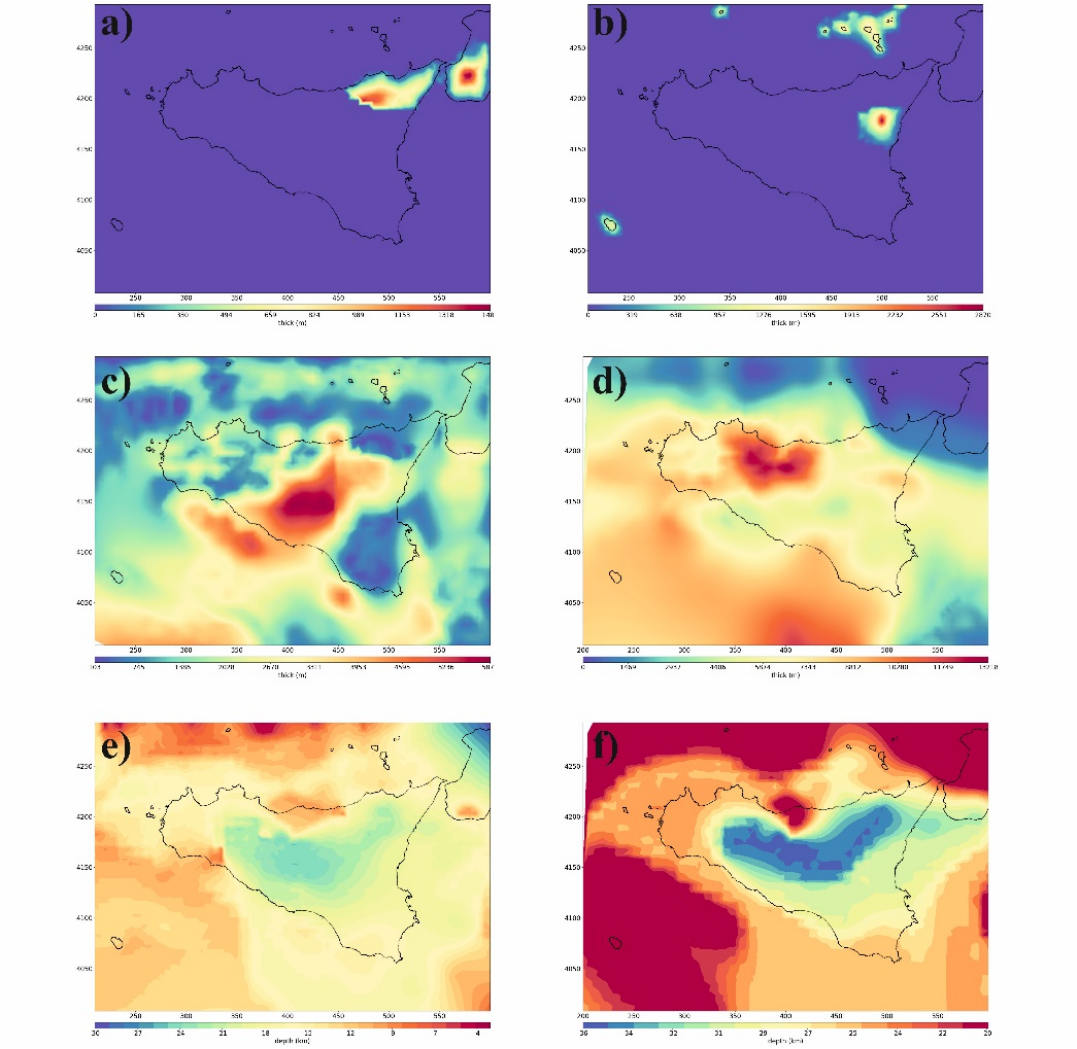


*Figure 2.3 - Thickness (m) of: a) Metamorphic Unit of the European plate, b) Volcanics domain, c) Paleogene-Quaternary deformed deposits (Paleogene-Quaternary), d) consolidated Meso-Cenozoic units (mostly carbonates). Top (depth in km) of e) the Crystalline Basement, f) the Moho depth. Coordinates are in EPSG:32633 – WGS84/UTM zone 33N.*

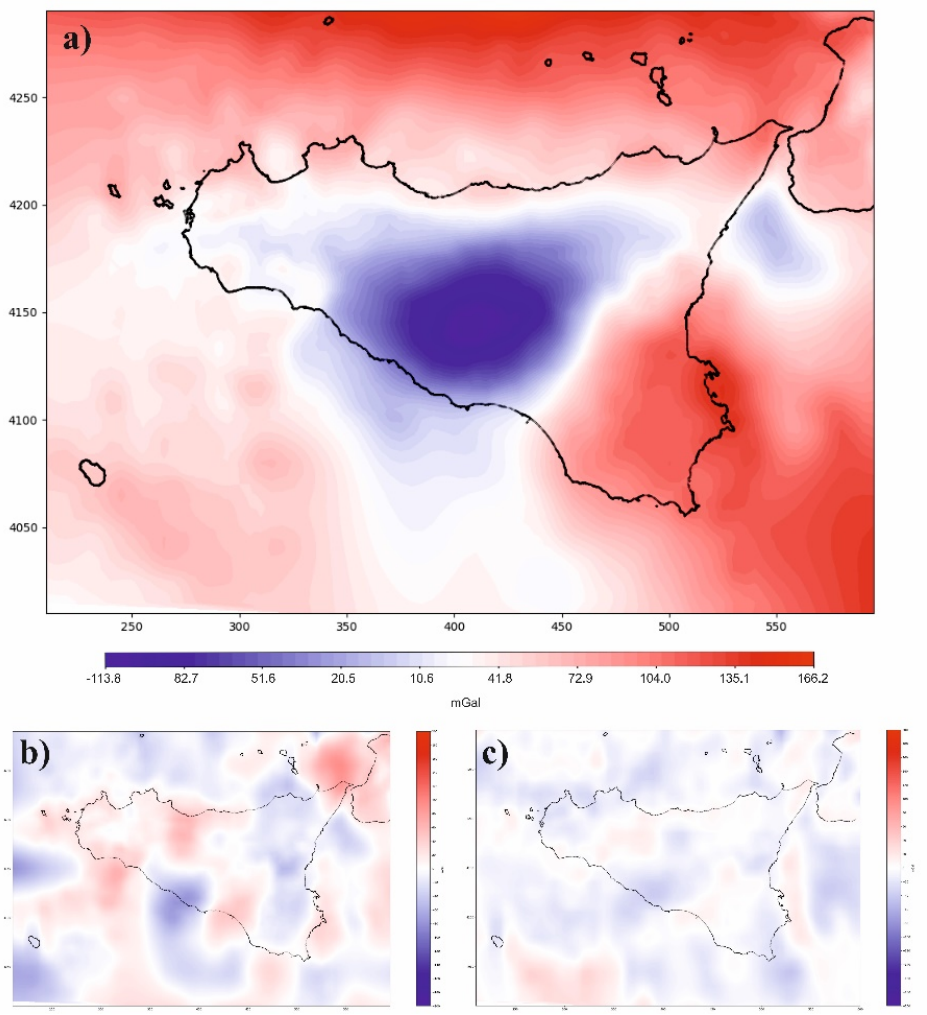


*Figure 2.4 – (a) the Bouguer anomaly (based on a Bouguer slab correction density of 2670 kg/m³) from ISPRA (the Italian National Institute for Environmental Protection and Research - Land Protection and Georesources Department). (b) residual gravity field obtained with IGMAS+ for initial model, (c) residual gravity field after Harvester module inversion applied to obtain the density configuration of the crystalline crust. Coordinates are in EPSG:32633 – WGS84/UTM zone 33N.*

## 2.4 Thermal modelling

The gravity-based 3D model is the input for the open-source software GOLEM (Cacace and Jacquey, 2017) in order to compute the 3D steady-state conductive thermal field of the study area. Thermal-hydraulic-mechanical and non-reactive chemical processes can be managed via the GOLEM software. It makes use of the flexible, object-oriented numerical framework MOOSE (developed at the Idaho National Laboratories), which provides a useful interface for the non-linear solver technology. In GOLEM, the governing equations of groundwater flow, heat and mass transport, and rock deformation are solved by the classical Newton–Raphson or by the free Jacobian inexact Newton-Krylow schemes. Non-linear feedback among the active processes is enforced by considering evolving fluid and rock properties depending on the thermo-hydro-mechanical state of the system and the local structure.

Following the assumption of steady-state conduction as the dominant heat transport process, the implemented solving equation reads as:

$$\nabla \cdot (\lambda \nabla T) - H = 0 \qquad \textit{Equation 2-1}$$

where λ is the thermal conductivity (expressed in W/mK) of the porous material (an average between its solid grain and pores), T the temperature (expressed in K) and H the radiogenic heat production contribution acting as a direct source of internal heat (expressed in $W/m^3$). The thermal properties, as well as the geometry of the investigated lithology, discretized into a Finite Element Model (FEM), have been implemented through the use of C++ language providing the main script for the subsequent numerical simulation. The FEM model shares the same resolution as the 3D geological model input horizontally (5 km), while it has been vertically refined with respect to the original geological model in order to maintain the element shape ratio close to one; each geological layer has been subdivided into separate Finite Element layers (refining process). In order to solve numerically the temperature distribution, the following set of boundary conditions has been imposed. All lateral boundaries have been closed to heat flow, and a spatially variable temperature distribution (first-order boundary condition) along the topmost model surface (topography and bathymetry) has been forced. The respective temperature distribution resulted from an interpolation of the yearly average

temperature from the dataset of the SIAS stations (Servizio Agrometereologico Siciliano, www.sias.regione.sicilia.it) for the onshore domains, whereas an average temperature of 17°C in the offshore domains consistent with the available data has been considered. In contrast to the top temperature constraint, the bottom temperature distribution has been assigned from the calculation of the mantle's input for regional context described hereinafter in section 3.1.1 and assumed from the regional outputs for high-resolution local domains described in Chapter 0.

# 3 Chapter 3 –Regional thermal modelling

The gravity-based geological model coupled with the rock properties for each layer, as well as the implementation of boundary conditions were used as a starting point to compute the regional thermal field of Sicilian area. The result of this numerical effort is the first 3D lithospheric-scale thermal model of the entire region.

The aim of this chapter is, therefore, to quantify the regional thermal field, as well as the structural control of the thermal configuration and its geodynamic implications. In doing so, the results of each proposed model have been discussed in terms of the lower boundary condition adopted. Each extracted model represents a family of numerical simulations, where the thermal rock properties have been systematically varied. The results based on the model's parameterization are discussed in the following chapter, also providing the best fit to the shallow available temperature measurements.

## 3.1 Gravity-based geological model

With the aim of validating the regional geological model, homogeneous density values have been attached for the five reconstructed thicknesses, together with the computed major density contrasts surfaces (moho, crystalline basement, carbonates unit, sedimentary cover, volcanic bodies and methamorphic complex).

As shown in Table 3.1, the considered values are distributed as follows: a homogeneous density value of 2550 kg/m$^3$ assumed as the average value of standard volcanic rock Anon, 1979.), a constant density value of 2780 kg/m$^3$, which is the mean value for the metamorphic unit (consisting of several lithologies) of the Peloritani metamorphic complex derived from Punturo et al. (2005), the average density value of 2020 kg/m3 for Paleogene-Quaternary deformed deposits resulting from the P-wave velocities conversion (Gardner's relation; Gardner et al., 1974) within the ViDEPI project database (see appendix A_3, A_4), the average density of Meso-Cenozoic Units of 2400 kg/m$^3$, computed from the P-wave velocities conversion (Gardner's relation; Gardner et al., 1974) within the ViDEPI project database (see appendix A_4), a 3D homogeneous density distribution for basement rocks of 2900 kg/m3 reported by Sgroi et al. (2012).

A heterogeneous density distribution in the upper mantle, obtained from a direct conversion of the S-wave velocity anomalies between 50 and 200 km depth (below sea level) as derived from the "CSEM Europe" mantle tomographic model (Fichtner et al., 2018), has been additionally considered (section 3.1.1, Figure 3.4). A model where the upper mantle density configuration has derived from the EU60 tomography (Zhu, 2015) did not result in any first-order changes in the gravity response and for the sake of readability, only the results obtained from the "CSEM Europe" mantle tomography will be discussed. The gravity residual calculated from the initial crustal configuration with the densities presented in Table 3.1 is shown in Figure 2.4b-c. The calculated gravity residual indicates positive values up to 200 mGal in the north-eastern Calabrian subduction domain, in the northern sector of the region, and along the Hyblean escarpment. In the Caltanissetta Basin and in parts of the Ionian domain, negative residuals between -120 and -150 mGal indicate local mass excess in the initial model. In the remaining parts of the inland and foreland domain, the gravity residual ranges between ±35 mGal, suggesting that the initial model already provides a good approximation of the observed regional gravity field.

*Table 3.1- Density values used for gravimetric regional modelling workflow.*

| | Dominant lithology | Density final model (kg/m$^3$) | Ref | Density reference model (kg/m$^3$) | Ref |
|---|---|---|---|---|---|
| Volcanic domains | Igneous rocks | 2.55 | (Anon, 1979) | 2.55 | (Anon, 1979)) |
| Metamorphic unit | Metamorphic-Igneous Rocks | 2.78 | (Punturo et al., 2005) | 2.78 | (Punturo et al., 2005) |
| Paleogene-Quaternary deformed deposits | Evaporites and sedimentary | 2.02 | (ViDEPI Project*) | 2.02 | (ViDEPI Project*) |
| Meso-Cenozoic Units | Mesozoic Carbonates and evaporites | 2.40 | (ViDEPI Project*) | 2.40 | (ViDEPI Project*) |
| Shallow Crystalline Basement Rocks | Metamorphic-Igneous rocks | 2.52 | Fatiando (Harvester module) inversion | 2.9 (value before inversion) | (Sgroi et al., 2012) |
| Deeper crust | Granodiorite | 2.85 | IGMAS+ inversion | | |
| Lithospheric mantle | Peridotite | (3.273-3.361) | Range from (Fichtner et al., 2018; Kumar, 2022) | (3.273-3.361) | Range from (Fichtner et al., 2018; Kumar, 2022) |

*data from the Gardner's relation (Gardner et al., 1974) applied to seismic velocity ViDEPI dataset.

Since the sedimentary and mantle parts of the model are well constrained, the observed residual anomalies are likely to be related to mass excess/deficit domains within the crystalline crust only. Indeed, a homogeneous density of 2900 kg/m³ has been considered for the crystalline crust in the initial model. In the second stage, a differentiation of this unit into two sub-units, a Shallow Crystalline Basement Rocks and a Deeper Crust, has been attempted, thereby also following available independent indications. This was done via the geophysical tool "Fatiando a Terra" (Uieda et al., 2013), which has been used to guide an inversion analysis of the gravity signal by considering the density configuration of the crust as a variable of interest for the inversion (Meeßen et al., 2018). For this purpose, the density of the Shallow Crystalline Basement Rocks has been set to 2520 kg/m³, consistently with previous works (e.g. Sgroi et al., 2012) (Table 3.1). For the density of the Deep Crust, 2850 kg/m³ has been assumed as a representative value, as this is consistent with the range of P-wave velocities observed from wide-angle seismic profiles in the area (Sgroi et al., 2012). The calculation sets the initial density perturbations along the base (i.e. the Moho) of a fixed mesh and propagates them vertically until the residual gravity reaches a prescribed minimum threshold. In this study, the initial seed distribution at 500 m above the Moho has been set and density perturbations within the continental crystalline crust have been introduced by thickening the Deep Crust after each propagation stage (500 m). The resulting interface separating the Shallow Crystalline Basement Rocks and the Deeper Crust units (Figure 3.1) has been subsequently integrated into the lithospheric configuration to obtain the final model.

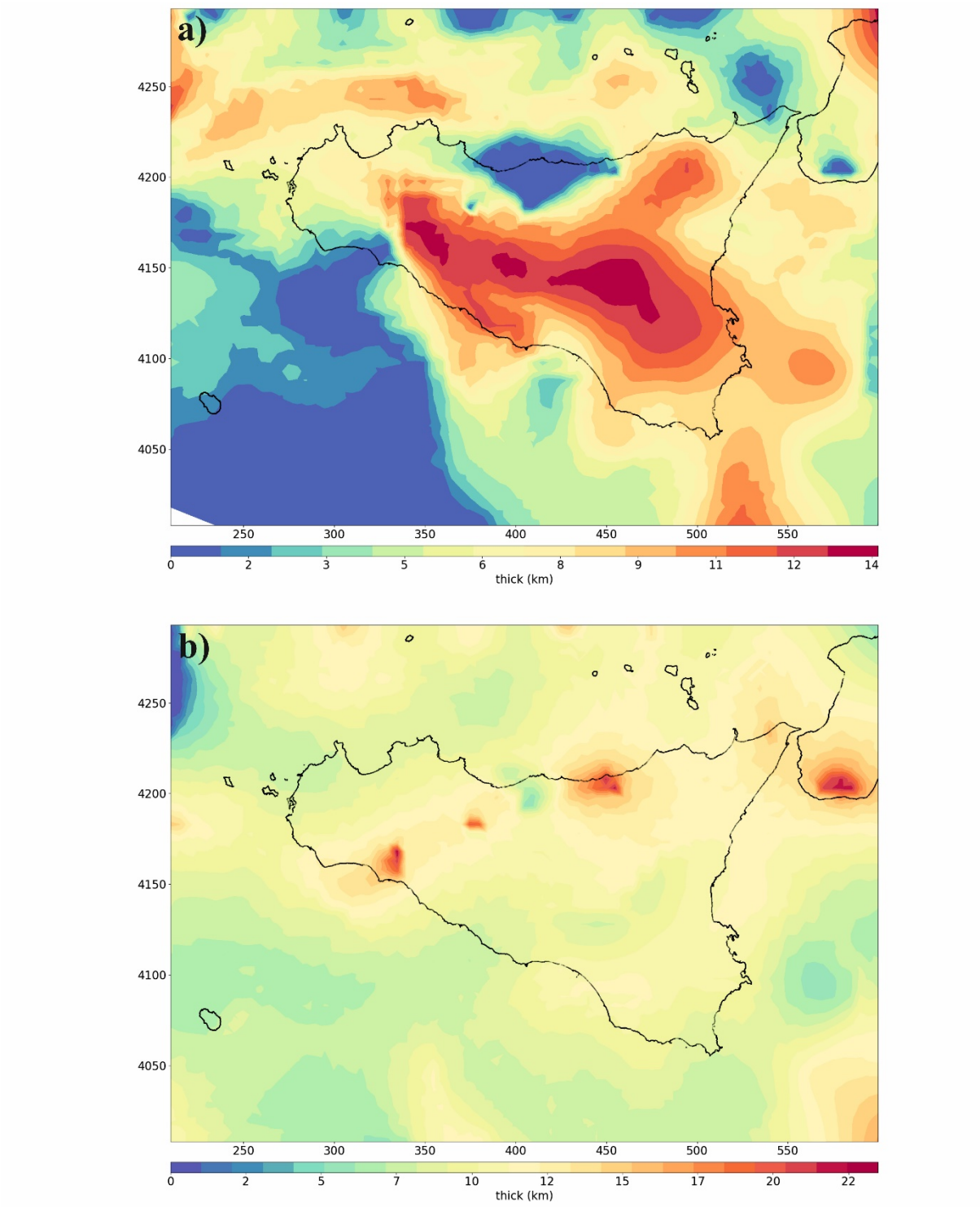


*Figure 3.1 - Upper (a) and lower crust (b) thickness from Fatiando inversion using Harvester module. Coordinates are in EPSG:32633 – WGS84/UTM zone 33N.*

### *3.1.1 Lower boundary constraints: Density and Temperature distributions in the upper mantle*

In order to better constrain the lower boundary condition, a heterogeneous density distribution for the upper mantle has been obtained from a direct conversion of the S-wave velocity anomalies between 50 and 250 km depth (below sea level) as derived from the "CSEM Europe" and "EU60" mantle tomographic model (respectively Fichtner et al., 2018 and Zhu et al., 2015). The velocity-to-density conversion has been performed following the approach described in Kumar (2022), which inverts temperature and density from mantle S-wave velocity given a predefined bulk mantle composition (appendix A_3). The approach relies on pre-computed look-up tables of temperature and pressure-dependent stable phase and mineral assemblages derived from a Gibbs free-energy minimization (Connolly, 2009; 2005) based on the augmented-modified version of a thermodynamic database (Afonso and Zlotnik, 2011), while the resulting inharmonic S-wave velocity is additionally corrected for anelastic attenuation and effects of partial melts (Kumar, 2022). To define a representative bulk mantle composition (Table 3.2), we have used the xenolith data available for the region (Bianchini et al., 2010; Ciliberto et al., 2009; Correale et al., 2012; Scribano et al., 2009; Tonarini et al., 1996, Figure 3.2).

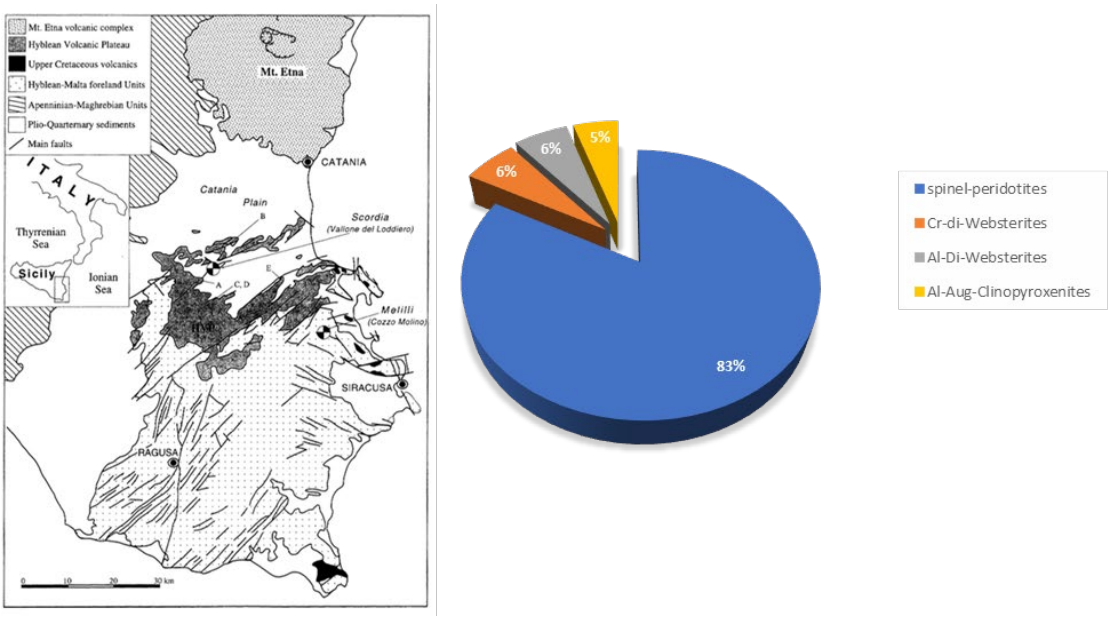


*Figure 3.2 - Xenolith data available for the region ( Bianchini et al., 2010; Ciliberto et al., 2009; Correale et al., 2012; Scribano et al., 2009; Tonarini et al., 1996).*

According to the petrographical and geochemical investigations of Tonarini 1996, Manuella 2013, Sapienza and Scribano 2000, Bianchini 2010, the Hyblean xenoliths represent the lithospheric mantle composition below the south-eastern sector of Sicily. The composition consists of anhydrous spinel-facies peridotites and subordinate pyroxenites/websterites (Sapienza and Scribano 2000). In detail, the Hyblean xenoliths are mainly represented by spinel-harzburgites (Punturo et al., 2000), in which olivine has a Mg# [$Mg/(Mg + Fe^{2+}$ )] ratio of 0.91 ± 0.01 on average, with NiO = 0.2–0.5 wt.%; orthopyroxene shows a Mg# of 0.89 ± 0.02 on average, with CaO <0.9 wt.%; clinopyroxene (Cr-diopside) exhibits a narrow compositional range ($En_{52} Wo_{47} Fs_{1}$–$En_{50} Wo_{43} Fs_{7}$); spinel has a Cr# [Cr/(Cr + Al)] ratio corresponding to 0.27 ± 0.02 and a Mg# from 0.67 to 0.80, on average (e.g., Scribano et al., 2009).

Therefore, for the assessment of a mantle composition considering depth from 50 to 250 Km, the evaluation of the average mineralogical composition has been based on harzburgite (Hz) samples from Tonarini 1996, which shows the mineralogical percentage of constituents.

In detail, for this study, two different compositions have been taken into account:

- *model (a)* - Average modal composition of the whole Harzburgitc suite analyzed by Tonarini et al., 1996 (Ol 62,6%, Opx 31,6% Cpx 2,8%, Sp 3,6%, XFe 0.125);
- *model (b)* - Weighted average modal composition considering Tonarini et al., 1996 compositions of Hz, Wbs and cpx-te based on the percentage of ultramafic whole rock distribution from Scribano et al., 2009 (Ol 51,9%, Opx 28,0%, Cpx 16,9%, Sp 3,6%, XFe 0.126).

Comparing the MgO (wt.%) vs. $Al_2O_3$ (wt.%) ratio for peridotites from Hyblean xenolites suite and the average global composition, it shows a significant separation between peridotites from the Hyblean Plateau and modern spreading ocean centers (MAR and SWIR), with respect to North Africa peridotites which are akin to the composition of continental lithospheric mantle and primordial mantle (Figure 3.3). Therefore, Hyblean peridotites are akin to abyssal peridotites rather than to continental mantle rocks from North Africa, in agreement with the model proposed by Scribano et al., 2006 of a fossil oceanic lithosphere.

(a) (b)

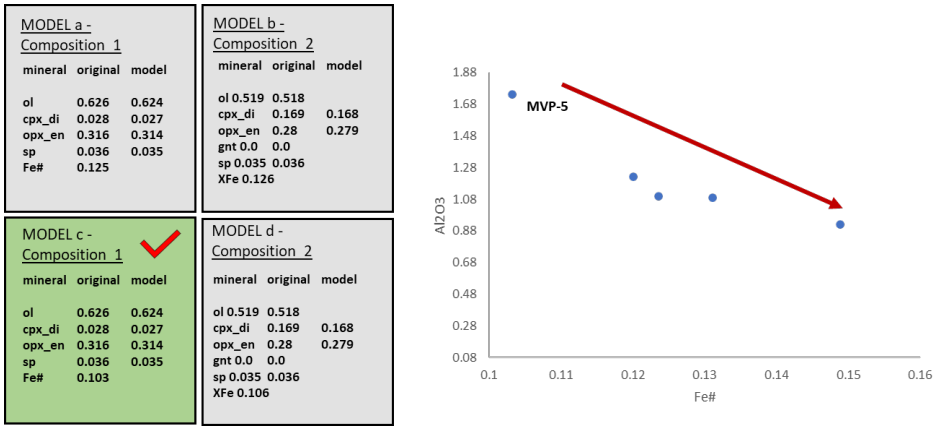


*Figure 3.3 - a) Average mineralogical composition used for the Vs conversion; b) depleted samples (tonarini, 1996)*

The iron content of compositions a) and b), respectively 0.125 and 0.126, seems to be incompatible with the average global values, probably due to the metasomatic petrogenesis of Hyblean harzburgites which took place in the shallowest portion of the lithospheric mantle. Since a decrease in the Iron content has a larger effect on the S wave conversion methods (Jordan, 1979; Goes, 2000), it is necessary to take into account a lower iron number which represents an average upper mantle composition. In this regard, the most spinel-rich sample from Tonarini 1996 (MVP-5, Figure 3.3b) has been taken into account, since it shows high contents of $Al_2O_3$ and high Mg# that reflect a low degree of depletion and represents the most primitive composition (associated to the depth investigated by the tomography). Therefore, recalculating the iron number, values of 0.103 for model (a) and of 0.106 for model (b) two different configurations have been obtained (respectively model (c) and model (d) Figure 3.3a).

*Table 3.2- Average major element concentrations (wt.%) for the lithospheric mantle used for the Vs conversion.*

| Major element | wt% |
|---|---|
| $SiO_2$ | 45.1 |
| $Al_2O_3$ | 4.6 |
| FeO | 7.6 |
| MgO | 38.1 |
| CaO | 3.1 |
| $Na_2O$ | 0.4 |

Thus, according to the more depleted nature of the upper mantle of the Sicilian domain (Tonarini et al., 1996; Scribano et al., 2009), an average pyrolytic composition has been assumed (Table 3.2). Along with the regularly spaced grid of the "CSEM Europe and "EU60" S-wave velocity model, the resulting voxel cube (x, y, z, computed density) loaded into the IGMAS+ model holds pointwise mantle density (and temperature) information laterally distributed every half a geographical degree (~43-55 km) and vertically spaced at 10 km distances. Figure 3.4 and Figure 3.5 show respectively the temperature and density values derived from the conversion of CSEM and EU 50-250 km b.s.l tomographies.

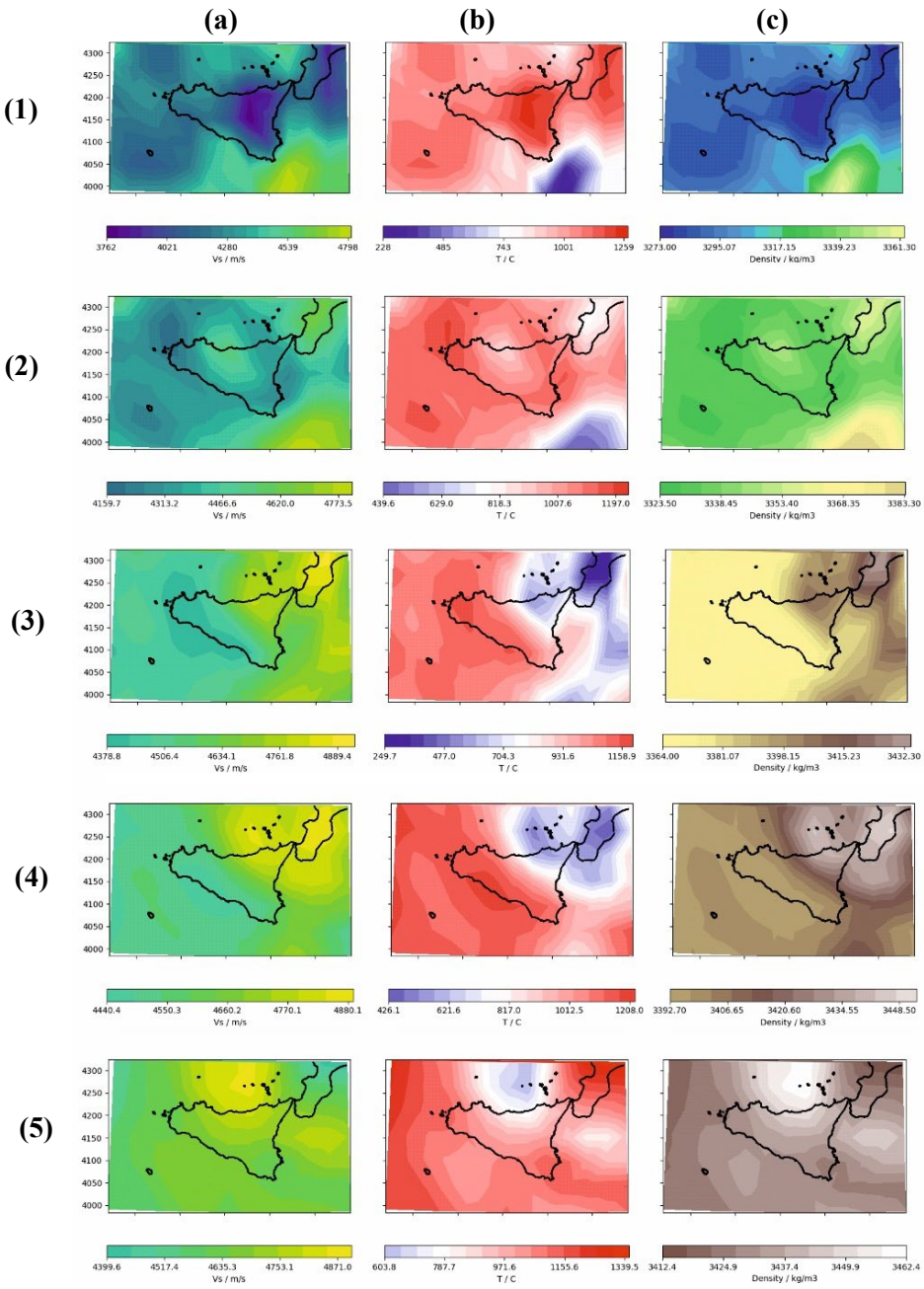


*Figure 3.4 –Temperature (b) and density (c) maps computed from the conversion of Vs (a) (CSEM mantle Tomography); slices from 50 Km (1) to 250 Km (5) depth b.s.l. (steps: 50 Km).*

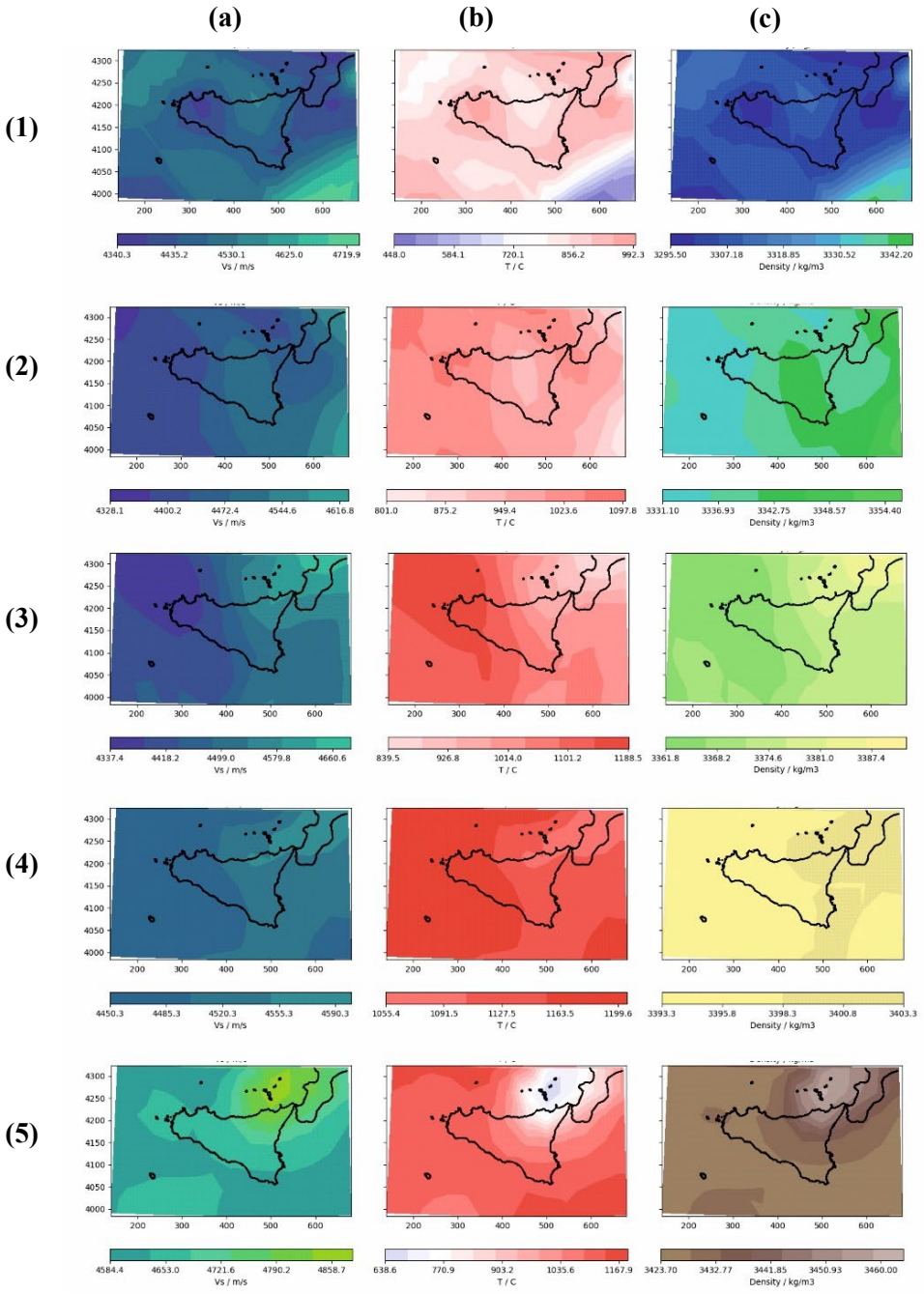


*Figure 3.5– Temperature (b) and density (c) maps computed from the conversion of Vs (a) (EU mantle Tomography); slices from 50 Km (1) to 250 Km (5) depth b.s.l. (steps: 50 Km).*

## 3.2 Thermal modelling

Concerning the regional area, direct constraints on the temperature or heat flow conditions at the Moho, however, are lacking. Therefore, a sensitivity analysis has been carried out by running models that differ in terms of the imposed lower boundary condition. In the first model (hereafter referred to as *Crustal Model*), the geological model has been cut along the Moho boundary (Figure 2.3f), where a constant heat flow (30 mW/m²) was assumed and considered as an average input value representative for the whole study area. In the second set of models, the effects of variable heat input from the underlying lithospheric mantle have been quantified. Therefore, the base of the model has been extended down to 50 km (b.s.l.) along which we assigned a variable temperature distribution derived from the conversion of the S-waves tomography models, namely CSEM (Fichtner et al., 2018, Figure 3.4) (*CSEM Mantle Model* hereafter) and EU60 (Zhu et al., 2015) (*EU60 Mantle* Model hereafter Figure 3.5). Figure 3.6 illustrates the temperature distribution obtained from the two input tomographies. The temperatures derived from the conversion based on the CSEM tomography model vary between 400°C beneath the Ionian Sea and higher than 1500°C beneath the Etna domain. From the significant positive thermal anomaly larger than 1500°C beneath the eastern sector (observed down to 80 km depth b.s.l., Figure 3.4), temperatures decrease towards the south-eastern and northern domains (temperatures below 1000°C) and towards the western side with a homogeneous temperature distribution at around 1400°C (Figure 3.6a). EU60 displays a similar trend in the regional thermal characteristics, though with lower magnitudes in the westernmost domains of the study area (Figure 3.6b). The temperature distribution at 50 km depth obtained from the conversion of the shear wave velocities from the EU60 tomography shows an increasing trend from east to west with the lowest temperatures (400°C-1000°C) in the south-eastern portion and the north-eastern domain, whereas higher temperatures (up to 1400°C) in the westernmost portion. The presence of a heterogeneous lithological configuration beneath Sicily (Table 3.1) results in a significant variability in rock thermal properties, namely thermal conductivity and radiogenic heat production as required for the thermal modelling (Table 3.3). The thermal conductivity was considered as an isotropic tensor due to the lack of data to constrain any preferential direction of heat conduction at the scale of our modelling. For the same reason, any functional behaviour of this parameter with respect to depth and/or temperature has also been neglected. Given the regional scale of our study, a constant

parameterization of each geological layer of the model has been adopted, chosen according to their dominant lithologies, which are obtained based on published studies (Table 3.3). The choice of a constant parameterization stems from the lithostratigraphic complexity of the Sicilian sedimentary and crustal rocks, which cannot be fully represented at the regional scale of the modelling. Therefore, the resulting thermal property values listed in Table 3.3 should be considered as reflecting effective properties for the different lithologies considered in the model. The modelling approach has relied upon data collected during recent years through the analysis of outcropping successions in Sicily and the interpretation of hydrocarbon exploration well logs augmented by laboratory investigations to acquire a range of variations for the thermal properties of each sequence (e.g. Abate et al., 2014; Galgaro et al., 2012; Gola et al., 2013; Di Sipio et al., 2013).

*Table 3.3 - Thermal modelling parameters used for the workflow.*

| | **Final matrix Thermal conductivity (W/mK)** | **Thermal conductivity range tested (W/mK)** | **Ref.** | **Final Radiogenic H. production ($W/m^3$)** | **Radiogenic heat production range tested ($W/m^3$)** | **Ref.** |
|---|---|---|---|---|---|---|
| Volcanic Bodies | 2.0 | 1.9-2.5 | (Clauser and Huenges, 1995) | 6.80e-7 | 6.80e-7 | (Vilà et al., 2010) |
| Metamorphic Unit | 2.9 | 1.9-2.9 | (R Cataldi et al., 1995; Sipio et al., 2013; Trumpy and Manzella, 2017) | 6.80e-7 | 6.80e-7 | (Vilà et al., 2010) |
| Paleogene-Quaternary deformed deposits | 2.9 | 1.5-3.0 | (Sipio et al., 2013) | 6.80e-7 | 6.80e-7 | (Caracausi et al., 2005) |
| Meso-Cenozoic Units | 3.8 | 2.5-3.9 | (Montanari et al., 2017a; Trumpy and Manzella, 2017) | 5.00e-7 | 5.00e-7– 1.0e-6 | (Caracausi et al., 2005) |
| Shallow Crystalline Basement Rocks | 3.0 | 1.9-3.5 | (Clauser and Huenges, 1995; Vilà et al., 2010) | 1.00e-6 | 1.00e-7– 1.00e-6 | (Vilà et al., 2010; Waples, 2001) |
| Deeper crust | 3.5 | 2.7-3.5 | (Clauser and Huenges, 1995; Vilà et al., 2010) | 1.00e-6 | 1.00e-7– 1.00e-6 | (Vilà et al., 2010; Waples, 2001) |

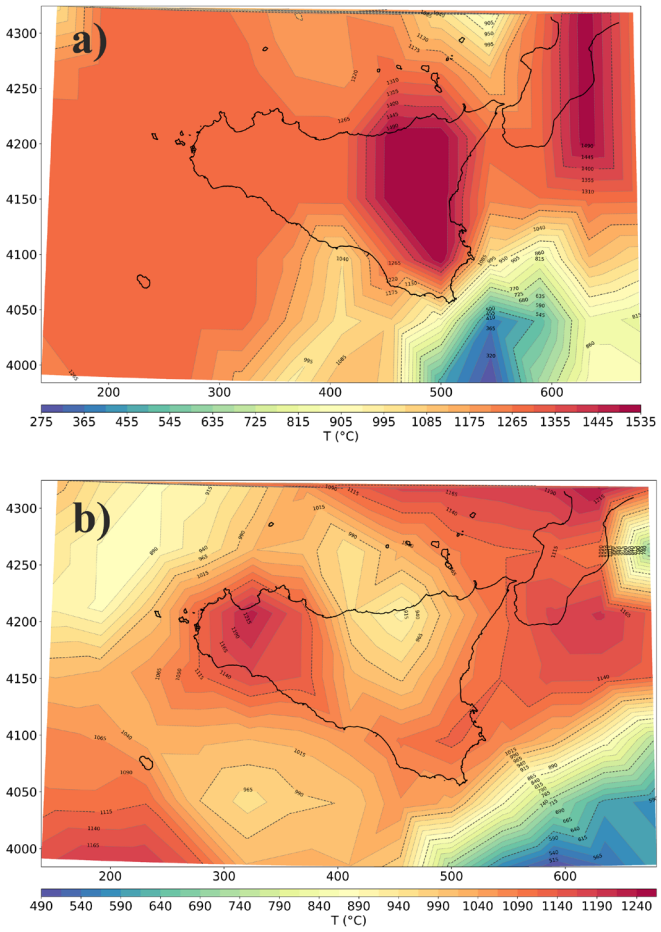


*Figure 3.6 – Temperature at depth of 50 km (below mean sea level) as derived from (a) the "CSEM Europe" mantle tomographic model (Fichtner et al., 2018) and (b) the "EU60" tomographic model (Zhu et al., 2015), both being imposed as alternative lower boundary conditions for the thermal modelling process. Note the different scales of the temperature intervals shown in the maps. Coordinates are in EPSG:32633 – WGS84/UTM zone 33N.*

### *3.2.1 Crustal Model.*

The main feature of this model is the presence of a temperature anomaly beneath the central sector of the study area cutting through all investigated depth (Figure 3.7). We interpret this feature as a result of the Moho topology (used as lower boundary condition) and the superposed thermal blanketing effects from the thick Paleogene-Quaternary deformed deposits (Figure 2.3c). Indeed, the positive thermal anomaly is located beneath the Caltanissetta basin, whereas colder conditions are modelled for the Hyblean carbonatic foreland areas and the north-western carbonatic domains, in the Sicily Channel domain and in the north-eastern sectors of the Metamorphic Complex. Spatial variations in the shallow thermal field, at depths of 1 and 2 km b.g.l., correlate spatially with the tectonic zonation of the area, with high temperatures being distributed according to the main tectonic structures, such as the Maltese-Hyblean escarpment. We notice that these

effects are no longer visible at depths deeper than 10 km. At such depth levels, variations in the thermal field are smoother, as they are caused by a constant heat input imposed along the Moho, thereby principally reflecting the topology of this boundary (Figure 2.3f).

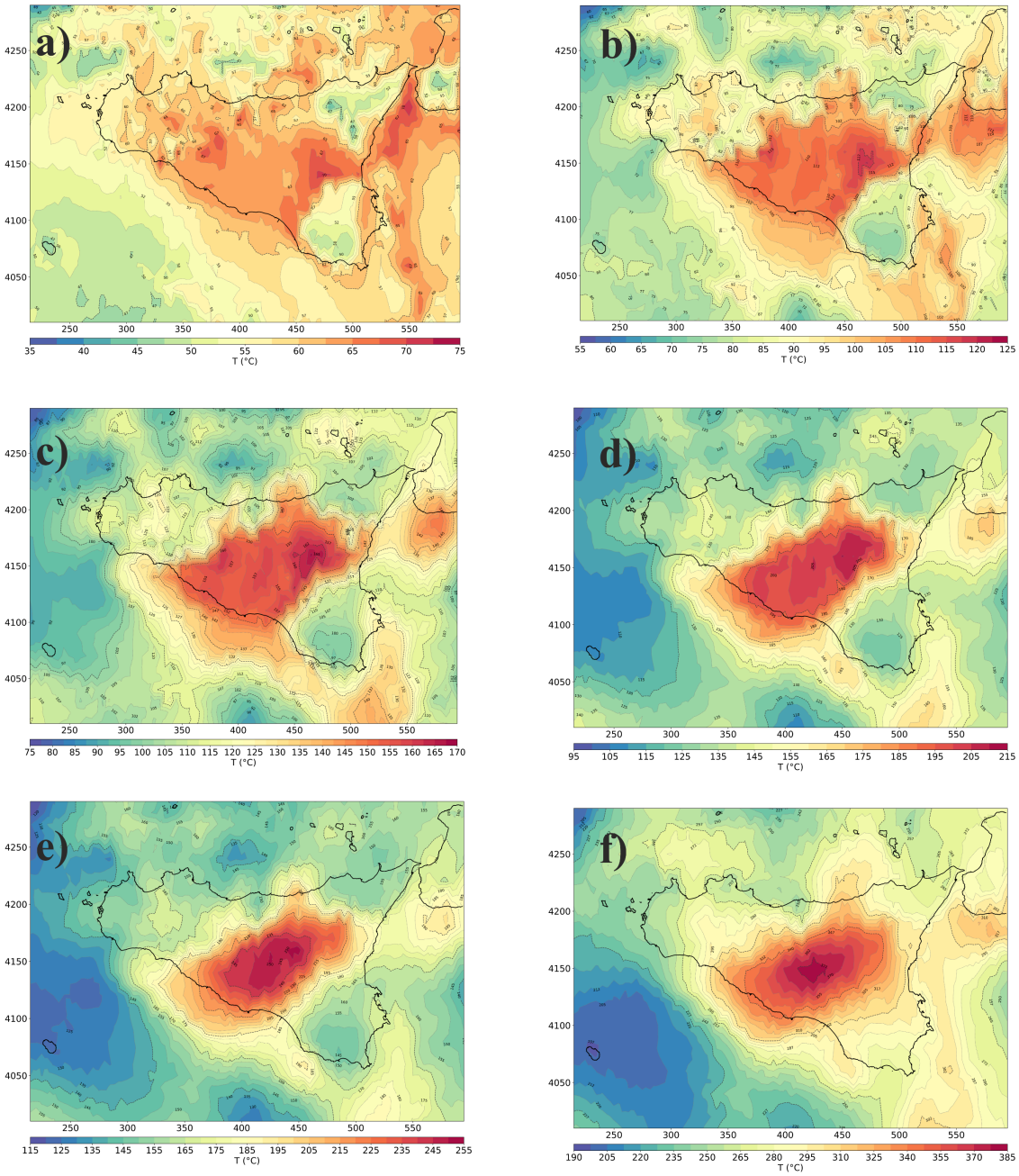


*Figure 3.7- Temperature maps at different selected depths below ground level (a: 1 km, b: 2 km, c: 3 km, d: 4 km, e: 5 km, and f: 10 km) derived from the Crustal Model, assuming a constant heat flow of 30 mW/m2 at the crust-mantle boundary. Coordinates are in EPSG:32633 – WGS84/UTM zone 33N.*

### *3.2.2 CSEM Mantle Model.*

The CSEM Mantle Model thermal field (Figure3.9) portrays positive thermal anomalies beneath local domains that are structurally linked to the presence of volcanic areas, such as the Aeolian Island Arc, Mt. Etna area and Pantelleria island. In detail, temperatures at 2 km b.g.l. are higher in these volcanic contexts (temperature >70°C) and noticed that an overall decrease in temperature beneath the Hyblean foreland and the carbonate north-western domain, where temperature are within a range of 50-70°C. The spatial distribution of these positive thermal anomalies at depths greater than 5 km shifts towards the eastern area, resulting in a thermal field significantly influenced by the thermal input from the mantle (Figure 3.6a).

### *3.2.3 EU60 Mantle Model.*

The computed thermal field distribution trend (Figure 3.9) is similar to the previous model (CSEM Mantle Model in Figure 3.8). In the shallower sedimentary parts (1-5 km depth b.g.l.), the thermal field is considerably influenced by the top boundary condition (topography) and the imposed surface temperature. This results in lower temperatures at 1 km b.g.l. (Figure 3.9). In fact, temperature not exceeding 40°C in the foreland domain and the north-eastern sector has been observed, while the highest temperatures (>50°C) are found in the active volcanic areas such as beneath the Aeolian Island Arc, Mt. Etna volcanic contexts as well as in the Sicily Channel area. In general, lowest temperatures are found within the Ionian area to south-east. Considering the significant thickness of sedimentary material, the Caltanissetta basin and the Gela Foredeep are characterized by temperatures reaching 150°C in their shallow portions (down to 5 km depth b.g.l.). The crustal thermal field shows a positive thermal anomaly in the depth range of 5-10 km b.g.l. concentrated in the western portions of the island and it seems to be correlates with the input of thermal energy from the lower boundary condition of the lithospheric mantle (Temperature from EU60 Tomography inversion Figure 3.6b). In addition, the presence of an additional positive thermal anomaly beneath the Ionian basin has been recognized. A similar trend is also visible at greater depths; in fact, between 10 and 30 km b.g.l., the thermal field seems to be no longer affected by the imposed upper boundary condition. In this case, positive thermal anomalies are localized in the western area of the island and the Ionian domain, as well the Hyblean foreland.

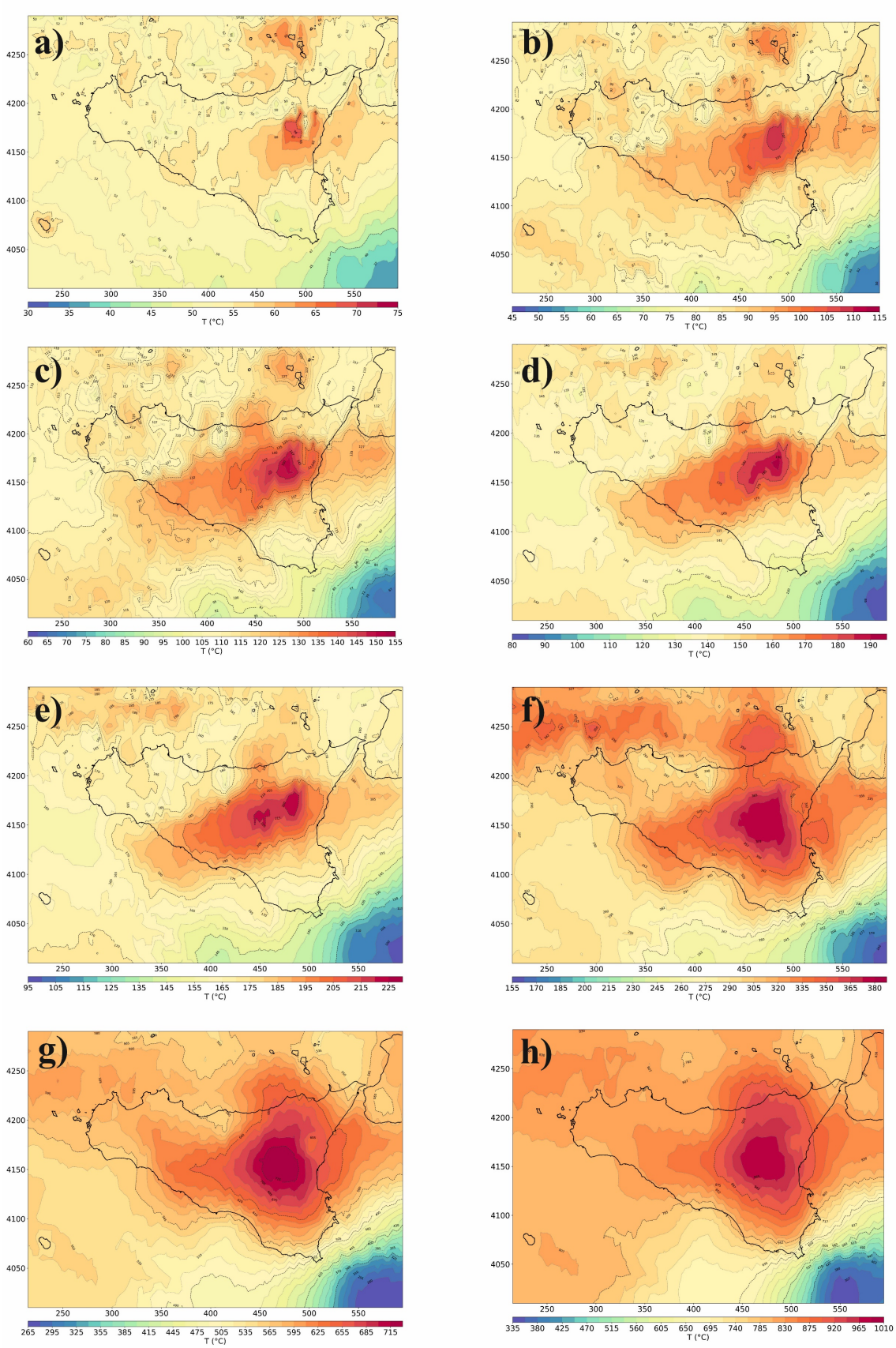


*Figure 3.8- Temperature maps through the thermal model implementing the mantle temperatures derived from the CSEM Mantle Model at depths below ground level of a: 1 km, b: 2 km, c: 3 km, d: 4 km, e: 5 km, f: 10 km, g: 20 km, and h: 30 km. Coordinates are in EPSG:32633 – WGS84/UTM zone 33N.*

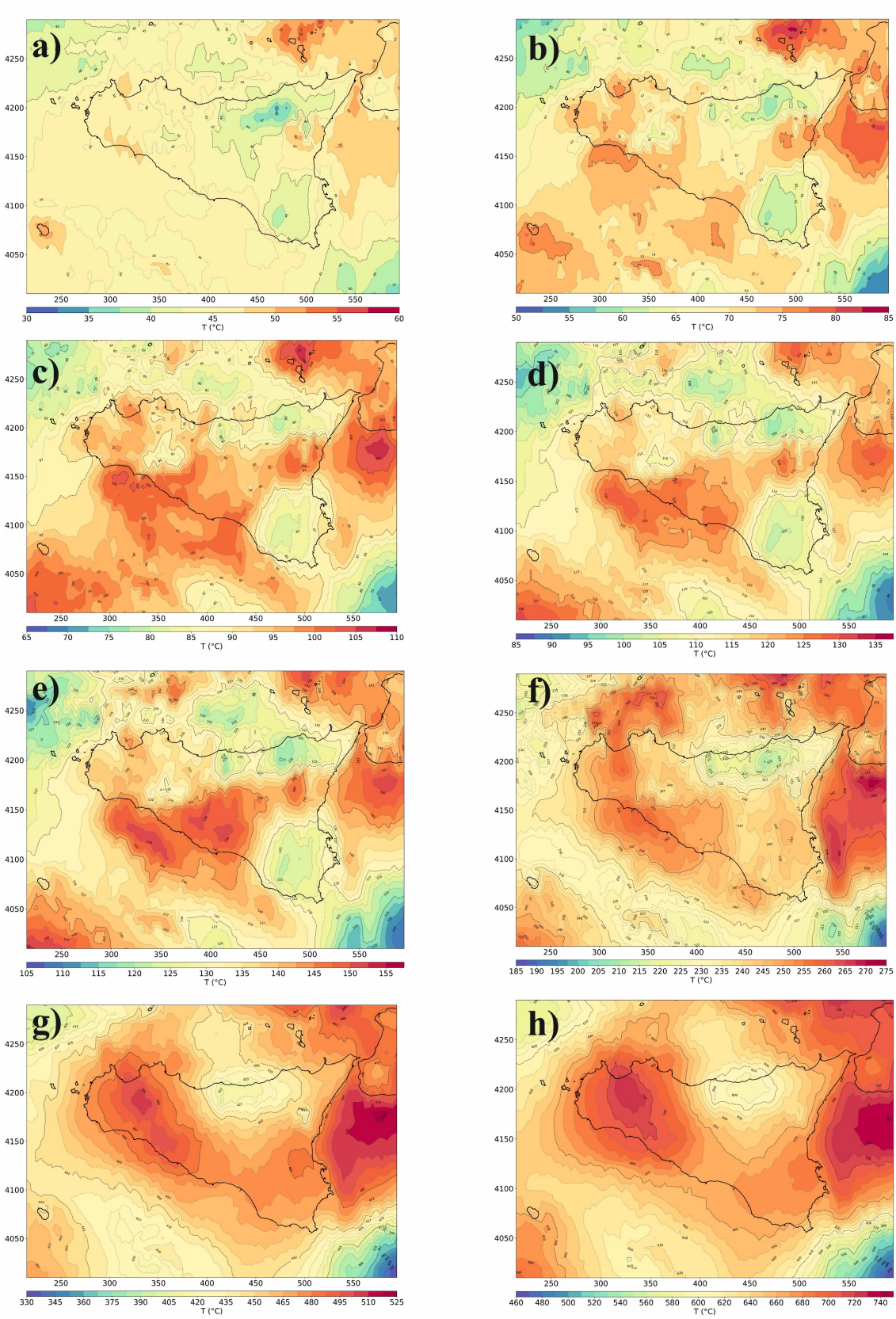


*Figure 3.9 - Temperature maps through the thermal model implementing the mantle temperatures derived from the EU60 Mantle Model at depths below ground level a: 1 km, b: 2 km, c: 3 km, d: 4 km, e: 5 km, f: 10 km, g: 20 km, and h: 30 km. Coordinates are in EPSG:32633 – WGS84/UTM zone 33N.*

## 3.3 Calibration against shallow temperature measurements (1-7 km depth b.g.l)

All different model realizations provide a coherent picture of the crustal thermal configuration in terms of its regional trends, which are controlled by resolved variations in the main structural units. However, variations in thermal rock properties result in local differences in the obtained temperature magnitudes at shallow, sedimentary depth levels. The regional scale of the model hinders to resolve the details of local lithostratigraphic variations mapped for the Sicilian sedimentary sequences. Although these local structural features do not affect to a first order the regional thermal configuration, it is likely that they exert control on a more local scale, that is the scale of direct temperature measurements. A model calibration is provided here by comparing the extrapolated data from each model realization against a dataset of measured temperatures available from the Italian National Geothermal Database (Cataldi et al., 1995; Trumpy and Manzella, 2017). The public dataset for Sicily consists of 1991 temperature data obtained from 361 wells drilled from the surface down to 6 km b.g.l. [measurements and bottom hole temperature corrected using the Squarci-Taffi empirical method (Della Vedova et al., 2001), where temperatures are extrapolated with a homogeneous gradient]. In addition to temperature data, other parameters were analysed including average gradient, calculated heat flux, main observed mineralization, permeability, and lithostratigraphic relationships. Such a data-oriented calibration introduces a source of epistemic bias due to an uneven distribution of available measurements and a lack of resolution of the local stratigraphy (Degen et al., 2021). Indeed, the aim is to attain the set of properties within the limits of the structural resolution of the input geological model that provides the best fit to the available measurements in order to derive implications for the shallow geothermal potential of the study area. Hence, to examine the local thermal configuration, the study area has been subdivided into three sub-domains of interest, each chosen according to a related tectonic origin: 1) the Hyblean Foreland; 2) the north-eastern domain (including the Mt. Etna area and the Aeolian Island Arc); 3) the western orogenic domain (including the Sicily Channel and the Pantelleria area) (Figure 3.10). In addition, the Root Mean Square Error (in °C) has been computed for each model as a function of depth to evaluate the suitability of the obtained results. Figures 3.12 to 3.15 display the temperature correlations for the Crustal Model (Figure 3.11), the CESM Mantle Model (Figure 3.12 and Figure 3.13) and the EU60 Mantle Model (Figure 3.14).

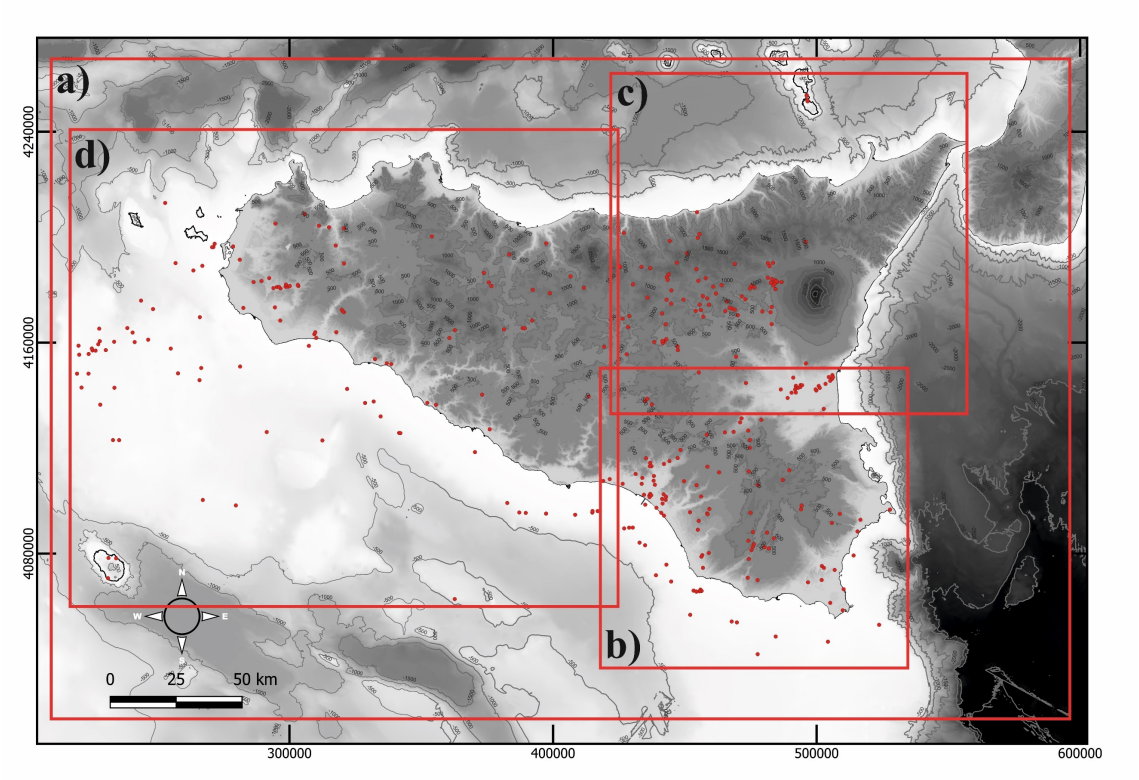


*Figure 3.10 - Dataset of wellbore temperatures from the updated Italian National Geothermal Database used for the comparison (red dots) and subdomain partitioning of the region. Red boxes display the subdomains used for the comparison between modelled and measured temperatures. In detail: a) Entire investigated area; b) Hyblean foreland domain; c) north-eastern domain; d) western domain. The isolines display the topography (DEM 2m) and Bathimetry (Emodnet project).*

The modelled temperature derived from the Crustal Model (Figure 3.11) shows a general good fit with the available measurements, with a minor shift in the correlation between the modelling results and the observations. As a common feature for all sub-domains, the modelled temperatures area slightly underestimate compared to the measurements with a maximum error of about 40°C at depths between 5 and 6 km. The underestimating trend of the observations could be related to the chosen boundary condition consisting of a constant heat flow along the base of the model. The imposed 30 mW/m² value has been considered as an average along the entire lower boundary of the model, so it likely provides a conservative estimate for the actual crustal heat flow beneath specific domains (e.g., volcanic areas). In these contexts, higher crustal heat flow conditions would rather expect, which would lead to higher temperatures in better agreement with the measurements. Concerning the CSEM Mantle Model (Figure 3.12), a systematic overestimation of the actual thermal gradient has been observed on a regional context with a maximum RMSE of 50-60°C at depths between 3 and 6 km. From the examination of the three sub-domains, this imbalance is mainly limited to the north-eastern sector,

where the misfit is significantly higher than in the Hyblean foreland and the western domain. This observation is an indication of an erroneous mantle contribution to the total heat budget within the north-eastern domain, which explains the overall overestimation of the resulting thermal gradient. In fact, from the analysis of the temperature map derived from the tomography conversion used as the lower boundary condition applied to the model, the presence of temperatures higher than 1500°C has been noted in relation of a local low-velocity anomaly in the tomography beneath the north-eastern sector (Figure 3.4c). An alternative interpretation for these anomalously low seismic velocities might be related to the presence of melts in the area (related to the Mt. Etna volcano and to the active subduction process), which we did not consider during the first conversion. For this reason, an additional simulation has been run. The resulting temperature from the first simulation has been corrected in the second run by eliminating the positive thermal anomalies accounting for the potential presence of melts beneath these domains. Thus, the resulting model provides an improved fit with the data (Figure 3.13).

Concerning the last analysed model, named EU60 Mantle Model (Figure 3.14), it shows a clear correlation for both the regional and local domains with a maximum error of around 25°C (in the Hyblean foreland; Figure 15b), resulting in the model being the best-fit.

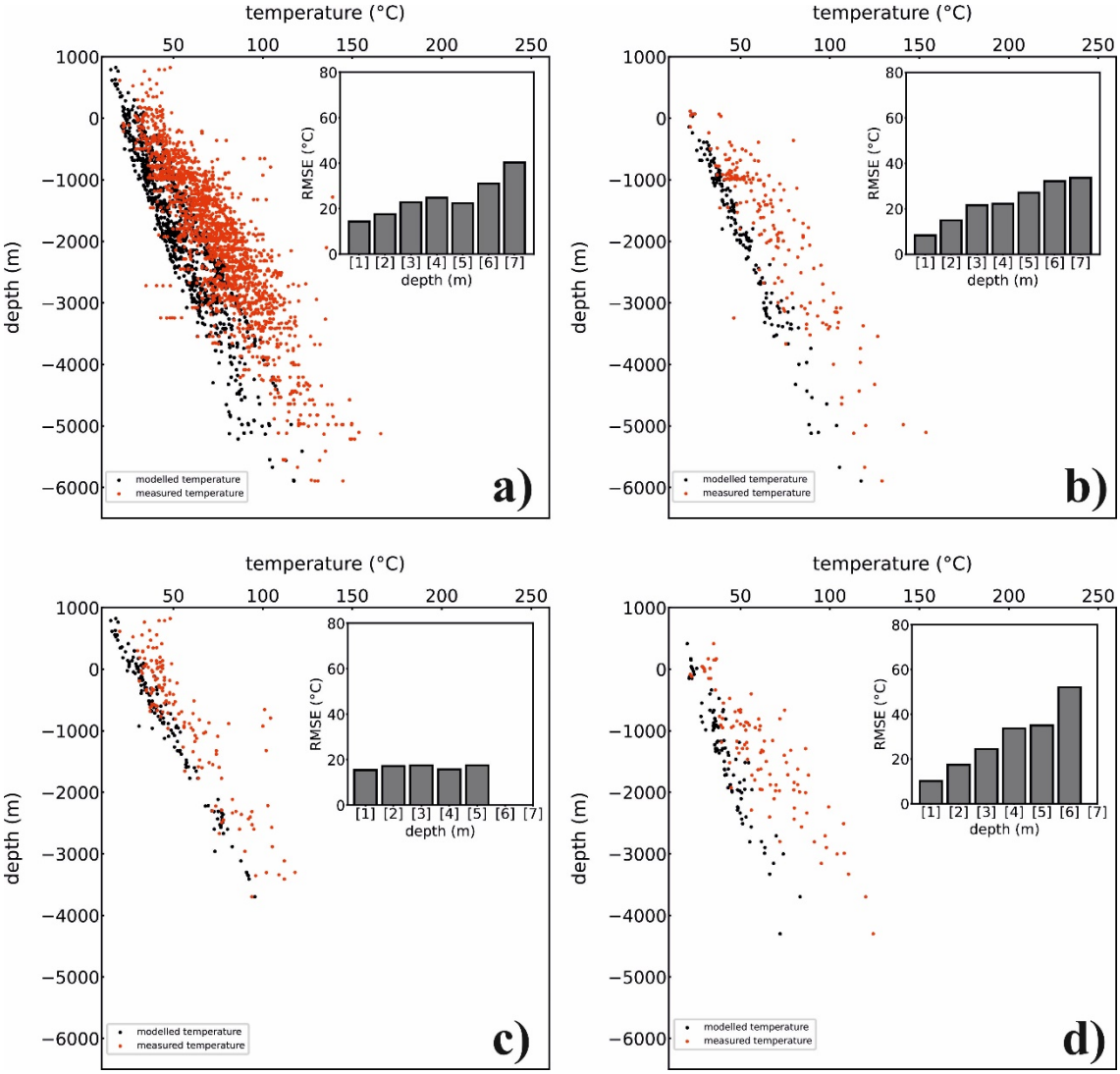


*Figure 3.11 - Temperatures modelled (black points) vs. measured (red points) for the Crustal Model. (a) Comparison between modelling results and available measurements for the entire domain. b) Model validation for the region of the Hyblean promontory; c) Model validation for the north-eastern domain; d) Model validation for the Western domain. The temperature comparisons are associated with the graph showing the Root Mean Square Error expressed in (°C) for different depth ranges expressed in meter (1 = [1000 - 0]; 2 = [0 - -1000]; 3 = [-1000 - - 2000]; 4 = [-2000 - - 3000]; 5 = [-3000 - -4000]; 6 = [-4000 - -5000]; 7 = [-5000 - -6000].*

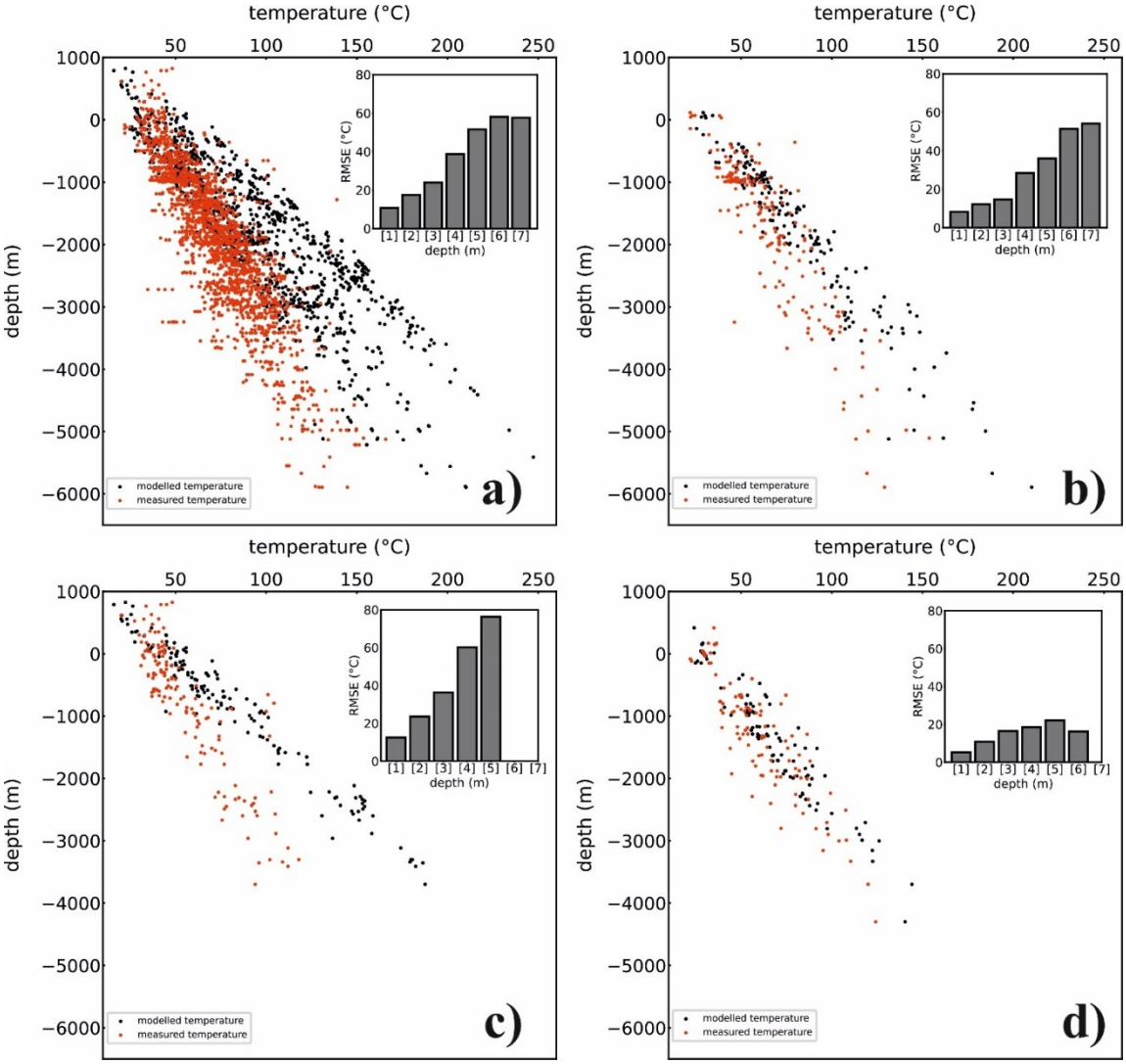


*Figure 3.12- Temperature modeled (black points) vs. measured (red points) for the CESM Mantle Model. a) Comparison between modelling results and available measurements for the entire domain; b) Model validation for the region of the Hyblean promontory; c) Model validation for the north-eastern domain; d) Model validation for the Western domain. The temperature comparisons are associated with the graph showing the Root Mean Square Error expressed in (°C) for different depth ranges expressed in meter (1 = [1000 - 0]; 2 = [0 - -1000]; 3 = [-1000 - - 2000]; 4 = [-2000 - -3000]; 5 = [-3000 - -4000]; 6 = [-4000 - -5000]; 7 = [-5000 - -6000].*

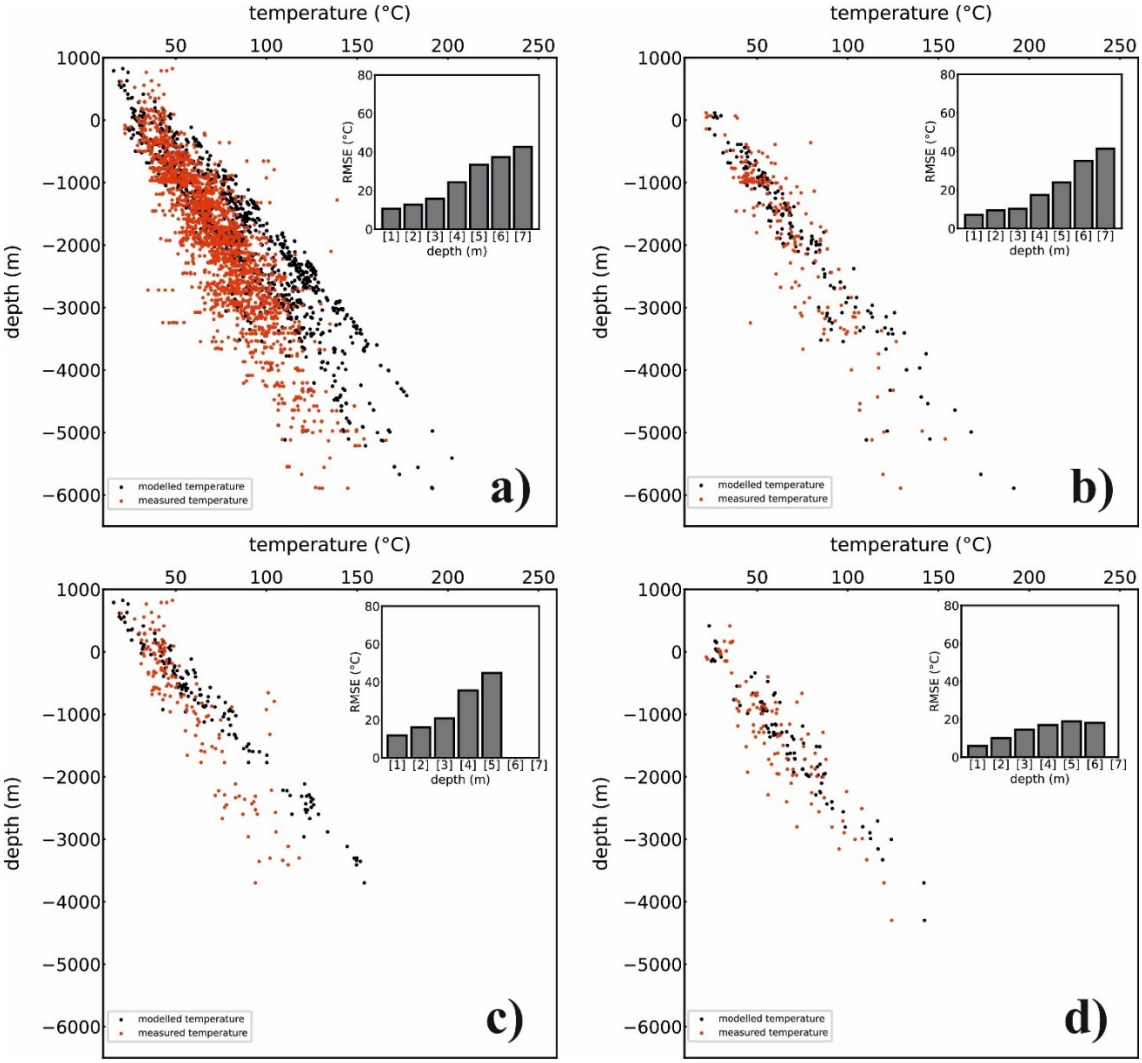


*Figure 3.13 - Temperature modeled (black points) vs. measured (red points) for the alternative interpretation of the CESM Mantle Model. a) Comparison between modelling results and available measurements for the entire domain; b) Model validation for the region of the Hyblean promontory; c) Model validation for the north-eastern domain; d) Model validation for the Western domain. The temperature comparisons are associated with the graph showing the Root Mean Square Error expressed in (°C) for different depth ranges expressed in meter (1 = [1000 - 0]; 2 = [0 - -1000]; 3 = [-1000 - - 2000]; 4 = [-2000 - -3000]; 5 = [-3000 - -4000]; 6 = [-4000 - -5000]; 7 = [-5000 - -6000].*

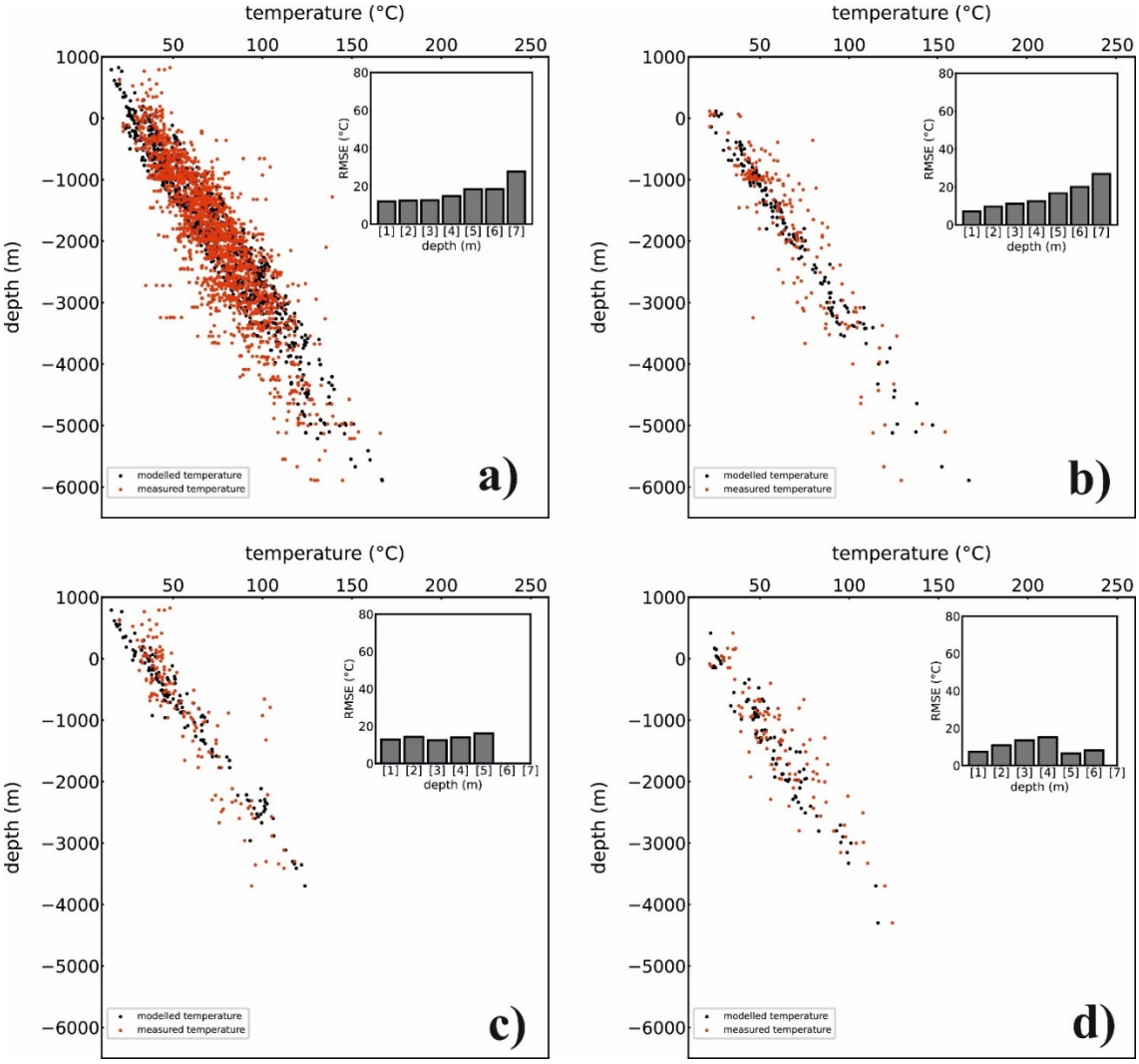


*Figure 3.14 - Temperature modeled (black points) vs. measured (red points) for the EU60 Mantle Model. (a) Comparison between modelling results and available measurements for the entire domain; b) Model validation for the region of the Hyblean promontory; c) Model validation for the north-eastern domain; d) Model validation for the Western domain. The temperature comparisons are associated with the graph showing the Root Mean Square Error expressed in (°C) for different depth ranges expressed in meter (1 = [1000 - 0]; 2 = [0 - -1000]; 3 = [-1000 - - 2000]; 4 = [-2000 - -3000]; 5 = [-3000 - -4000]; 6 = [-4000 - -5000]; 7 = [-5000 - -6000].*

## 3.4 Regional Geodynamic implications

The heat distribution in the shallow crust is principally controlled by the insulating properties of the low conductive sedimentary rocks at the top of the stratigraphic successions. This blanketing effect is especially relevant beneath areas covered by the thick succession of the Paleogene-Quaternary deformed deposits of the orogenic units (Gela Nappe and Caltanissetta Basin), located above a thickened highly radiogenic crust. There, the temperature gradient is higher than in the other domains of the study region. On the other hand, high altitude domains (i.e., the Peloritani Mountains) bear a more conductive crystalline basement that causes efficient heat transfer, finally resulting into lower shallow temperatures.

The *Crustal Model* with a homogeneous heat flow fixed at 30 mW/m$^2$ along its base allows to determine the effects of the main crustal structures found in the area on the regional thermal field. The highest temperatures in the first 3 km b.g.l. are localized along structures such as the Hyblean-Maltese escarpment, the overlapping front of the orogenic chain and the subduction front of the Calabrian succession (Figure 3.7). The temperature misfit beneath the subdomains of the Hyblean promontory and the western portions of the investigated area (Figure 3.11) is indicative either of the relevance of including a spatial variability in the thermal energy input, or of local conditions where the heat flow at the Moho is likely higher than the average value of 30 mW/m$^2$ imposed in this model (Figure 3.15b). With the aim of quantify such variability in the crustal heat flow two additional sets of models that also integrate a portion of the lithospheric mantle has been carried out. By means of these lithospheric-scale models the contribution of the mantle to the crustal thermal field has been computed and therefore further investigated the deeper thermal configuration in the area. Concerning the best-fit lithospheric model, the *EU60 Mantle Model* (Figure 3.8), it displays pronounced positive thermal anomalies along the collision zone (overlapping front), highlighting a clear distinction between the different crustal domains. The spatial extent of the thermal anomaly is most prominent between 3 to 6 km depth and is indicative of the presence of a geothermal reservoir beneath the central domain, which spatially correlates to the Carbonate units. In addition, the correlation found between these thermal anomalies and the thickness of the crystalline basement point to an elevated radiogenic heat production within this layer as a result of the structural process. The lack of thick clastic sedimentary covers above the Mesozoic carbonate domains of the Hyblean foreland and western areas manifests in a lower

thermal gradient, which is found down to 5 km in depth. The increase in the thermal gradient below 5 km can be over correlated to an elevated radiogenic heat production from a relatively thick crystalline basement. The deeper portions of the thermal model (below 10 km of depth) are mainly influenced by the basal input temperatures and the radiogenic heat production contribution.

Regarding the lower boundary conditions applied to the extended lithospheric models (CSEM Mantle Model and EU60 Mantle model), the conversion obtained based on the CSEM and EU60 tomography models provides several interesting aspects, among which is the presence of a clear distinction between the temperature distribution at 50 km for both conversions (Figure 3.6). There is a significant difference in the resulting temperature maps derived from the two tomographies, with the CSEM showcasing a regional positive thermal anomaly in the eastern area (Figure 3.6a), while highest temperatures are found in the western domain in the EU60 model (Figure 3.6b). Maximum temperature derived from the conversion of the shear waves from CSEM tomography are up to 1580°C at 50 km, which extends down to 80 km depth in the eastern sector. By considering the CSEM temperature for the thermal modelling, an overall misfit (overestimation) against measured temperatures has been observed (Figure 3.12). This could be related to the presence of bodies characterized by a different rheological behavior, which have not been considered in the first conversion. Petrological and geochemical investigations (Viccaro and Cristofolini, 2008; Viccaro et al., 2011; Viccaro and Zuccarello, 2017) suggest the presence of a rather shallow partially melted zone below the Mt. Etna area extending between 50 and 80 km of depth, which can be referred to as the feeding source of Etnean magmas. By correcting the temperature from the CESM model because of the presence of melts at 50 km, it was possible to improve the overall correlation between the modelled versus observed temperature and the average RMSE for the eastern domain (Figure 3.13c). An additional observation is that the presence of cold bodies beneath the north-eastern sector (temperature around 900-1000°C) in the CSEM tomography from 50 km to 250 km could be linked to the active subduction process occurring in the area recognized in literature (Scarfì et al., 2018; Calò et al., 2012). Interestingly, the thermal field derived from the CSEM model allows us to image the subducting Ionian slab and therefore to distinguish the surrounding mantle. The vertical temperature distribution displays low-temperature bodies (700°C < T <1000°C) from 50 to 250 km deep toward north-west. It is also possible to interpret the presence of a cold lithospheric mantle with temperatures between 400 and 600°C in the south-eastern

area as a robust characteristic in the CSEM tomography. Such a negative anomaly distribution could be related to a denser body, thereby suggesting the presence of an imbricated colder oceanic domain. The analysis conducted on the EU60 Mantle Model display a systematic bipartition of the thermal field between the eastern and western side at a depth of 50 km of the investigated domain. In this regard, temperatures reaching 900°C and heat fluxes of 80-90 mW/m$^2$ at the Moho (Figure 3.15a-b) illustrate that there is a significant correlation to the active volcanic areas. The thermal conditions, cause-effect of the different tectonic processes which have affected the study area, has been observed and illustrate a good correlation with the temperature and heat flux at moho depth for surroandings areas (i.e. the lithospheric north-thyrrenian modelling by Verdoya et al., 2005)

A further analysis of the distribution of the lithospheric thermal field allows us also to discriminate different active geodynamic contexts. Based on the work on mantle Helium fluxes (Caracausi et al., 2005) in the western portion of Sicily, we can structurally correlate both the high thermal gradient and the surface heat flux to the active rifting in the Sicily Channel (Della Vedova et al., 2001), thereby highlighting an important link of the lithosphere thermal field with mantle dynamics through deep-reaching inherited fault systems.

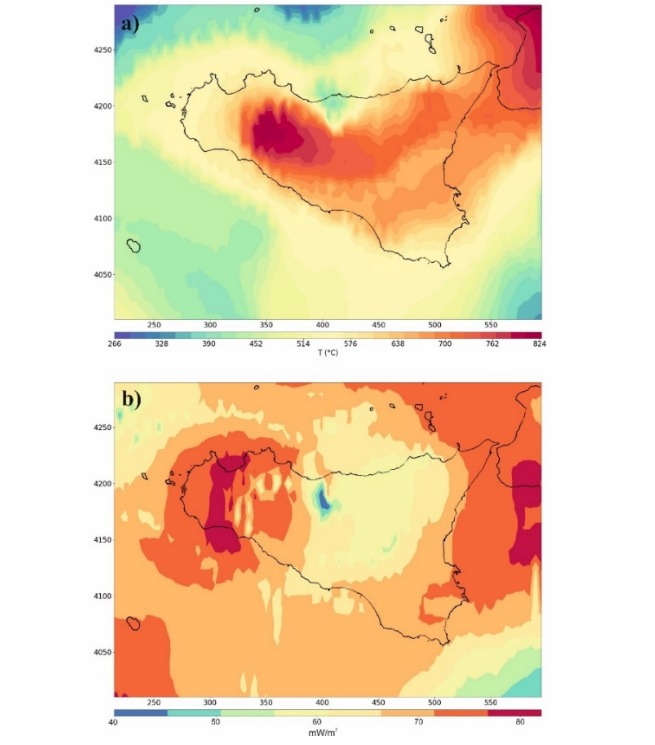


*Figure 3.15- Temperature (a) and Heat flow distribution (b) at Moho depth for the EU60 Mantle Model.*

## 3.5 Regional Geothermal implications

Sicily represents a very stimulating context for geothermal exploration, as it is characterized by the presence of a complex geodynamic setting with large lithological variability. Evidence of high heat flow and thermal gradients suggest huge unexplored potentials (Della Vedova et al., 2001; Montanari et al., 2015; 2017a; Abate et al., 2014; Santilano et al., 2016; Di Sipio et al., 2013; Gola et al., 2013; Trumpy et al., 2015). The 3D thermal models proposed in this research highlight some of the controlling factors of the shallow and deep thermal field distribution and put into evidence the low-to-moderate thermal regime of Sicily, emphasizing the large geothermal exploitation potential of the region. Concerning the shallow thermal field, it is mainly influenced by the boundary conditions assumed at the top of the model and by the distribution of its low conductive sedimentary covers (thickness and distribution). Maximum temperatures of 100°C at depth of 3 km along the foredeep and orogenic domains, with differences of about 30°C for the Carbonate units (70-75°C) to the north-west and the Metamorphic Complex, Peloritani and Nebrodi chains have been observed. Medium/High thermal gradients, ranging from 35°C/km to 45°C/km, especially within the Mesozoic carbonate units capable of guaranteeing excellent medium-enthalpy geothermal potential in some portions of the island, have been recognized at depths between 2000 and 4000 m below ground level. According to various studies on the geothermal potential in Sicily, it is possible to identify the location of the geothermal reservoir in the carbonate units. Therefore, they represent the most promising geothermal target to be investigated. At the top of the formation, temperatures of about 150°C are observed in the central area of the Caltanissetta basin, while the foreland areas show temperatures influenced by the surrounding surface conditions. Although this depth range is suitable for the exploitation of medium-enthalpy resources, it is worth noting that the whole regional territory at shallow depths (between 1000 and 2000 m) consists of temperatures suitable for the exploitation of low enthalpy geothermal energy (shallow district heating) or direct utilization of the heat (geothermal heat pump). The values of thermal conductivities applied to the main sedimentary rocks that provide the best fit with the available data (Table 3.3) are in the upper spectrum of the range tested, although they appear partly in contrast with the values derived through a sole gravity modelling approach (Table 3.1). This leads to a systematic overestimation of the measured shallow temperatures, which is independent of the lower boundary condition adopted. This finding points to two

processes that have not been considered so far but deserving further investigations: (1) the possible influence related to coupled heat and fluid transport; (2) the presence of an out of equilibrium system mainly related to a thermal signal from still ongoing deep magmatic processes. Nevertheless, these modelling outcomes reveal a high level of structuration of the resulting thermal field to local heterogeneities in the stratigraphic sequences in the subsurface of Sicily, which can be only approximated to a certain degree within a regional model. Further observations need therefore to be gathered on the sedimentary configuration to refine the starting model and to provide a better resolution on the generated thermal field at the local scale of the available measurements. In addition, the variations of the thermal field over time and the contribution of other influencing factors (e.g. fluids) must also be assessed in future studies. Indeed, Sicily is an area of active volcanism that may have not reached thermal equilibrium. We try to account for this partly by using the information on the deep mantle temperature given by shear wave velocity variations, that reflect the present-day deep thermal field independent of its state of equilibrium. Thus, the considered approximation is partly justified by the choice of the lower thermal boundary condition. To properly quantify related transient effects, dynamic models involving mantle convection as well are needed, but they go far beyond the scope of this study. Indeed, this research is intended as an incentive step, providing a base for other detailed future works. In addition, defined subdomains where these transients are relevant have been observed, and the results only provide an approximate solution to the present-day crustal thermal state. By relying on this data integration, the wide range of geological conditions making up the subsurface of Sicily has been discerned, also evaluating its impact on the resulting thermal resources at depth. The proposed 3D model of Sicily thereby allows to constrain areas with important geothermal anomalies, such as the volcanic zones of the Aeolian Island Arc, the Etnean area and the Sicily Channel Rift Zone, which are suitable areas for the exploitation of medium-to-high enthalpy resources. The model also suggests that low-enthalpy resources are available over extended areas of the region, especially in the carbonate layers. All these aspects make Sicily a potential pilot region for geothermal exploration and exploitation studies in southern Italy. Being the first effort in a complex geological setting, the research provides a solid workflow aimed at the quantification of the potential geothermal resources and their associated exploitation.

# 4 Chapter 4 – Thermal modelling: a case study from South-Eastern Sicily

Based on the thermal conditions extrapolated from the best-fit regional numerical model EU60, a local high-resolution area has been investigated. Following the same workflow described in chapter 2, in this case the high-resolution thermal modelling stage was based on a newly acquired gravimetric dataset, useful to validate the starting three-dimensional geological model. The results of the numerical simulations will be discussed in terms of computed temperature at different depths, systematically validating them with the available shallow temperature measurements. In addition, to evaluate the interaction between rheological, thermal, and tectonic conditions, the influence of the most important geological discontinuities has been analysed. In the end, the resultant best-fit thermal model has been used to investigate the possible exploitation of the low enthalpy geothermal potential throughout open-loop systems evaluating the local geothermal potential as a function of different geological settings.

In this section, therefore, the methods and the outputs of the thermal modelling as well as the exploitation analysis will be discussed.

## 4.1 Hyblean Foreland

### *4.1.1 Elements of geology*

The Hyblean foreland is located in the south-eastern area of Sicily, and it is part of an emerged portion of the Pelagian Block (Burollet P. F., et al., 1978). The region has an extension of about 4500 $Km^2$ and is considered a link between the orogenic domain of the Apennine-Maghrebid chain and the African plate (Lentini, et al., 1987; Lentini, Carbone, 2014). It is separated from the other orographic elements of Sicily by a depressed area along the north-west margin, known as “Avanfossa di Gela” (Lentini F. and Vezzani, 1978), which includes the “Piana di Vittoria” to the south-west and the “Piana di Catania” to the north-east (structural scheme in Figure 4.1).

The investigations define the Hyblean sector as a raised area characterized by a still debated continental crust (Henriquet, M., 2019), which tends to thin and flex towards the north-western portion forming the so-called “Avanfossa Gela-Catania”. Through the information obtained from oil exploration wells carried out in 1960 (Patacca E., et al.,

1979) the stratigraphic succession has been reconstructed. The entire geological setting is characterized by a predominantly carbonates succession consisting of basic carbonates layers (Cretaceous and the Quaternary age). In detail, they represent the roof of a Mesozoic sequence, extended from the Middle Triassic.

A scheme of the tectono-stratigraphic evolution of the Hyblean area envisages the coexistence of two distinct adjacent palaeogeographic domains:

- The Syracusan domain, emerging between Agnone and Syracuse and, to the south, along the Ionian coast up to Capo Passero, consisting of associations of shallow-sea lithofacies with a predominantly carbonate succession significantly influenced by outcropping and submarines (age <1.4 Ma) volcanic products (Schmincke, U. et al., 1997, Schiano, P., et al., 2001);
- The Ragusa domain, located in the central-western area of the Hyblean plateau, which is characterized by deep sea lithofacies with a succession of calcareous and marly-calcareous pelagic lithofacies. In addition, the presence of terrigenous deposits is related to the eastern domain dismantling (Carbone, S., et al., 1987). These characteristics indicate that the western Hyblaean successions were deposited within a deep basin, contiguous to the eastern shallow-sea areas, now separated by a different altitude (>100 meters).

According to a detailed stratigraphic reconstruction, the diversification of the two discussed domains (Syracuse and Ragusa Domains) can be associated with the upper Triassic (237-201 My). The distinction could be related to a rifting phase affecting the platform facies of the Gela unit (deepest recognized Formation), giving rise to the basin deposits (Streppenosa Formation). On the structural heights, however, a carbonate sedimentation of modest depth was established (Siracusa Formation). In the Jurassic-Cretaceous interval the Hyblean area was characterised by the sedimentation of a carbonate succession of a pelagic environment (Buccheri, Chiaramonte, Hybla and Amerillo Formations). In the Upper Cretaceous, the growth of submarine volcanic edifices, partly exposed in the area of Capo Passero, Syracuse and Augusta, profoundly modified the physiography of the sedimentation basins, determining the distinction between the two palaeogeographical domains (Lentini, et al., 1978). In the Lower Miocene, the boundary between the two domains was attested at the height of the Avola Mountains, where we recognise the lateral transition between the Climiti Mountains Formation, typical of the shallow-sea domain, and the Ragusa Formation, attributable to the deeper-sea basin. Finally, in the Lower Tortonian-Messinian period this limit,

corresponding to the lateral transition between the shallow-sea successions of the Palazzolo Formation and the Tellaro Basin Formation, has been located along the valley of the Tellaro River (Romagnoli, et al., 2015).

The topographic levelling of the two Hyblean sectors occurred with the contribution of at least two different processes:

- The progressive filling of the western areas of the basin by sedimentary successions of Tertiary age.
- The effects of tectonics that determined the new configuration of the region.

The role of the tectonics was certainly decisive in the sedimentation of the Plio-Quaternary deposits of the Hyblean Mountains, currently located in the most recent structural depressions. Along the northern and western margins, these deposits represent the outermost offshoots of the Gela Avanfossa, in discordant support of the flexural Hyblean successions. Along the eastern margin of the plateau, Quaternary deposits represent the filling of graben structures, located transversally to the Ionian coast (e.g., Augusta Basin and Floridia Basin). The latter consist mainly of calcarenites passing upwards and laterally to clays (Pliocene sup-Pleistocene inf.). Finally, Middle Pleistocene-Superior Pleistocene coastal facies deposits develop along the current coastlines and can be correlated with various marine terraces (Bianca, et al., 1999).

Concerning the structural conditions, considerable fault systems responsible for the area's current high seismicity have been recognized in the Hyblean area. The main tectonic lineaments consist of high-angle fault systems, which are distributed over three distinct preferential orientations (Figure 4.1):

- NNE-SSO direction, as well as the direction of elongation of the entire plateau (Comiso-Chiaramonte system);
- NE-SW forms the Pozzallo-Ispica-Rosolini system, which controls the steps along the south-eastern edge of the Ragusa plateau;
- Scicli-Ragusa fault line system;
- Tellaro Line, an imposing NW-SE shear zone along the valley of the Tellaro river, delimiting the Ragusa and Syracuse domains (Romagnoli, et al., 2015);
- NE-SW oriented fault system of Avola Fault.
- Scordia-Lentini Graben, a large structural depression filled by Pleistocene marine sediments with NE-SW orientation;

- Pedagaggi-Lentini-Agnone Graben, characterised by northward dipping faults.

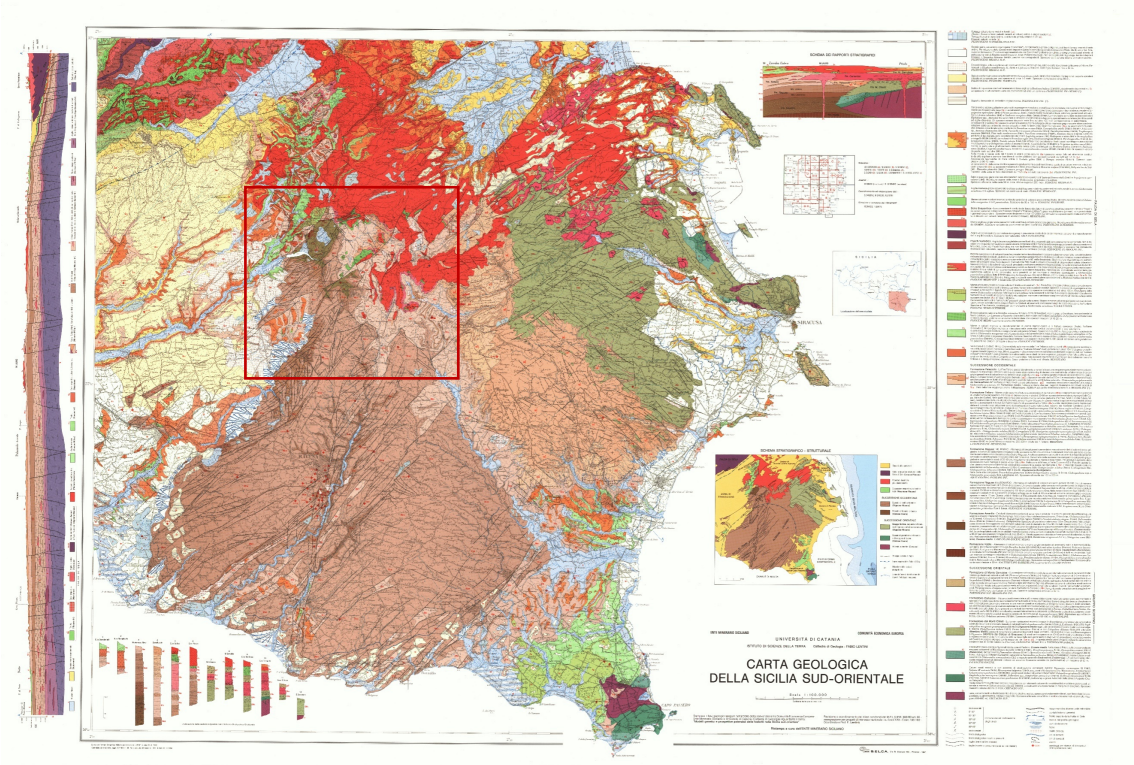


*Figure 4.1 - Geological map of southeastern Sicily (Lentini, 1987); the red box illustrates the area of local high-resolution modelling phase.*

### *4.1.2 Hydrogeological setting*

Based on the available hydrogeological dataset (ISPRA; Arpa), the hydrogeological setting of the Hyblean plateau can be divided into two main sectors (Figure 4.3) (Piano di gestione del distretto idrografico della Sicilia, https://www.regione.sicilia.it/istituzioni/regione/strutture-regionali/presidenza-regione/autorita-bacino-distretto-idrografico-sicilia/pianificazione/piano-di-gestione-direttiva-2000-60/ciclo3 (November 2022)):

- *south-western sector*, characterised by a homogeneous structure consisting of a carbonate succession.

  The sector is subdivided into two main water bodies, the Ragusa and the Vittoria Plain water body. Considering the Piana di Vittoria domain, the first aquifer is located in the Pleistocene sandy calcarenitic soils (at an average depth of 50 to 100 m), and a second deeper aquifer is confined by the marls of the Tellaro

Formation. The depth of the second aquifer varies depending on the geological-structural characteristics of the lithologies involved, moving towards the NW to the transition zone of the Gela-Catania Avanfossa. Locally, the presence of a non-continuous aquifer intercalated within the evaporitic series has been observed. The supply of the western sector mainly derived from the effective infiltrations within the Carbonate massif. In this respect, the major springs are located in the margin area (e.g. Sorgente Cifali, Diana in the Ragusa territory).

In the south-western sector, mainly characterised by the carbonate successions of the Ragusa Formation, the first aquifer is semi-confined and is located in the calcarenitic formation of the Irminio Member at an average depth of approximately 100-150 m below ground level. At a greater depth, a more productive aquifer is located in the limestone marly series of the Leonardo Member and separated from the shallowest portion by marly and clayey terms. Both aquifers are characterised by secondary permeability (karstification and fracturing) and low porosity. Sometimes the tectonic structures cause direct contact between the two aquifers. The karst dissolution phenomena began from the earliest uplift phases of the plateau (late Tertiary) and continued throughout the Quaternary period, generating increasingly articulated systems. Low and medium productivity are related to the alluvial deposits, conoids and recent sands aquifers.

- *north-eastern sector*, which is generally divided into four water bodies: the Lentinese basin, north-eastern Syracuse, southern Syracuse and the Augusta-Priolo plain.

  The different geochemical signature of the above-mentioned water bodies mainly depends on the water-rock interaction and on the directions of groundwater flow. In particular, in the northern portion from Monte Lauro to the Lentini plain (flow direction towards N-NE), the substratum is locally composed of Miocene altered volcanites (argillification processes) that make the top impermeable. Along a NE-SW alignment, a structural high separates the body of water described above from an adjacent mixed aquifer (Augusta Basin) where the alternation of volcanites interbedded with the carbonate succession has been recognized.

  The Syracuse domain is constrained to the north by the Melilli-Monti Climiti graben (structural high with an ONO-SE direction) with flowing water towards SW. The main aquifer involves the limestones of the Palazzolo formation and the

Monti Climiti formation. This carbonate series superimpose on the Miocene marls of the Tellaro formation to the west and is covered, in the Cassibile and Siracusa-Solarino area, by Plio-Pleistocene sediments. In general, this aquifer shows transmissivity values ranging from 0.1 to 9.0 × $10^{-3}$ $m^2/s$, as well as relatively high permeability due to karstification. The latter is a process that has influenced the local Miocene carbonate series since its emergence. The Augusta-Priolo water body consists of coarse sands and calcarenites (maximum thickness of 20 m). The clay substrate shows thickness from a few tens to a few hundred metres. The lack of clay occasionally connects the sands and calcarenites with the lower permeable terms (hydraulic continuity). The aquifer within the above-mentioned rocks, is exclusively fed by local infiltration and is largely drained by local watercourses.

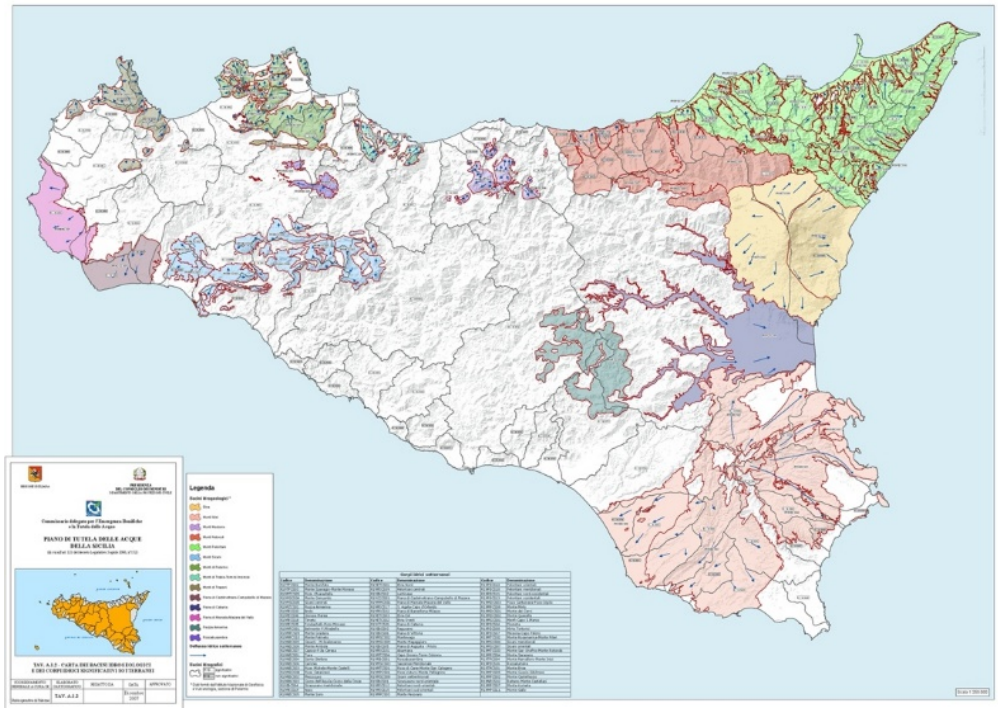

*Figure 4.2 – Hydrogeological basins distribution in Sicily (Arpa, Regione Sicilia)*

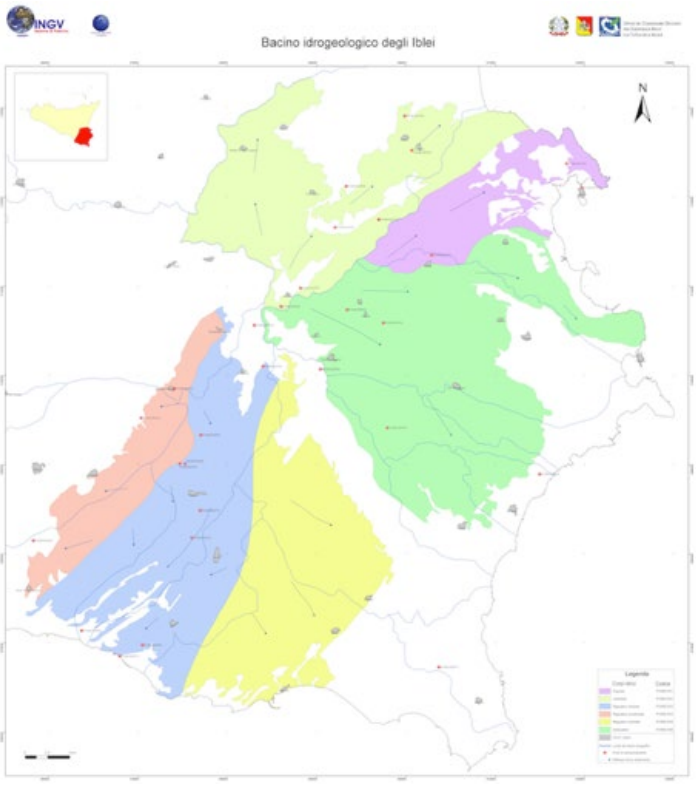


*Figure 4.3- Hydrogeological basin of the Hybean area (IGV, Arpa, Regione Sicilia)*

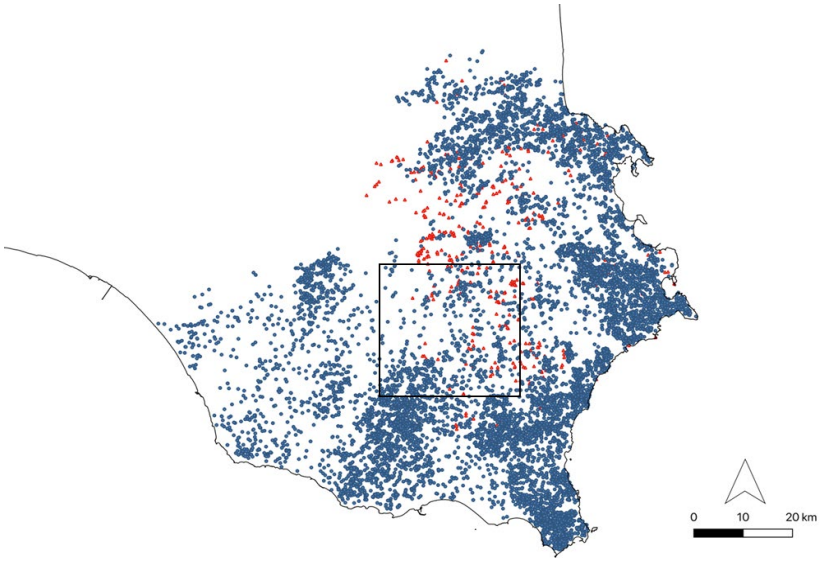


*Figure 4.4- Hydrogeological dataset (ISPRA, Genio civile Siracusa, Ragusa). Red dots illustrate the springs; Blue dots show the distribution of hydric wells.*

## 4.2 Case study

### *4.2.1 3D gravity-based model*

The investigated area is located between the Syracuse and Ragusa domains, with a total extension of 930 $km^2$. The reconstruction of the detailed stratigraphy was based on the analysis of previous geological and geophysical investigations, mainly linked to the hydrocarbon exploration wells available dataset (VIDEPI project). Table 4.1 illustrates the implemented formations that were considered. To solve the occurring computational problems some units have been combined.

The acquired dataset has been implemented, and the stratigraphy and thicknesses of the formations have been processed using the statistical interpolation algorithm of the PETREL software (Kriging). Successively, the main tectonics features (described in section 4.1.1) were introduced in the modelling phase. To detail the shallowest domain, the geognostic dataset from ISPRA and the Sicilian Region Archives (Genio Civile di Siracusa) have been consulted and implemented in the geological reconstruction process. In order to detail the gravity response of the carbonate sequence (up to 5 km depth), as part of a collaboration agreement between the University of Catania and the Maurel&Prom company, the new gravimetric survey, performed as part of the geological exploration of the investigated area, has been analized. Figure 4.6 shows the coverage of the acquired dataset. By means of IGMAS+ software (Schmidt et al., 2020), the Bouger and Free-air anomaly acquisition has been used to investigate and validate the density distribution of the different considered formations. A lithology-dependent density value (Table 4.1) has been assigned to each geological unit. In the first attempt, 11 different density layers have been considered: (1) a homogeneous density value of 2500 kg/m3 for volcanic rocks reported by Anon, 1979; (2) an average density value of 2000 kg/m3, for the Evaporitic series; (3) a constant density value of 2500 kg/m3, which is the mean value for the Palazzolo Unit; (4) the average density value of 2200 kg/m3 for the Tellaro Unit; (5) the average density of 2300 kg/m3 for the Ragusa unit; (6) the average density value of 2500 kg/m3 for the Amerillo Unit; (7) the average density value of 2400 kg/m3 for the Hybla Unit; (8) the average density value of 2400 kg/m3 for the Buccheri – Chiaramonte Unit; (9) the average density value of 2500 kg/m3 for the Modica Unit; (10) the average density value of 2450 kg/m3 for the Noto-Streppenosa Unit; (11) the average density value of 2670 kg/m3 for the Gela Unit. The density value for the considered units was

obtained from the P-wave velocities conversion (Gardner's relation; Gardner et al., 1974) within the sonic logs of the ViDEPI project database (see appendix A_4).

In order to constrain the density distribution of the lower boundary condition, the upper mantle density configuration has been introduced in the gravity model (voxel process on IGMAS+). From the direct conversion of the S-wave velocity as derived from the "CSEM Europe" mantle tomographic model (Fichtner et al., 2018) described in section 2.3.1, the density heterogeneities at the base of the model (20 Km) have been computed.

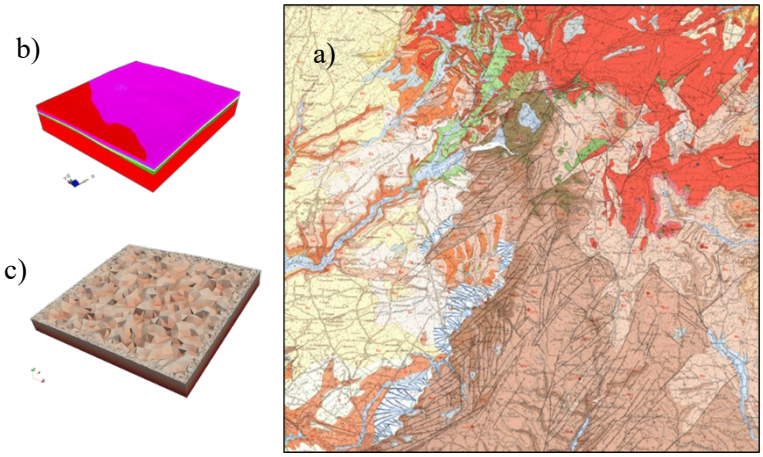


*Figure 4.5 - a) Geological configuration of the local model domain. b) development of the 3D geological model; c) section of the reconstructed mesh.*

After the first stage of the units' configuration (Figure 4.5b), the analysis on the new gravimetric dataset has been carried out on the IGMAS+ software to validate the proposed configuration. Figure 4.7a and 4.8a illustrate respectively the Bouger anomaly and Free-air map of the area. The two maps display a positive gravity anomaly in the western sector. Figure 4.7b and 4.8b show the modelled gravity distribution for Bouger anomaly and Free-air anomaly. To validate the proposed stratigraphy and layer's thicknesses, the measured values has been compared to the modelled ones by an inversion process (figure 4.7c and 4.8c). The calculated gravity residual (Bouger) indicates positive values up to 20 mGal in the central domain, with NE-SW trend. In the Vittoria Plain and in some parts of the eastern subdomain, negative residuals between -18 and -2 mGal indicate local mass excess in the initial model. In the remaining parts of the inland and foreland domain, the gravity residual ranges between ±10 mGal, suggesting that the initial model already provides a good approximation of the observed local gravity field (Figure 4.7).

Figure 4.8 illustrates the variation of Free-air anomaly. The computed values are consistent with the measured data, providing a good fit between the proposed geological setting. The residual Free-air anomaly vary between ±8 mGal except for the westernmost domain (probably due to the lack of dataset coverage).

In conclusion, the gravity-based validated geological model will be useful for the reconstruction of a three-dimensional mesh through the MeshIt software (Cacace, 2017) (Figure 4.5c). In fact, the managing of tetrahedrons properties will provide the basis for the subsequent thermal modelling stage.

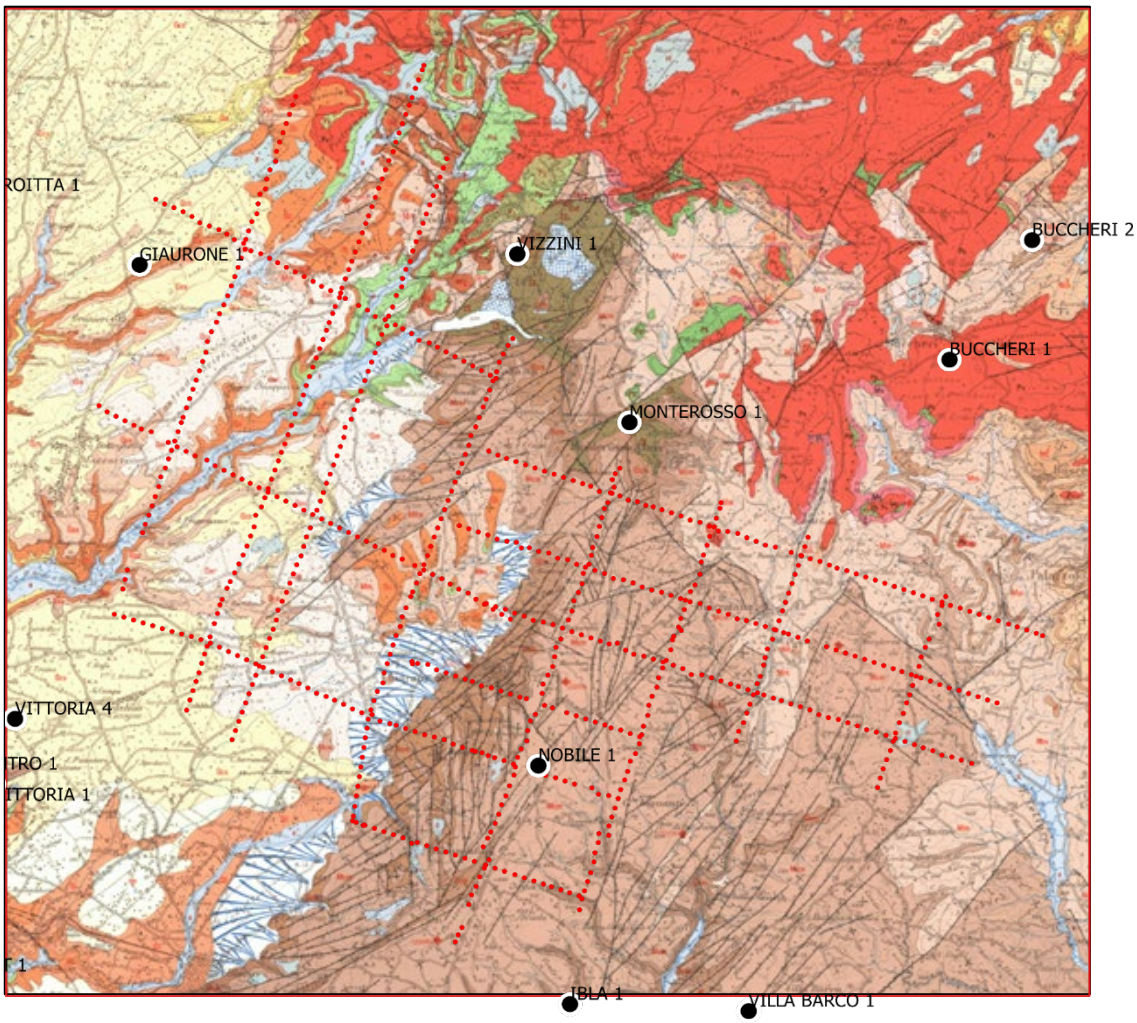


*Figure 4.6 - Location of the measure station for the new gravimetric survey (Maurel&Prom). Black dots display the location of the available well logs in the area.*

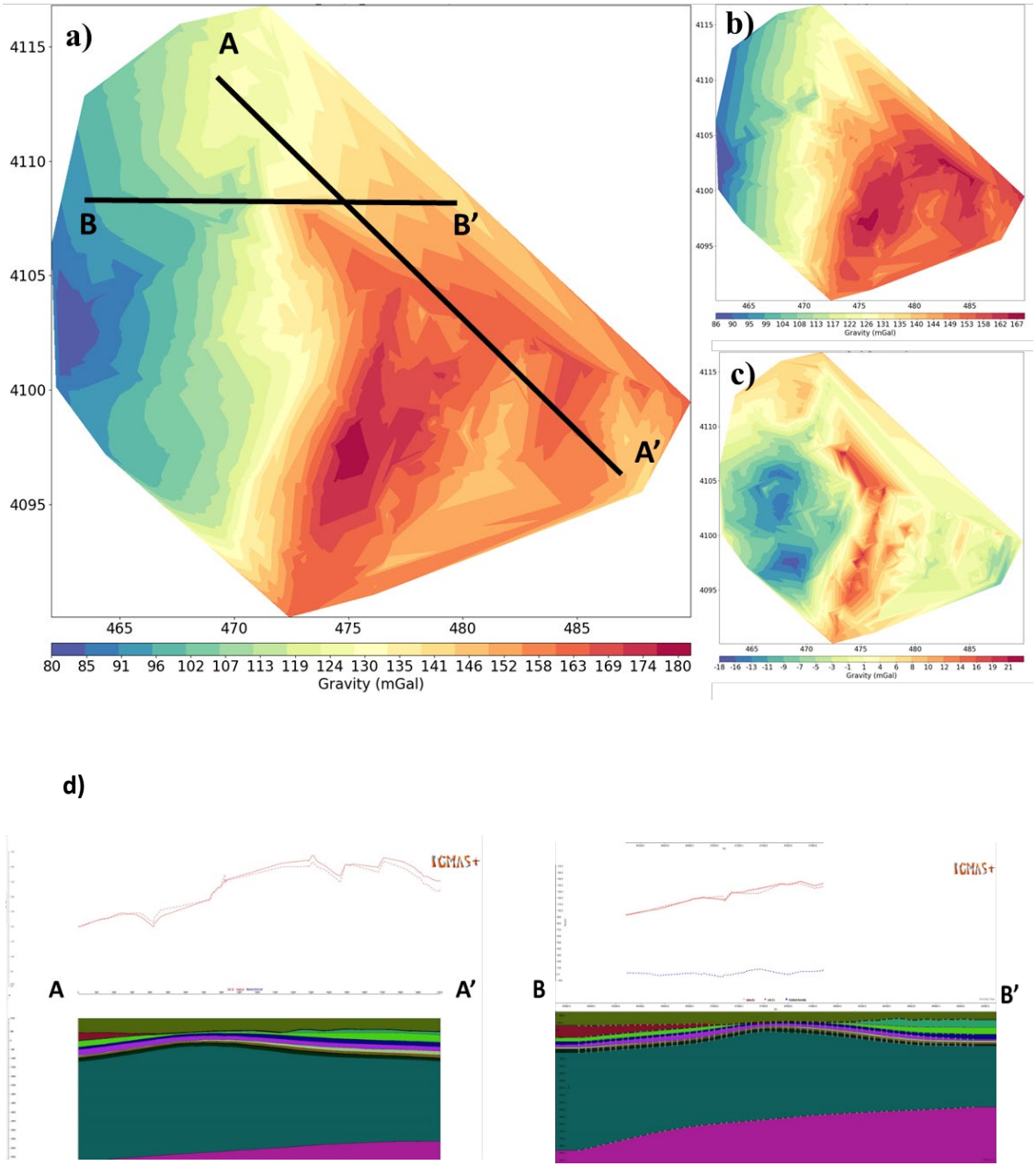


*Figure 4.7– Bouger anomaly (mGal) maps of the local domain. a) measured Bouger anomaly values; b) calculated Bouger anomaly (IGMAS+); c) residuals (IGMAS+) d) Gravimetric analysis of model sections (Bouger anomaly). Red line measured, red dotted line calculated, blue line residuals..*

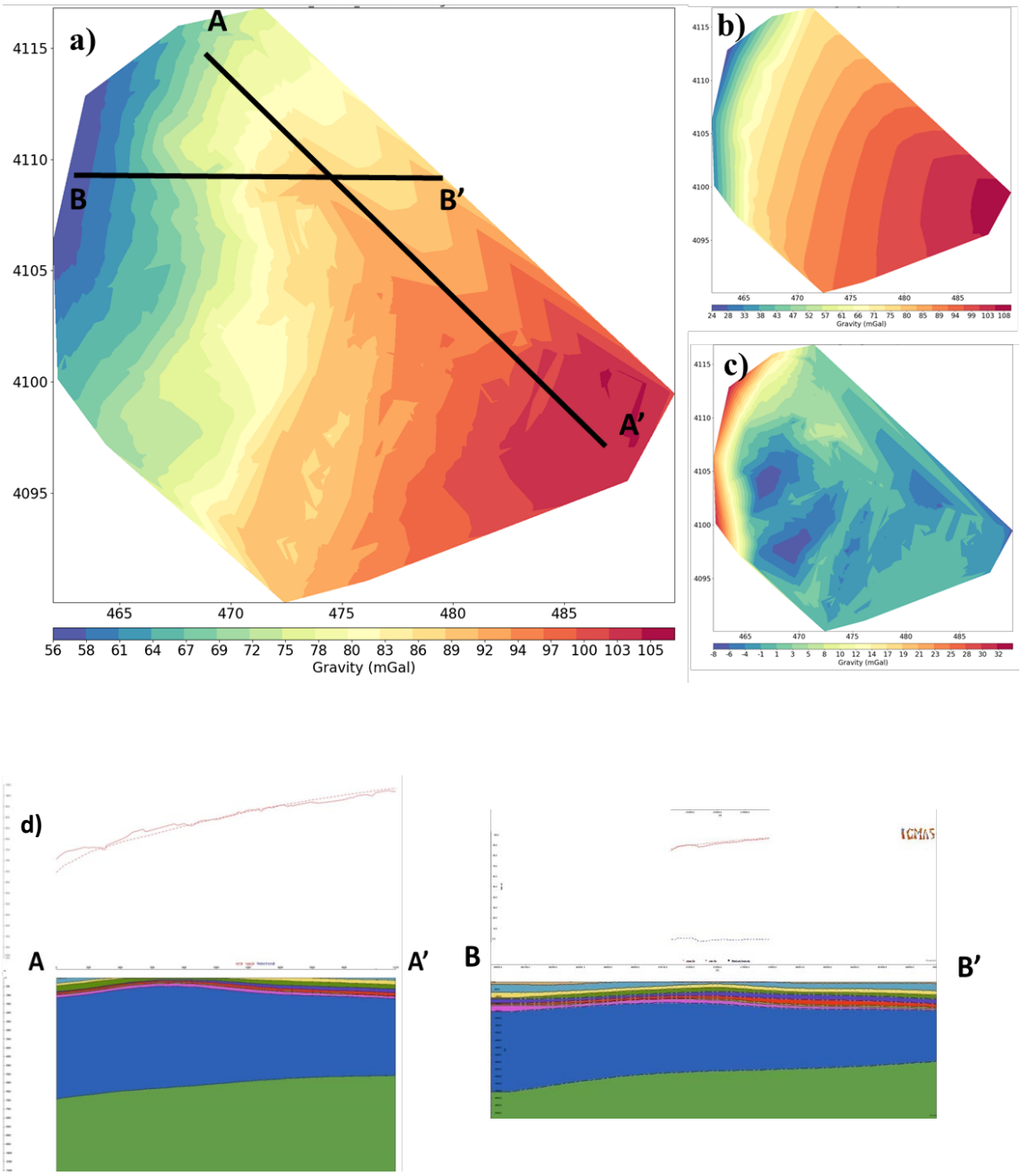


*Figure 4.8 - Free -air (mGal) maps of the local domain. a) measured Free -air anomaly values; b) calculated Free -air (IGMAS+); c) residuals (IGMAS+); d) Gravimetric analysis of model sections (free-air anomaly). Red line measured, red dotted line calculated, blue line residuals.*

*Table 4.1 - Density values used for gravimetric local modelling workflow.*

| Unit | Dominant lithology | Density final model (kg/m$^3$) | Ref |
|---|---|---|---|
| Hyblean volcanic rocks | Igneous rocks | 2.50 | (ViDEPI Project*) |
| Evaporitic series | Sedimentary rocks | 2.000 | (ViDEPI Project*) |
| Palazzolo unit | Sedimentary rocks | 2.020 | (ViDEPI Project*) |
| Tellaro unit | Marls | 2.200 | (ViDEPI Project*) |
| Ragusa unit | Limestones and marls | 2.300 | (ViDEPI Project*) |
| Amerillo unit | Mesozoic Carbonates | 2.500 | (ViDEPI Project*) |
| Hybla unit | Clay (marls and limestones intercalating) | 2.400 | (ViDEPI Project*) |
| Buccheri-Chiaramonte unit | Limestones | 2.400 | (ViDEPI Project*) |
| Modica unit | Limestones | 2.500 | (ViDEPI Project*) |
| Noto-Streppenosa unit | Organic rich shales (limestones and marls intercalating) | 2.450 | (ViDEPI Project*) |
| Gela unit | Dolomite sequence | 2.670 | (ViDEPI Project*) |

*data from the Gardner's relation (Gardner et al., 1974) applied to seismic velocity ViDEPI dataset.

### *4.2.2 Hydrogeological setting*

The case study is located within the so-called Southern Syracuse groundwater body (Figure 4.3). The latter affects most of the Province of Syracuse with the exclusion of the northern portion, whose major population centres are Noto, Avola and Palazzolo Acreide. Due to its hydrogeological characteristics and its great areal extension, it is one of the most important hydrogeological basins in south-eastern Sicily. Morphologically, the body of water consists of a series of horst-graben blocks that slope towards the easternmost sector of the area. Similarly, the carbonate plateau is affected by deep incisions such as Anapo, Cassibile and Cavadonna rivers degrading towards the Syracuse plain. From a lithological point of view, the aquifer is made up of a succession of carbonate, Calcareous-Calcarenitic deposits ranging in age from the Upper Cretaceous to the Tortonian with both vertical and lateral heteropy phenomena. The area in question is often characterised by aquifers placed on different levels, separated by semi-permeable media, and interconnected thanks to the presence of structures and faults affecting the different lithologies. As part of the research conducted, it was possible to carry out a survey on the identification of water extraction points (census performed at the offices of "Genio Civile di Siracusa"), extrapolating significant data on the characterisation of the aquifer, which was then useful for the definition of the heat exchange reservoir. Among the main parameters studied, the static and dynamic water level, as well as the flow rate values, made it possible to draw up a thematic map (Figure 4.9) regarding the piezometric level of the area. Analysing the existing literature (Aureli, A., 1993), the aquifer has a primary permeability >10-4 cm/s and shows strong transmissivity (values between 0.1 and 9 $m^2/s$) (Ruggieri, R., 1990). The bottom of the aquifer is made up, in some areas to the east, of strongly altered and argillified Cretaceous volcanites, while other carbonate formations of a more ancient age in hydraulic continuity follow below the limestones for a large part of the area. In the south-western sector of the basin of reference, particularly between the towns of Buscemi and Palazzolo Acreide, and extending even further southwards, a semi-impermeable marly-calcareous formation (Tellaro Formation) is located and interspersed between the more markedly calcareous terms. In the sector where the carbonate terms outcrop, the watercourses, through erosion and dissolution, have carved their beds into deeply sunken gorges (quarries), often reaching the piezometric level. With regard to the flow of groundwater in the aforementioned body of water, it occurs with a general direction from west to east along radial directions, from the highest topographical areas

(Monte Lauro) towards the lower peripheral areas, while in correspondence with the deep valley incisions, there are manifestations of variation of the river regime from draining to feeding the water table. This is mainly linked to the piezometric lowering produced by the considerable exploitation through boreholes.

In general, local soil permeability is subject to marked decreases both vertically and laterally due to fracture sealing and/or contact with low permeability marls. For these reasons, groundwater discharges occur along the entire length of the Hyblean Plateau margin (Ruggieri, R., 1990). The basin is fed directly by effective rainfall through infiltration into the network of fractures that desiccate the carbonate substrate, whose water table has both free and confined flow conditions in relation to the local and particular fracture conditions. The vulnerability of this water body is high due to the widespread fracturing and karstification affecting the carbonate strata. The analysis of the hydrogeological characteristics of the aquifer pertaining to the study area allowed for the evaluation of its potential for exploitation as a heat exchange reservoir for the implementation of low-enthalpy geothermal plants in an open-loop configuration. Furthermore, the flow rate values which were useful for the design of possible extraction and production wells in low-enthalpy geothermal projects were taken into consideration.

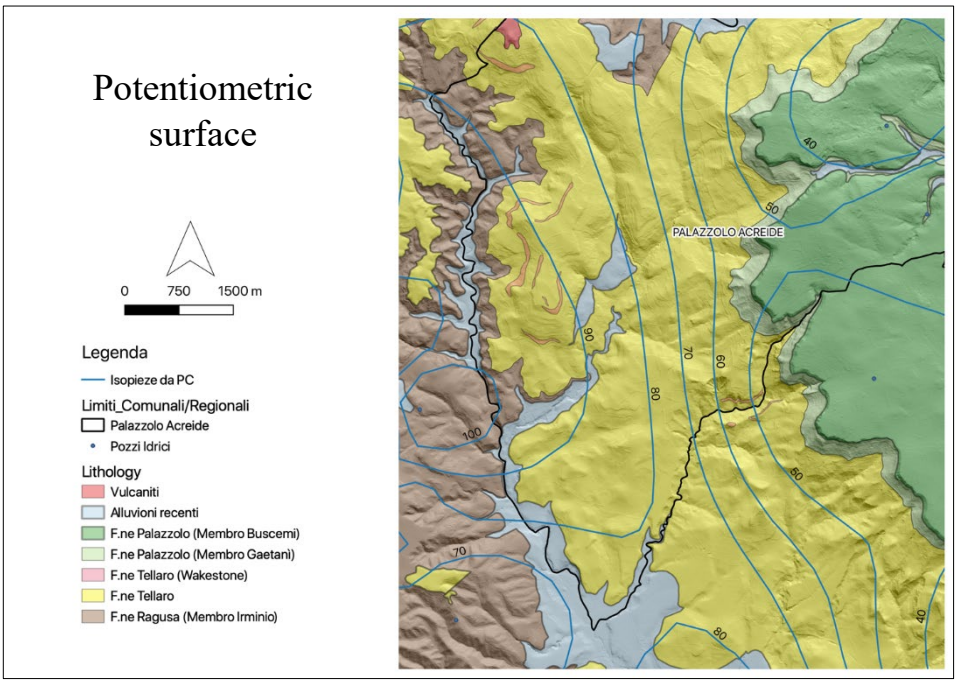


*Figure 4.9 - Potentiometric surface derived from the linear interpolation of dynamic water state (data from Genio Civile Siracusa)*

## 4.3 Thermal modelling

The thermal modelling of the Hyblaean case study has been conducted following the same methodological approach used for the regional thermal modelling testing phase (see chapter 2). In contrast to the choice of the lower BCs for the regional model, in this regard, they have been obtained using the best-fit regional model "EU60" as a starting point. In this case, the temperatures at the depth of 7 km below ground level (EU60 mantle model derived temperature as described in section 3.3.1) have been extrapolated from the regional model block and imported as a lower boundary condition for the local modelling phase, while the temperature extrapolated and interpolated from the meteorological station of SIAS (Servizio Agrometereologico Siciliano, www.sias.regione.sicilia.it) remains the top boundary condition. Given the high-resolution scale of the case study, a detailed parameterization of each Meso-Cenozoic layer of the model has been considered. As previously discussed, the implemented geometries and thicknesses have been obtained from the convergent interpolation algorithms of scatter information implemented in the PETREL software (©Schlumberger) of the published dataset for the investigated area (lithologies per each considered boreholes in VIDEPI project and Geothopica project). With reference to the thermal properties, Table 4.1 illustrates them as reflecting effective properties for the different lithologies described in section 4.2.1. In this regard, we relied upon data collected during recent years through the analysis of outcropping lithologies (Geological Map of Sicily - Lentini, Carbone 2012) and subsurface successions in Sicily from the interpretation of hydrocarbon exploration well logs together with laboratory investigations to attain a range of variations for the thermal properties of each sequence (e.g. Abate et al., 2014; Galgaro et al., 2012; Gola et al., 2013; Di Sipio et al., 2013).

### *4.3.1 Steady-state thermal model simulation*

The gravity-based geological model with the rock properties chosen for each layer and the set of top and bottom boundary conditions have been used to compute the local thermal field. The result of the numerical modelling stage is the high-resolution (lateral and vertical resolution of 200m) 3D thermal model of the studied area. The results, based on the iterative simulation of four different model parameterizations, are discussed below with the aim of providing the best fit between the shallow temperature measurements and the modelled ones. Four different thermal conductivity configurations have been considered providing four different simulations as follow: 1) average thermal conductivity values, derived from literature dataset (Trumpy et al. 2017), as a function of each Meso-Cenozoic lithologies; 2-3-4) min, max and average values from Di Sipio et. Al, 2013, in particular; (2) average thermal conductivity of 1.7 W/mK for the entire succession; (3) average thermal conductivity of 2.5 W/mK for the entire succession; (4) average thermal conductivity of 3.7 W/mK for the entire succession. It is important to note that simulations 2-3-4 consider the iterative process for thermal conductivity range values from 1.7 to 3.7; here we illustrate the steps 1.7 W/mK, 2.5 W/mK, 3.7 W/mK. To evaluate the interaction between the major tectonic structures and the propagation of the thermal conditions, an additional simulation has been therefore analysed. Thus, a fifth model setup has been performed to evaluate the integration of the main tectonic structures of the Hyblean context described in section 4.1.1. Three refined areas consisting of major faults have been added to the starting mesh of the 3D model and an average thermal conductivity value for each layer of the entire succession has been considered. The trend of the calculated thermal field distribution for the first simulation stage (1) (Figure 4.10) seems to be significantly influenced by the imposed surface temperature. For example, at 1 km b.g.l. (Figure 4.10a) the temperature does not exceed 38 °C in the northern-central sector, while the surrounding areas are characterized by lower temperature values (< 20 ° C). Due to the considerable interconnected fractures of the carbonate succession, the western and eastern domains of the area, including vast portions of the Ragusa Formation outcrop and the Gela forefoot (Vittoria plan), are characterized by temperatures between 17°C - 20°C. The investigated thermal field displays in the central sector a positive thermal anomaly for depth between 1-5 km b.g.l. which could be connected to the thermal energy input from the lithospheric mantle as a possible consequence of the bulge of the

Hyblean foreland (Henriquet et al., 2019) and the subsequent shallower depth of the Moho surface, as well as the outcrop of the deep lithologies.

The thermal conductivity variation in the second stage of simulations 2-3-4 (Figure 4.11, Figure 4.12, Figure 4.13), which consider values of thermal conductivity of 1.7-2.5-3.7 W/mK, did not influence the distribution of the thermal field observed, and can be therefore neglected.

Although the first stage of the modelling does not consider the tectonics features of the area, the preferential orientation of positive thermal anomalies may reflect a contribution of the tectonic component to the heat transfer. In this regard, the positive thermal anomalies, located in the meridional sectors of the area, could be therefore correlated to the major tectonic structures (Figure 4.14). In fact, NE-SW oriented thermal anomaly could be correlated to the Scicli fault system and NW-SE oriented positive thermal anomaly could be related to the Tellaro Faults. The trend is visible at different depths, from 1 to 7 km below ground level, where the thermal field is no longer affected by the

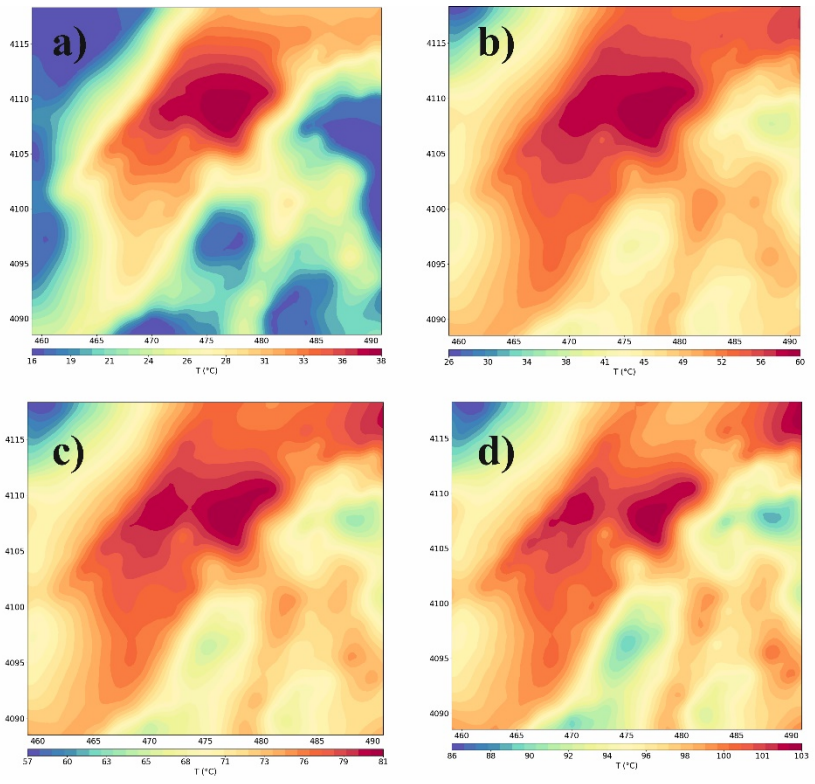


*Figure 4.10- Temperature maps at different selected depths below ground level (a: 1 km, b: 2 km, c: 3 km, d: 4 km) assuming an average thermal conductivity value of 1.7 W/mK. Coordinates are in EPSG:32633 – WGS84/UTM zone 33N.*

imposed upper boundary condition. By the integration of tectonics components, simulation 5 displays how the faults' systems could represent a preferential pathway for the heat transmission in the subsurface. Although the simulation did not shows an increase

in the modelled temperatures the general trend confirm a contribution from the deeper level depicting the tectonic configuration of the deeper crust (Figure 4.14).

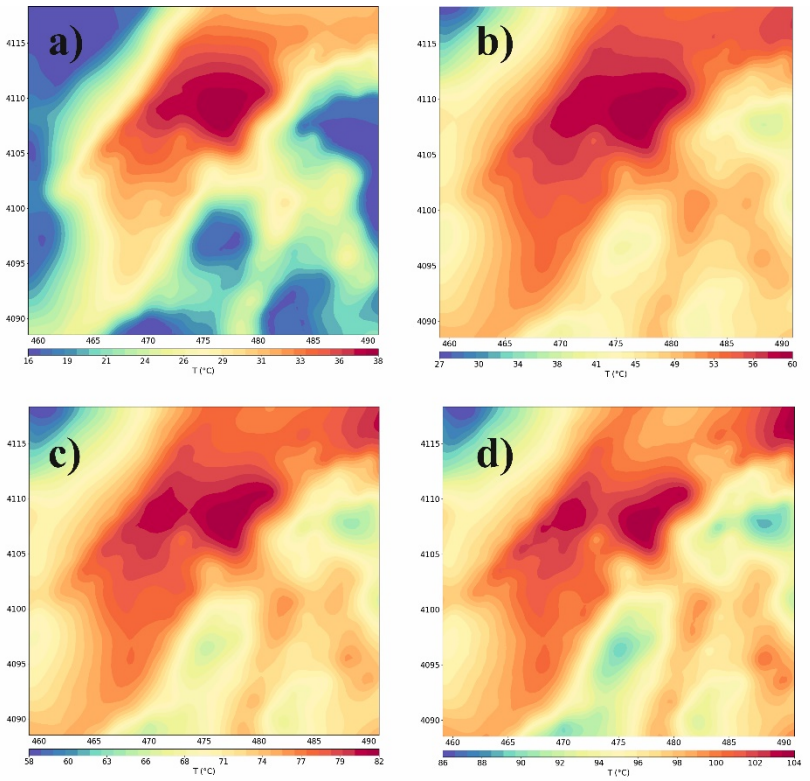


*Figure 4.11- Temperature maps at different selected depths below ground level (a: 1 km, b: 2 km, c: 3 km, d: 4 km) assuming thermal conductivity values for each lithology. Coordinates are in EPSG:32633 – WGS84/UTM zone 33N.*

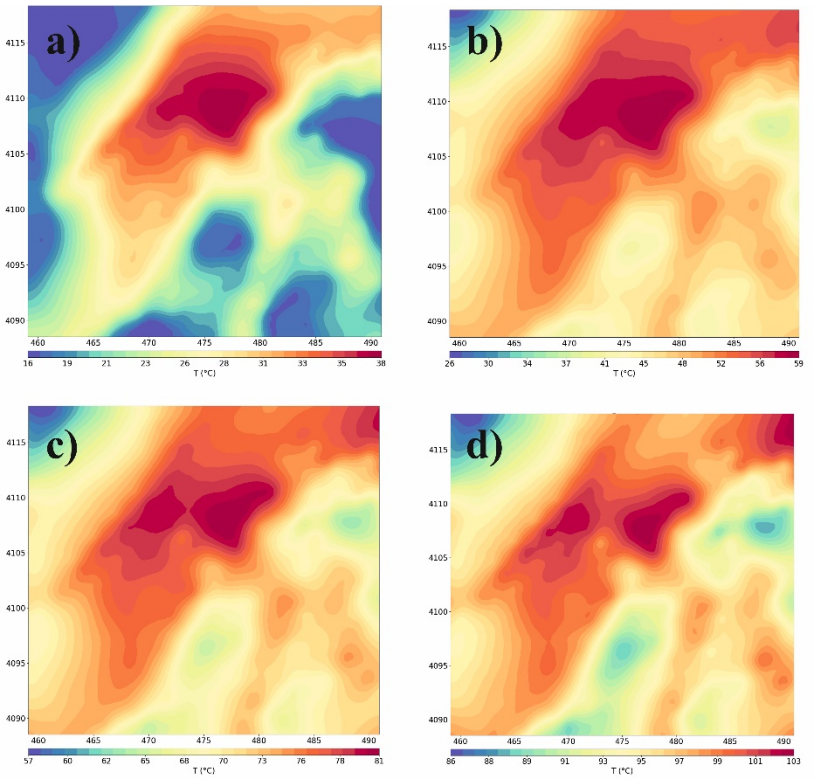


*Figure 4.13- Temperature maps at different selected depths below ground level (a: 1 km, b: 2 km, c: 3 km, d: 4 km) assuming an average of thermal conductivity values of 3.7 W/mK. Coordinates are in EPSG:32633 – WGS84/UTM zone 33N.*

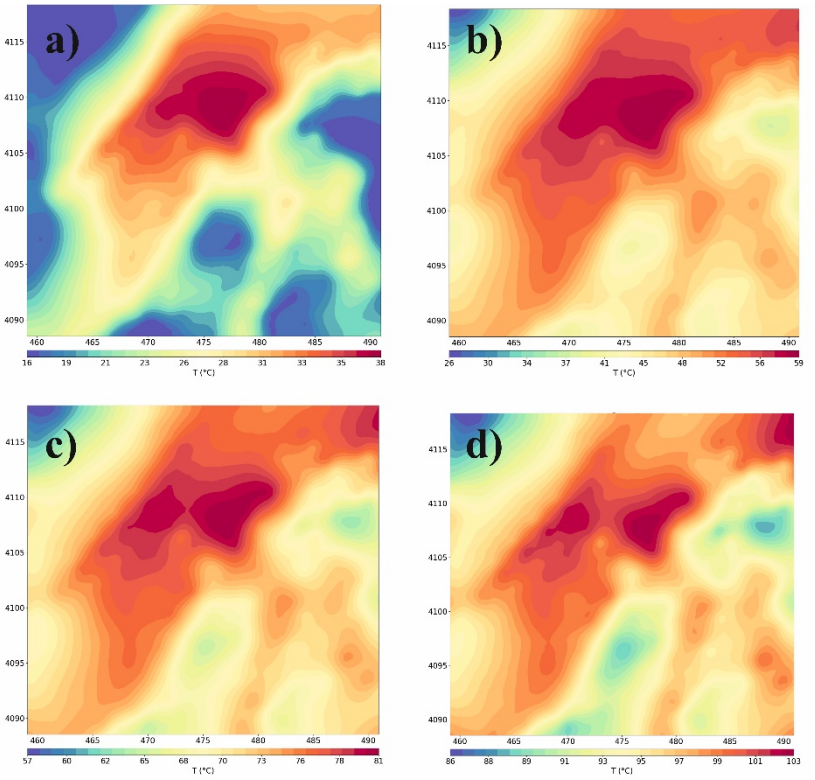


*Figure 4.12- Temperature maps at different selected depths below ground level (a: 1 km, b: 2 km, c: 3 km, d: 4 km) assuming an average thermal conductivity value of 2.5 W/mK. Coordinates are in EPSG:32633 – WGS84/UTM zone 33N.*

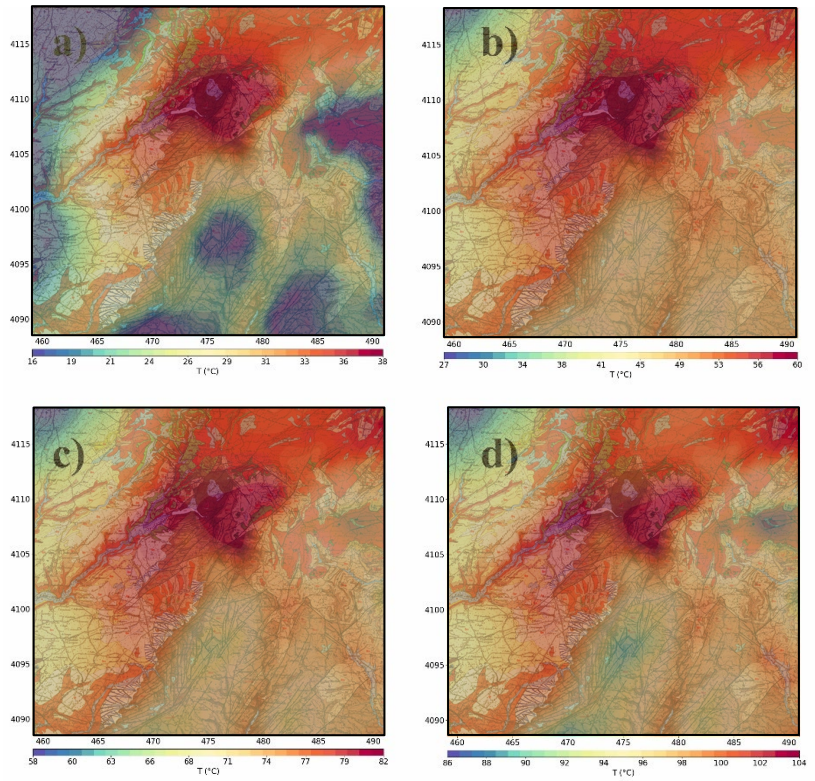


*Figure 4.14- Temperature maps at different selected depths below ground level (a: 1 km, b: 2 km, c: 3 km, d: 4 km) assuming an average thermal conductivity per each unit. The major tectonics features are included in the modelling phase and superimposed on the thermal maps. Coordinates are in EPSG:32633 – WGS84/UTM zone 33N.*

### *4.3.2 Observed versus modelled temperature: validation against 1-2-3-4 Km depth (b.g.l)*

As discussed in section 3.3, the regional scale of the thermal modelling phase shows limitations on the definition of the local thermal field. The high-resolution investigation aims to display how the Sicilian sedimentary sequences mostly control the variability of thermal conditions on a local scale. The calibration of the high-resolution thermal model is provided by comparing the results obtained from the numerical thermal simulation, (in steady-state condition) described in section 4.3.1, compared to the available dataset from the Italian National Geothermal Database (Cataldi et al., 1995; Trumpy and Manzella, 2017). To compare the measured and modelled temperature in the specific area, a selection of 6 drilled wells inside the pilot area has been picked from the public dataset (Figure 4.6). [Measurement and temperature of the bottom hole corrected using the empirical method Squarci-Taffi (Della Vedova et al., 2001), where temperatures are extrapolated with a homogeneous gradient]. In addition to temperature data, parameters including mean gradient, calculated thermal flux, main observed mineralization,

permeability and lithostratigraphic relationships have been analysed. The modelled temperature derived from the steady-state thermal simulations displays a good fit with the available temperature measurements. Modelled temperatures are therefore consistent with the measurements with a maximum Root Mean Square Error of about 25°C at depths between 3 and 4 km, in line with the previous regional Hyblean domain calibration (Figure 3.14b, Figure 4.15a). The thermal outputs also illustrate how the tectonics could play a key role and represent a controlling factor for the thermal conditions (Figure 4.15b). In this regard, it is possible to note how the positive thermal anomalies reflect the tectonic distribution of the area. To better constraint the possible interaction between faults and thermal conditions, supplementary simulations, implementing the tectonic condition, have been carried out. The implementation of the main tectonic structures during the simulation stage results in a marked improvement of the adjustment of the modelled temperature compared to the measured ones, with maximum RMSE of 10°C between 3 km and 4 km b.g.l (figure 4.15b). This defines the best configuration in terms of temperatures variation. The tectonic component, then, becomes a key element in heat transport. In addition, new evidence could be related to the integration of others geo-tectonic structures. In this regard, the implementation of this new element will be further investigated.

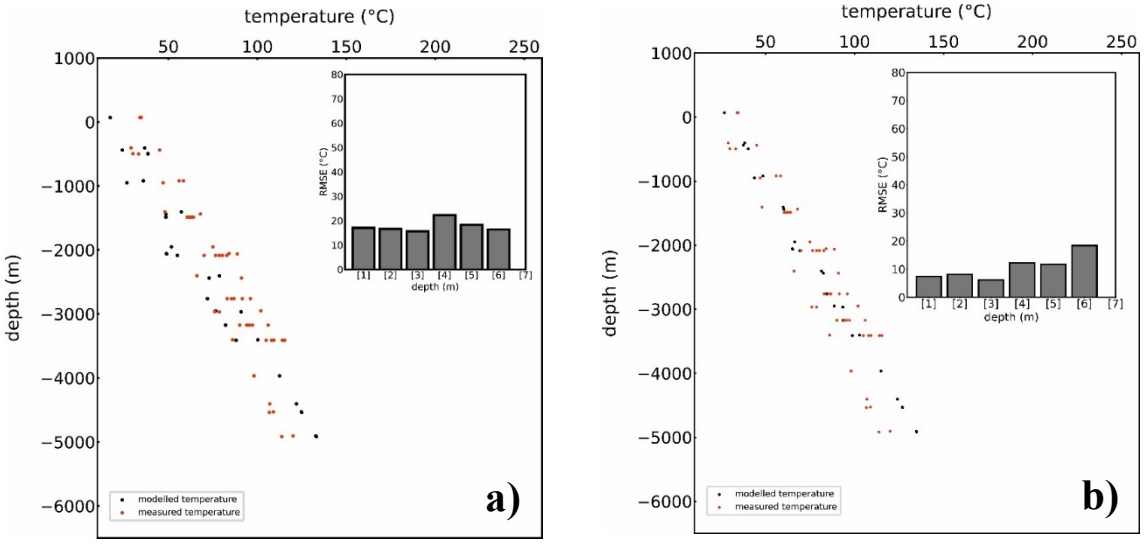


*Figure 4.15- Temperatures modelled (black points) vs. measured (red points) for the local Model (thermal cond. 2.5 W/mK) a) simulation without tectonics; b) simulation with tectonics. The temperature comparisons are associated with the graph showing the Root Mean Square Error expressed in (°C) for different depth ranges expressed in meter (1 = [1000 - 0]; 2 = [0 - -1000]; 3 = [-1000 - - 2000]; 4 = [-2000 - -3000]; 5 = [-3000 - -4000]; 6 = [-4000 - -5000]; 7 = [-5000 - -6000].*

## 4.4 Numerical simulations of a low-enthalpy open-loop system

In order to simulate the thermal and hydraulic response of the modelled reservoir, an operational activity of a low enthalpy geothermal system over a period of 10 years has been analysed. In this case study, a micro-domain of the modelled area has been considered (Figure 4.16). The type of plant considered in the case study concerns an open-loop geothermal system (direct use) where technology relies on the fact that the water reservoir remains at a relatively constant temperature throughout the year, warmer than the atmospheric temperature during the winter season and cooler in the summer. This type of approach takes into account the presence of the injection and extraction wells, as well as the geothermal heat pump that benefits from transferring the heat stored in ground water into a building during the winter, and from transferring it out of the building and back into the ground during the summer. The ground, in other words, acts as a heat source in winter and a heat sink in summer (Banks, 2009).

With the aim of evaluating the thermal disturbance on the hydrogeological conditions, the simulation takes into account two different doublet systems, each consisting of an injection and a production well, whit a distance of 30 linear meters between each other.

The area consists of three different geological layers: the Ragusa Unit (gray layer in Figure 4.16), the Tellaro Unit (red layer in Figure 4.16), the Palazzolo Unit (green layer in Figure 4.16). The Ragusa Unit represents the target reservoir (main aquifer), the upper Tellaro formation acting as a cap rock, while the Palazzolo formation represents a different superimposed aquifer. The extent of the model domain is 10x10x0.5 km in the x, y, and z directions. Because of computational reasons, the water table has been considered as the top of the hydrogeological model (considering a pressure on the top of 0.1 atm). Taking into account the hydrogeological setting of the area (described in section 4.2.2), the target reservoir for low enthalpy purposes has been located at a depth of approximately 100-500 m b.g.l. For the numerical simulation, the adopted reservoir boundary conditions included: a constant temperature fixed along the top of the reservoir (T 20 °C, corresponding to the measured temperature from wells in that area), heat input at the base of the model (T (°C) at 500 m depth from the interpolation of the extrapolated thermal gradient of approximately 0.03 °C/Km), and hydrostatic pressure along all lateral borders of the domain. The open-hole section of the two wells extends for approximately 200 m vertically in the reservoir, therefore the 140-340 m b.g.l depth was considered as

depth of the open-loop geothermal simulation. In addition, the injection has been considered at the top of the reservoir while the production has been considered from the base of the modelled reservoir. The open-hole section of the wells has been integrated as one-dimensional finite elements and the homogenization of the resulting governing equations is done by considering the surface area of the well bore as scaling parameter. The primary condition of the system, before the injection/extraction from operation wells, is described by running a steady-state simulation (with the same boundary conditions as described above) without considering any operational activity. The following step of simulation take into account the transient condition applied to the first steady state running.

A schematic representation of the main geometry is illustrated in Fig. 4.16, and all properties are listed in Table 4.1. Figure 4.17 illustrates the reservoir state at the beginning of the simulation. It is possible to observe the evolution of the reservoir temperature as resulting from the dynamics of the interactions between the different components of the system (i.e. reservoir matrix, fluid and geothermal wells) and it shows how the simulator can be effectively applied to 3-D modelling of low enthalpy geothermal reservoirs.

*Table 4.2 - Hydrogeological and thermal properties*

| | **Thermal conductivity [W/m/K] (bulk)** | **Specific heat capacity [J/m³/K] (bulk)** | **long. dispersivity/ trans. [m] dispersivity [m]** | **Porosity [%]** | **Hydraulic conductivity [m/s]** | **T BCs (K/m)** | **Thickness [m] / length [m]** |
|---|---|---|---|---|---|---|---|
| Layer 1 (Aquifer) | 2.5 | 800 | 1/0.5 | 0.45 | 0.00311 | 0.3 | 30/50 |
| Layer 2 (Aquitard) | 2.2 | 2400 | 1/0.5 | 0.15 | 0.001 | 0.3 | 100/150 |
| Layer 3 (Aquifer) | 2.6 | 800 | 1/0.5 | 0.25 | 0.00311 | 0.3 | 200/300 |
| Wells | 0.65 | 4200 | - | 1 | 1000 | | 100 |

*Table 4.3 – Doublet Simulation (case studies)*

| **Case Study** | **Injection temperature[°C]** | **Injection temperature [°C]** | **Mass flow rate [kg/s]** | **Aquifer thickness [m]** |
|---|---|---|---|---|
| Case_1 | 30 | 26 | 4.2 | 100 |
| Case_2 | 30 | 26 | 4.2 | 100 |

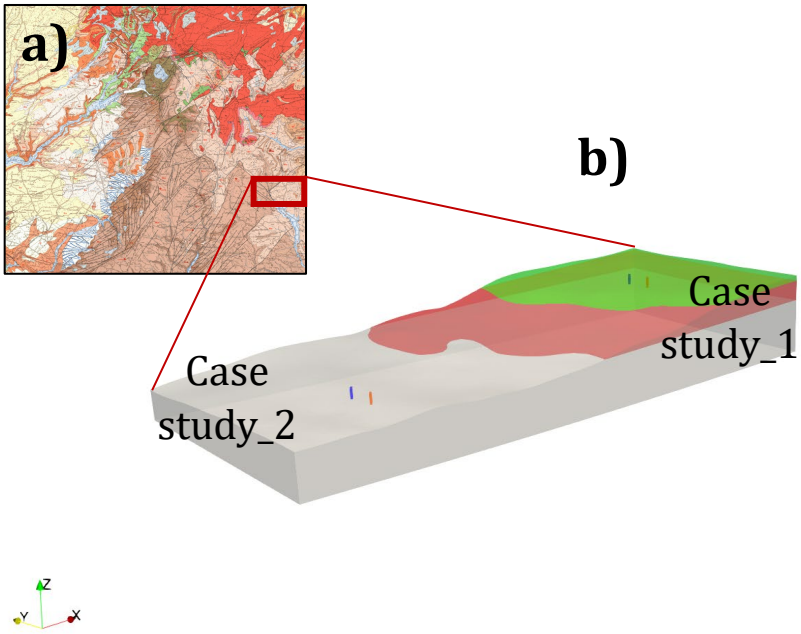


*Figure 4.16 - a) location of the modelled area; b) schematic representation of the main geometry of the modelled area. Blue lines represent the location of the injection wells, while red lines show the location of the extraction wells.*

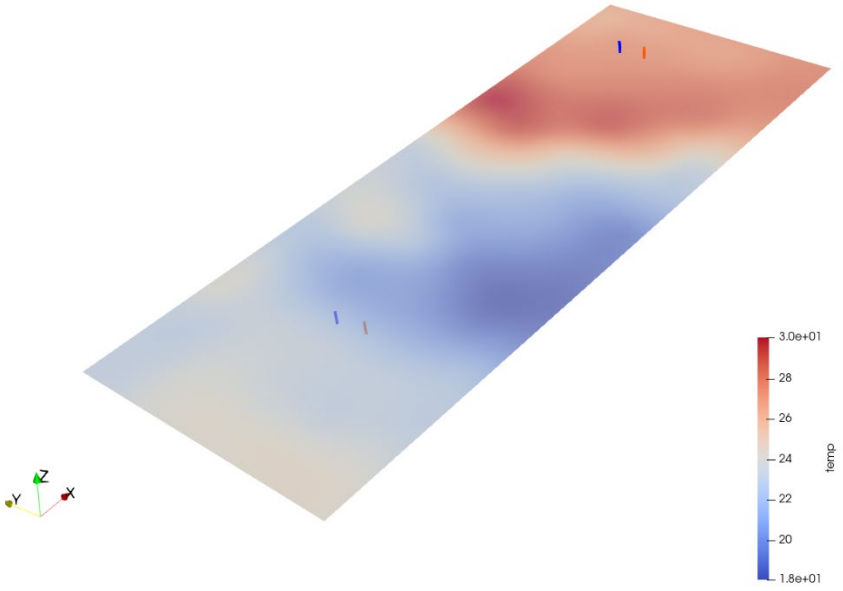


*Figure 4.17 – Micro domain simulation slice at 240 m above sea level (time 0).*

## 4.5 Sustainability over time

With the aim of identifying the best configuration of an open-loop geothermal plant, it was possible to simulate different configurations (borehole distances, operating flow rate, temperature variations etc.). The purpose of applied numerical geothermal modelling is based on the evaluation of the possible variation of the reservoir conditions with the aim of maintaining the geothermal reservoir thermal situation. In detail, the modelling stage has been implemented to evaluate the hydraulic and thermal effects of the low enthalpy geothermal system operation, which is characterized by 2 extraction wells and 2 injection wells; the main characteristics of which are summarised in Table 4.2, while the location of the wells is shown in Figure 4.16.

The injection of a fluid with different temperatures in the subsoil (seasonal geothermal inversion cycle, higher in summer and lower in winter), could cause the lack of efficiency of the entire heat exchange system as well as affect the biological equilibrium conditions. The optimal configuration (section 4.4) allowed to simulate the operation of the plant for a period of 10 years in summer and winter cycles. Temperature variations at injection and extraction points were analysed to assess the influence of the heat exchange with ground water. For example, the temperature condition at the top and bottom of the reservoir considered is represented in figure 4.18. In particular, the figure shows the final condition during the last step of the simulation (summer period), where at the top of the reservoir a sharp increase in temperature is observed (Figure 4.18b), while at the bottom (taken from the extraction well) a temperature in line with that of the relevant aquifer is observed (Figure 4.18a). In order to better constrain local temperature changes, the graphs in the figure show the temperature changes in the injection (Figure 4.19b-4.20b) and extraction (Figure 4.19a-4.20a) wells. It is possible to observe how the inversion of the seasonal geothermal cycle affects temperature fluctuations in the injection wells, without destabilizing the aquifer over a period of 10 years. In addition, with the aim of verifying the complete efficiency of the system as a function of time, the temperature changes in the extraction wells were analysed. Figure 4.19 and Figure 4.20 show temperature decreases of 0.5 C. This allows to validate the distance between the injection and extraction wells for each doublet system considered. In this regard, multiple simulations were performed to identify the threshold to preserve the efficiency of the entire plant, which is of about 20 meters.

By means of numerical simulations, the geothermal open loop systems could be useful for several applications. Among the possible exploitation of a low temperature reservoir (~30 °C), as in the above-mentioned example, heating of homes, drying of fruits, greenhouses, aquaculture could be included with no alteration on the natural thermal field conditions.

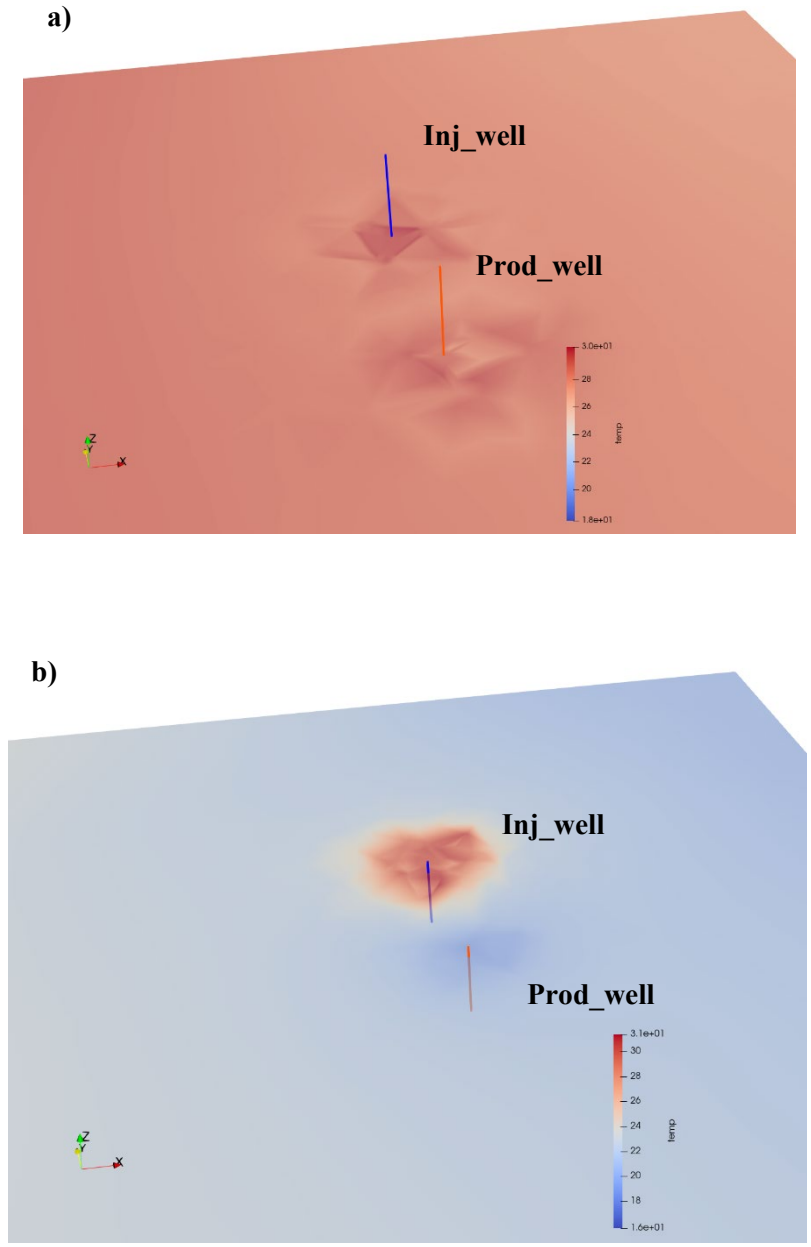


*Figure 4.18 - Reservoir temperature distribution in case study 1 a) example of the reservoir top temperature perturbation in the last step of the simulation (summer); b) example of the reservoir bottom temperature perturbation in the last step of the simulation (summer).*

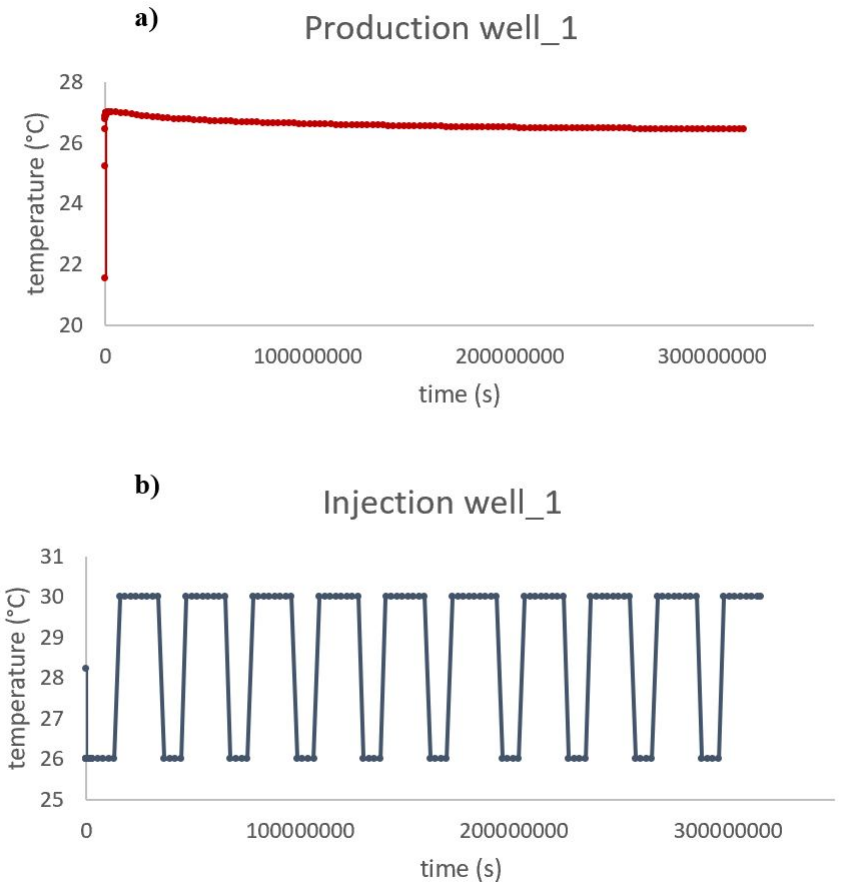


*Figure 4.19 – Temperature variation for doublet in case study_1 over time for production (a) and injection (b) well.*

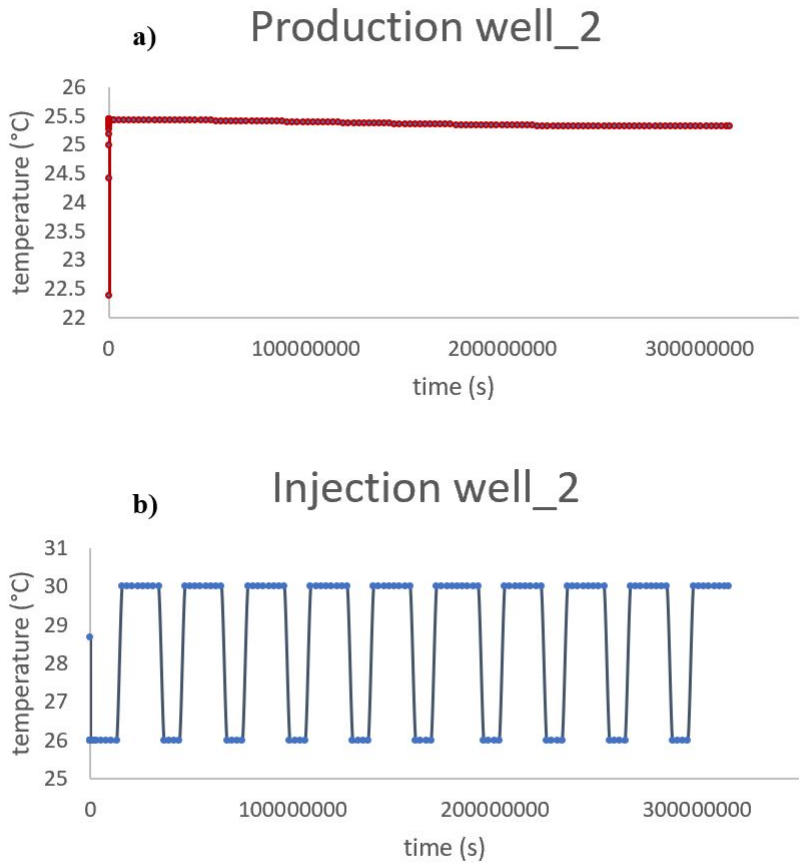


*Figure 4.20– Temperature variation for doublet in case study_2 over time for production (a) and injection (b) well.*

# 5 Chapter 5 – Products

The modelling of the thermal field at depths which are advantageous for geothermal exploration results in the development of useful tools for the subsequent exploitation of the renewable resource. Accordingly, the definition of 2D temperature thematic maps was carried out to obtain temperature depictions for depths mainly between 1 and 5 km. With the aim of making the thermal modelling work as an interactive tool for the Sicilian geothermal field investigation, it was possible to integrate the 3D modelling outcomes in a web portal that allows querying of the punctual thermal conditions of the studied areas. The web project takes the name of STORAGE - project (acronym of Sicilian Temperature pORtAl for Geothermal Exploration - project). The name intentionally identifies both the subsoil property of storing heat and the function of data space in a web platform. These aspects, combined with the logo, represent the main elements of the project: the Earth's internal heat, the modelling of the subsoil through a tetrahedral meshing process and the exploitation of the resources through heat exchangers (Figure 5.1). The basic concept is to provide a web platform that can be used by both academics and experts in the field for the characterization of geothermal resources in Sicily.

In this section, the applied methodology and the obtained results will be clarified.

## 5.1 Project conceptualization

Among the essential components of the correct planning of geothermal resources exploitation, the identification of subsoil temperature is crucial. In the regional thermal modelling stage, exposed in chapter 3, the outermost layers of the earth's crust have been analysed and different resolutions of the three-dimensional model have been identified considering the best-fit models for the subsequent analytical steps (Crustal Model, CSEM Mantle Model and EU60 Model in chapter 3). In order to provide a standard dataset, temperature-depth values have been extrapolated and analysed by using open-source software Paraview. In detail, temperature-depth values have been acquired from the best models' slices (obtained from the linear interpolation post-processing of the starting dataset) both for the regional model and for the local one. In the studied regional thermal field, the vertical extension of the model (lithospheric scale) allowed us to investigate the temperature conditions up to lithospheric depth; this allows us to investigate the

geothermal conditions as well as the geodynamic implications. Temperature horizontal slices at depths of 1, 2, 3, 4, 5, 10, 20, and 30 km below ground level have been studied (Figure 3.7, Figure 3.8, Figure 3.9). While the lithospheric scale resolution is useful to define the rheological characteristics of the regional context, the thermal condition of the most superficial portions of the crust has significant repercussions in the exploration of the exploitable geothermal resource. In this regard, the focus on depths ranging from 1 to 5 km below ground level for a local domain has been considered. In order to facilitate the investigation of subsurface temperatures and to make the main outcomes of the modelling phase accessible and interactive, the Sicilian Temperature pORtAl for Geothermal Exploitation – project shows significant perspectives. The idea of a web portal for the exploration and exploitation of geothermal resources represents the first step towards the correct management of geothermal resources in Sicily, but also a driving force for the growth of the still not widespread geothermal culture in Italy. The investigation of geothermal characteristics on a local scale (high-resolution case study described in chapter 4) enables us to define and describe the concept of "Geothermal Micro-zonation". Following a national-scale approach like the Geothermal Zoning of the Italian territory (https://unmig.mise.gov.it/index.php/it/dati/risorse-geotermiche/zonazione-geotermica-del-territorio-italiano - March 2017), which involved the Ministry of the Environment and the Protection of the Territory and the Sea, the representatives of the universities and scientific community, and the regional administrations mainly interested in geothermal projects and sector operators, the micro-scale approach would guarantee an incentive to identify and characterize the suitable areas for the exploitation of geothermal resources. In fact, the involvement of local structures like the municipal, provincial, and regional administrations would allow the development of a pervasive structure capable of reference market triggering, providing a reference tool to plan the exploitation of geothermal resources and to involve entrepreneurs in the sector as well.

## 5.2 Database

The web portal https://storageproject.it/ is based on a standard database derived from best-fit models. In that respect, the dataset has been obtained from a postprocessing analysis of the best-fit thermal models and provides 10 standard grids of temperature values horizontally distributed in order to attain data standardization. In this first attempt, for the regional and local (higher vertical resolution) approach, the depth from 0 (ground level) to 5 km depth (step of 1 km) below ground level was chosen according to

geothermal exploration purposes. In detail, 5 grids are referred to the regional model and 5 grids concern the higher resolution local model. The grids have been extrapolated assuming standard depth (1-5 km below ground level). Each horizontal slice is characterized by a regular grid of nodes with a resolution of 5 km on a regional scale, while for the high-resolution local model, the distance between nodes is 200 meters. Thus, the nodes represent the boundaries of the tetrahedrons which display the major thermal properties (appendix A_5). Among these, the temperature is extrapolated for each depth from the starting model and the average temperature gradient at the interrogated depth. Regarding the geographical extension, the regional dataset covers a 300 x 400 km area of the Southern Italy domain from Lon 38° to Lat 35° (WGS84) with a resolution of 5 km between the nodes of a regular grid, while the high-resolution area of about 930 $km^2$ (Lat 37.20° Lat 37.21° WGS84) is made up of an irregular grid with 200 meters between the nodes, located in the south-eastern zone of the regional context (Hyblean domain). Both models display a higher lateral boundary resolution (ratio of 2/5).

The obtained database has been implemented as a files archive (raw dataset and processed maps) in the repository section inside the web page (Figure 5.7) and made readable as a text file within the computerized structure (PHP, SQL, JAVA language) to generate the interactive version of the database.


*Figure 5.1– Visual identity of the STORAGE project*

## 5.3 Methods

The structure used to manage the database (described in section 5.2) is controlled using a PHP (Hypertext Pre-processor) code that allows the visualization and querying of the best-fit thermal model described in chapters 3 and 4. PHP is an open-source scripting language, run on the server side, which is mainly used to create dynamic sites. Every operation performed on the Web involves a client and a server. A client is a device (such as a browser) that requests a remote server. The remote server, through a scripting language (such as PHP), interprets the client's request and sends a response (such as an HTML page, a JSON object, or an XML) to the client. At this point the client can interpret, in turn, the response received and provide it to the user; in the case of the browser, it will receive an HTML page which will be shown to the user. PHP is a language for server-side scripting, which is a language that resides in a remote server and which at runtime interprets the information received from a client thanks to the Web server, processes it, and returns a result to the client that has formulated the request (Figure 5.2). For example, suppose you access a page on a website where you can log in. From our browser within a page (for example www.storageproject.it) we will enter our credentials for authentication.

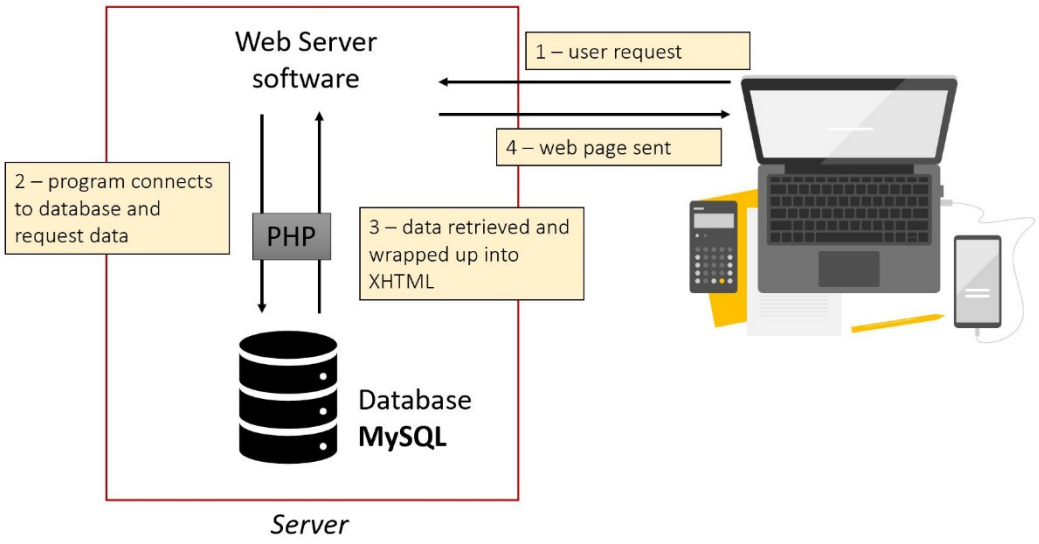


*Figure 5.2 – Client-server workflow for STORAGE project.*

The actions that are performed are the following:

(1) the browser requests the credentials to the remote server via the HTTP protocol;
(2) the Web server receives the request and interprets it, verifying that the data sent is correct;
(3) the Web server returns a response to the client which may be different depending on whether the requested resource is available or not.

What PHP does is to precisely process the data transmitted through an HTTP request and provide an adequate response to the client. In our case, the language has the task of verifying that the login data are correct and returning a different response depending on the validity of the information received. While standard markup language for documents designed to be displayed in a web browser (client-side languages), such as HTML, CSS, or JavaScript, is interpreted directly by the browser when opening a page, PHP code already runs on the web server, where PHP scripts generate HTML statements, which are then transmitted to the browser. The latter does not receive the actual code (the PHP script), but simply the result of the executed script. The main scope of PHP is server-side programming. In addition, the SQL language used for the query operation and the Java script implemented in the Maps features (API Google) management have been implemented. The scripting language is characterized by wide database support and can be used on any platform, which allows to modify the source code (Figure 5.3).

In detail, the *Storage Project* PHP code is structured as follows:

1. Connection to the starting database (input of T-depth CSV files for the regional and local scale model);
2. visualization tools on the home page (for example the coordinates management slot in WGS84 and UTM33N geographical reference systems or the map viewer tool);
3. validation of the investigated database according to the possible regional or local scale observation;
4. control on the closest nodes to the clicking area of the map (through the calculation of the mean quadratic difference on the four points closest to the point of interest);
5. management of the buffer zone of the models; in this regard, the buffer of 0.11 ° sexagesimal degree has been introduced to neglect values outside the boundary from the calculation.

After the analysis of the starting model outputs, the significant temperature-depth value slices (in terms of geothermal exploitation) have been extrapolated. Thus, trough the implementation of the database in the PHP code, it will be possible to perform spatial queries on the thermal field obtained from the preliminary modelling phase (see Chapter 2). The thermal model on a regional scale will be managed by various functions with the possibility of increasing the resolution on a pilot area, which is defined as micro-zonation domain.

```
12
13  function exec_query( $query ) {
14      global $link;
15      $results = mysqli_query($link, $query);
16      $r = mysqli_num_rows( $results );
17      if ( $r == 0 ) {
18              return array();
19      }
20      else {
21          $ret = array();
22          while( $item = mysqli_fetch_assoc( $results ) ) {
23              $ret[] = $item;
24          }
25          return $ret;
26      }
27  }
28
29
30      $situazione = 0; // valori non settati
31      $celta = "";
32      if(isset($_GET)) {
33          if(isset($_GET["scelta"])){
```

*Figure 5.3 – Example of the PHP code used in Storage project.*

## 5.4 Web Portal

To improve the distribution and develop a web portal for the exploration of geothermal resources in Sicily, the best-fit thermal model, obtained from the first modelling phase, has been uploaded within the set-up code, providing several visualization tools. The "Web portal" section of the online platform is the most important aspect of the entire project and consists of a page characterized by a division dedicated to the interactive map which displays the study areas (blue rectangle for the regional domain and red one for the local domain in Figure 5.5d) and a section related to the outputs (Figure 5.6a-b-c). The information division is made possible by visualizing a query section structured as follows: coordinates query slot and area (district) slot. Despite the wide geographical extension of several municipal areas, the research tool was inserted to evaluate the average temperatures (Lat and Long of the municipal area from ISTAT), but also with the aim at the future implementation of municipal high-resolution geothermal zonation (Figure 5.5b).

There are primarily three methods for handling portal queries:

1. managing the municipalities' latitude and longitude values in Sicily Figure 5.5b);
2. exerting control over latitude and longitude values (Figure 5.5c);
3. selecting the desired location on the interactive map (Figure 5.5d).

Based on the choice, it will be possible to obtain the temperatures (at different depths) at the selected point (example in Figure 5.6c) as well as the temperature gradient (average for the selected depth). The calculation of the temperature in areas without data coverage derives from the linear interpolation between the four nodes closest to the selected point according to a weighted average (Figure 5.4). The output also incorporates information regarding the geographic location of the nodes of the grid (if we are considering the dataset from regional modelling or local micro-zonation modelling Figure 5.6a), the depth below ground level, the temperature values per each point, the depth below sea level, the average gradient for a specific thickness, and the average gradient for the first 5 km below ground level. In addition, to facilitate the correlation between temperature and depth for a drilling project the temperature-depth values below ground level were implemented (Figure 5.6c).

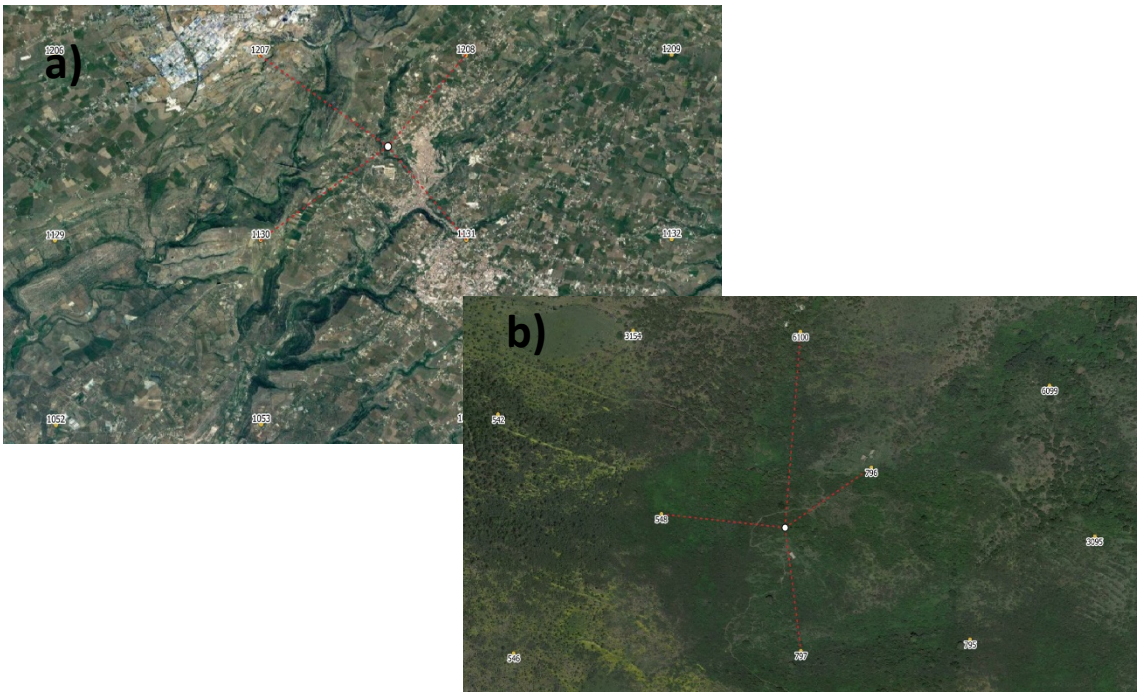


*Figure 5.4 – Nodes interpolation according to a weighted average between the four closest values to the selected point in the area. a) example of regional data interpolation (lateral resolution of 5 km); b) example of local domain interpolation (geothermal microzonation area with lateral resolution of 200 m).*

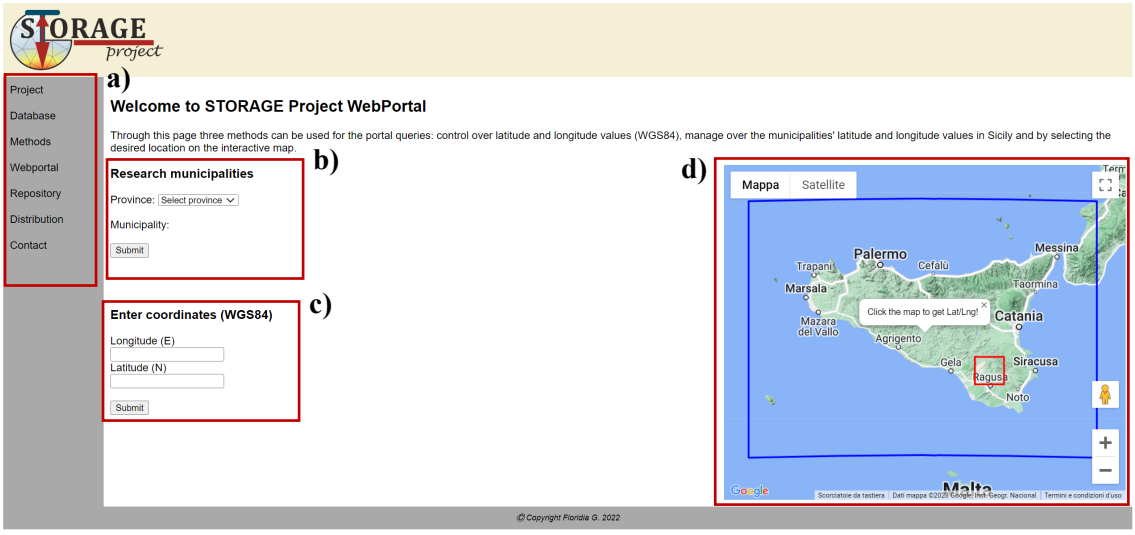


*Figure 5.5 – Web portal page. a) bullet interactive menu; b) research by municipalities tool; c) research by coordinates; d) interactive maps (blue polygon: regional modelling area, re polygon: local domain area).*

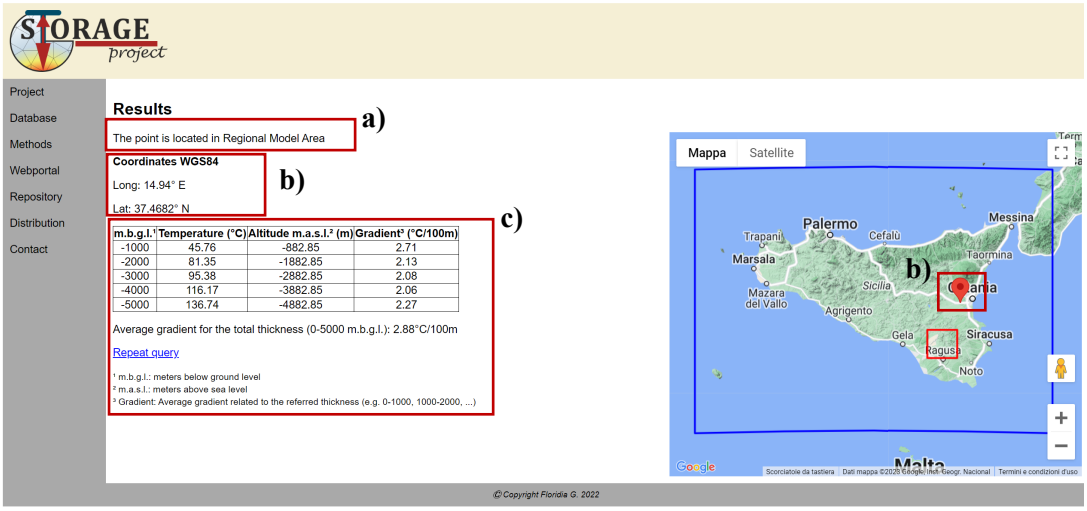


*Figure 5.6 – Outputs of the research. a) location of the selected point in terms of referred database; b) location of the selected point (coordinates in WGS84); c) tables with numerical results; d) interactive maps (blue polygon: regional modelling area, re polygon: local domain area).*

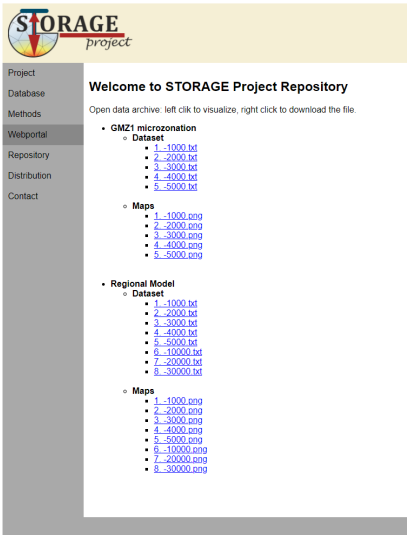


*Figure 5.7– On-line repository: visualization and downloading of the regional and local dataset obtained from the thermal modelling stage.*

## 5.5 Distribution

The first release of the STORAGE project is implemented in an online platform using the domain at the following link: https://storageproject.it. One of the most important aspects of the STORAGE project is its full accessibility, as well as the open future implementation (including third parties) with increasingly updated data deriving from high-resolution local case studies. The updated dataset will be useful for improving the reference thermal model, with the aim of obtaining a more and more consistent dataset. For this reason, the developed code allows the implementation of multiple models as well as the possibility of integrating multiple reference geothermal properties. In this way, it will be possible to integrate different datasets, making the portal updated and complete. In the first phase, the distribution of the web page will be subject to limitations, such as prior registration with credentials, and the requests must be supported by scientific reasons. In addition, in this preliminary stage, temporary credentials have been applied (user: user; password: StorageProject2022@). At a later stage, the portal could take on the characteristics of a real open source.

# 6 Chapter 6 – Industrial Application

The final stage of the research project aims at investigating its industrial applications, together with a study of the development of new materials for the geothermal resources exploitation, referred mainly to the low enthalpy geothermal systems. Throughout the collaboration between the University of Catania and the EarTherm company, the investigation of innovative compounds characterized by Carbon Fibre (CF) as an innovative additive for the development and configuration of the probes and grout in a geothermal heat pump system (hereafter GHPS) has been analyzed. In this regard, the experiments mainly concerned:

- the improvement of the thermal properties by the research and development of new configurations for vertical geothermal probes, by considering CF mixed compounds implemented in standard polyethylene probes;
- the improvement of the mechanical and thermal characteristics of standard grout used as filling boreholes material in low enthalpy geothermal plants, by adding CF mixed compound.

The use of Carbon Fiber powder, mainly derived from industrial waste, constitutes an essential element for the development of a circular economy, and supports the European challenges about the “End of Waste” process and reduction of environmental impact, suggesting new perspectives for economic development and sectorial work.

In this section, the applied methodology and the obtained results will be described.

## 6.1 State of play

Although the efficiency of a shallow geothermal installation is chiefly based on the chemical and physical characteristics of rocks and hydrogeological aspects of the subsurface, the total heat extracted from the subsoil also depends on the intrinsic thermal exchange characteristics of probes and grout materials. New configurations and solutions aimed at enhancing the performance of components are therefore of considerable interest in this field of research. Innovative combinations of different materials and configurations are therefore necessary to improve mechanical properties and thermal response, and to preserve the exceptional workability and commercial advantages of the finest elements

available on the market. The shallow portion of the subsoil exhibits significant heat stored, since below an average depth of 20 m the temperature remains constant showing values comparable with the average annual temperatures at the surface depending on the latitude (Midttømme, K. et al., 2008, Banks, D., 2009). This represents an optimal condition for the use of heat exchanger systems with open or closed-loop configurations to supply thermal energy (Banks, D., 2009). Currently, significant thermal dissipation occurs between the soil, the bentonitic grout as filler, and the heat exchanger, which finally causes a reduction in the performance of the entire system's efficiency. Standard materials, currently used in the market, at present do not allow optimal heat exchange between the soil and the system. Therefore, in order to improve the whole performance of the geothermal installation, the above-mentioned components (probes and grout materials) should be enhanced. The experimentation of new materials for improving the characteristics of standard geothermal probes and the search for new grout mixed materials have been extremely limited throughout recent years. For example, polyethylene is currently used in the production of low enthalpy geothermal probes (DIN 8074 standard) (Kavanaugh, S.P. et al., 1997). It has completely replaced metallic materials such as copper and stainless steel used in past installations, which, although characterized by high thermal conductivity, have shown technical problems of a different nature (for example stray currents, corrosion), coupled with expensive production costs (Banks, D. et al., 2009, Stober, I. et al., 2013). As a matter of fact, polyethylene is a polymer, with good chemical composition, thermal expansion, flexural strength, compressive strength, and limited production costs. In this regard, all properties of polyethylene, such as ductility, flexibility, transportability on site, workability and easy installation make it the best compromise in terms of quality/cost ratio for any type of GHPS (Stober, I. et al., 2013, Vasile, C. et al., 2005). However, polyethylene exhibits very low thermal conductivity between 0.40 W/mK and 0.45 W/mK. Being basically a thermal insulator, it can be considered scarcely adequate for heat exchange purposes (Abesser, C. et al., 2010, Ball, D.A. et al.,1983). Among the components affecting the performance of the whole geothermal system, alongside the configuration of the geothermal probes (hybridized materials still little explored), the chemical-physical characteristics of the filling bentonitic concrete, making contact between the surrounding ground and the heat exchangers, represent a still little explored issue (Abesser, C. et al., 2010). It has the main function of transmitting heat and responding to specific conditions, like particular geological settings (Ball, D.A. et al.,1983, Badenes, B. et al., 2020,

Mendrinos, D. et al.,2017), where it must follow specific characteristics of mechanical resistance, ensuring the waterproof insulation of the system. Excellent thermal conductivity and specific mechanical characteristics are not ensured by standard cements currently available on the market. For example. Ball, et al.,1983, Badenes, et al., 2020, Mendrinos, et al.,2017, Viccaro, 2018 point out mixtures of aluminium, graphite, bentonite and superplasticizer materials which are useful for the enhancement of the entire system. For instance, the results illustrate how graphite increases by about three times the mechanical and thermal conductivity characteristics of the cement mortar, as well as optimizes the efficiency and the consequent cost reduction of the entire plant system. With the aim of improving the heat exchange without neglecting the mechanical properties of the materials used for probes and grouts, it was possible to evaluate the response of materials such as Carbon Fiber (CF) applied to the geothermal systems' compounds.

## 6.2 Carbon Fiber Powder: an innovative additive for hybrid geothermal systems compounds

The limitations due to the isolating properties of the materials currently used in geothermal systems (geothermal probes and grout) led us to the experimental idea of using alternative and innovative mixed compounds (Stober, I. et al., 2013, Mendrinos, D. et al.,2016). The research of new solutions which can be useful to improve the heat exchange performances of geothermal heat pump systems (GHPS) regarding the probes and grout filling materials, encouraged our research towards hybridized geothermal components (Badenes, B. et al., 2020, Mendrinos, D. et al.,2017) and hybrid grout (Viccaro, 2018). Indeed, it was chosen to consider polyethylene probes and pure standard grout doped with Carbon Fibre Powder (a mixture of pure carbon fiber and resin). Carbon Fiber powder (hereafter CFP), due to its workability characteristics, is suitable for use as an additive material useful to 1) set new configurations on polyethylene geothermal standard probes; 2) improve the heat exchange characteristics of mortars filling geothermal boreholes in low enthalpy geothermal systems (Katzman, H.A.et al. 1994, El-Hage, Y. et al., 2018). In addition, the utilization of CFP as a new material for geothermal applications is part of a new vision involving the development of innovative systems compounds resulting from possible industrial waste. In this regard, the application of CFP

provides circularity in the industrial production processes supporting the actual sustainable trend of the “End of Waste” concept.

Pure Carbon Fibre is a material characterized by exceptional mechanical properties and high thermal conductivity (~14 W/mK) (Bhatt, P. et al, 2017, Katzman, H.A. et al., 1994, El-Hage, Y. et al., 2018) that would allow a significant increase of the thermo-mechanical performances of the geo-exchange compounds. These improvements make the hybridized compounds highly suitable for their use as efficient components in geothermal installations, reaching on the whole better economic competitiveness than standard materials on the market (Viccaro, M., 2018). CF shows particular physical and mechanical characteristics that, properly applied on a polymeric material such as, for example, standard polyethylene, allow a significant increase in the thermomechanical performance of the geo-exchange system. It is important to note that the exclusive use of CF for the construction of the geothermal probes cannot be considered as a realistic solution, since the required economic investment would be too high and cannot be compensated even considering the significant benefit in terms of thermal conductivity and heat exchange. In addition, the CF pipes can only be made of rods, as the finished product is rigid and consequently lacking in flexibility, and also with a limited length (6 m–max value), implying the use of hydraulic joints and not allowing any easy procedure during transport and any movement in the installation site.

The research in testing a new composite product combining good physical-mechanical characteristics of polyethylene and high thermal conductivity of CF has been conducted with the aim of rethinking the classic single and double U geothermal probes (Mendrinos, D. et al.,2017, McCray, K., 1997, Roumeli, E. et al. 2014). Since polyethylene does not appear as the optimal material for heat exchange in the subsoil, the identification of materials with higher thermal conductivity (>1 W/mK), compared to the polyethylene, can represent a turning point in the primary heat exchange in GHPS. CFP was taken into consideration in order to design such new components (section 6.3.1). In addition to the contribution of geothermal probes setting in the heat exchange, the entire operation of a low-temperature geothermal system, and in particular the heat transfer efficiency between subsoil and probes, is also significantly influenced by the nature of the filling mortar (Mahmoud, M. et al., 2021; Viccaro, M., 2018). The standard filling materials (current on the market) do not usually guarantee an optimal heat exchange; for this reason, it is important to develop new materials to improve heat exchange, as well as to maintain low

production costs. With the aim of improving heat exchange between probes, grout and subsoil, the use of mortars hybridized with carbon fiber was investigated also in this case. The improvement of the thermal characteristics and the experimentation on mechanical and thermal properties on CFP additive grout materials for GSHP systems result in a very eligible mixture that can be used as an effective sealing grout into boreholes for geothermal probe installations. Furthermore, the utilization of CFP compounds both for geothermal probes configuration and for its mixing with pure materials in filling grouts leads to an exponential increase in GSHP system efficiency, as well as in the recycling process minimizing the environmental impact (<CO2 emissions). The final production cost becomes a very important aspect, as it governs the entire process of setting up geothermal systems. In fact, although pure materials have a non-negligible cost (Naslain, R., 2000), their purchase and/or use in a not completely pure form could certainly contribute to lowering the final costs. In addition, potential economic benefits, especially in the recycling process of waste materials and in the development of a circular business model related to the recycling of CF, have been investigated.

## 6.3 Methods

### *6.3.1 Development and testing of Innovative Probes*

The testing phase of innovative setup solutions has provided various experimentations to determine the best configuration for the implementation of CFP and subsequently to prove the thermal response of a prototype system.

In this regard, by means of EarTherm Laboratory equipment (Figure 6.1a), a series of grooves with a constant section (width of 1 cm and depth of 1.5 mm) have been carried on the circumference of the 3-m-long polyethylene pipe. These grooves have been then filled with CF powder developing two different settings: (1) I50 configuration; and (2) I80 configuration. These configurations have been respectively based on 5 radial grooves coated with CFP, with a defined distance of 50 cm (I50), and 3 radial grooves coated with CFP with a defined distance of 80 cm (I80) (Figure 6.1b). According to the testing protocols (International Ground Source Heat Pump Association, 2016), before the thermal characterization, a first hydraulic testing phase, with an operating pressure of 5–6 bars, was carried out on each probe. Subsequently, thermal conductivity tests were performed to compare the heat exchange performances of the hybrid CF-polyethylene (I50–I80) and compared them to the standard-polyethylene probes currently available on

the market (ST). The methodology used to measure the exchange temperature consists of an electrically operated heating cable with a heat output of 49 W/m and a maximum temperature of 58.7°C, fixed with 3 clamps, arranged and spaced from each other with a pitch of about 6 cm (Figure 6.2a) on the entire pipe. The thermal test has been carried out in a static fluid regime, and each probe sample has been filled with 1.6 liters of water. This configuration allows the investigation of the heat transfer via the conduction process. The thermal test is divided into three steps:

1. heating phase to verify the response times of the thermal conductivities during the transmission of heat by conduction;
2. cooling phase to evaluate the thermal dispersion by conduction;
3. heating/cooling phase in order to determine the possible effect of thermal inertias.

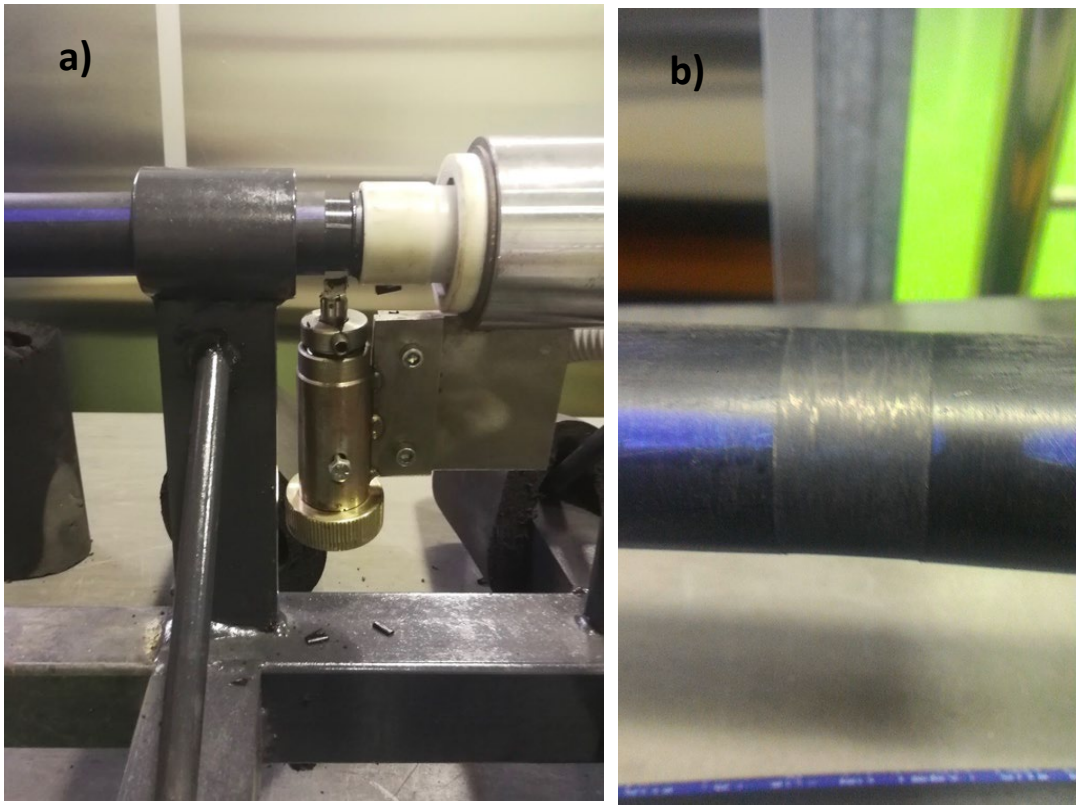


*Figure 6.1- a) Setup of the thermal test for the hybrid polyethylene probe and (b) detail of the temperature detection system S3 and heating cable component.*

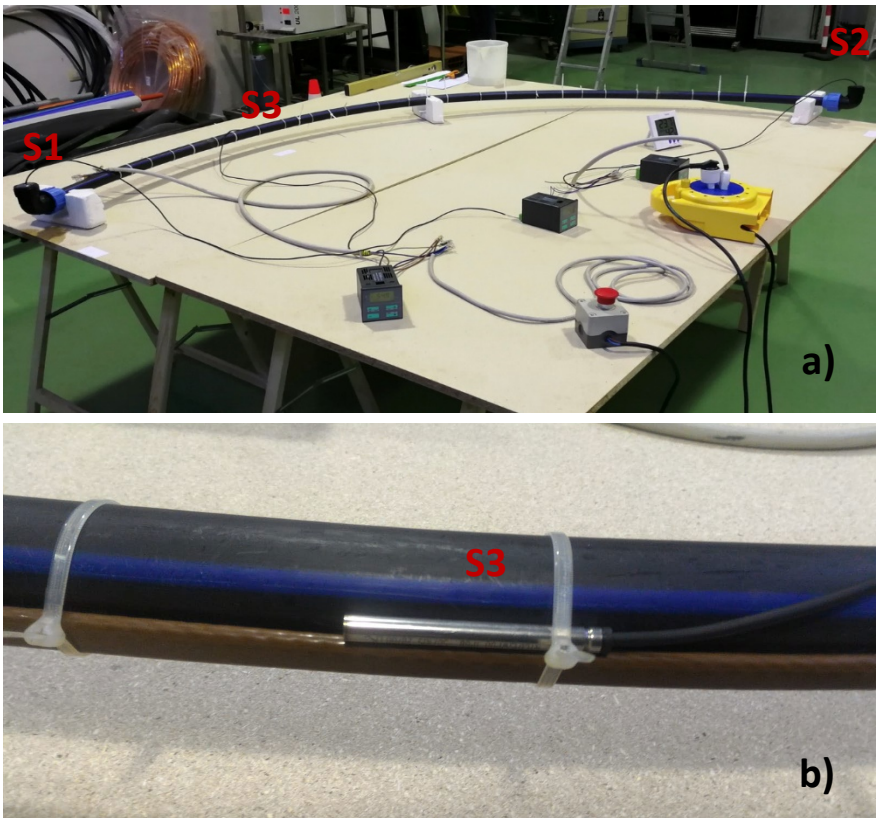


*Figure 6.2- Production of the innovative probes with radial carbon fibre (CF) rings and (b) finishing of the radial CF rings.*

### *6.3.1.1 Geo-Exchange Prototype System*

Based on the best thermal output configuration, after the hydraulic and thermal analysis, it was possible to develop the prototype geo-exchange systems which are useful to reproduce, on a small scale, the heat exchange that occurs between the elements of a geo-exchange system: subsoil - grout - probe (Wang, S. et al, 2020, Shonder, J.A., 1999).

For the development of the prototype system, "U" type geothermal probes were incorporated and cemented inside two PVC cylinders of 1.05 m in height and a diameter of 200 mm. In particular, a standard polyethylene probe cemented inside a premixed commercial mortar (Figure 6.3a) and a I50 radial probe fixed inside a hybridized bentonite mortar (1.5% graphite additive) (Figure 6.3b) have been analysed.

In order to obtain a realistic probe-mortar assembly, the filling grout underwent a 28-day curing process inside a PVC mold. After the drying phase, the cement-probe column was installed inside a larger diameter column equipped with a heating cable characterized by an operating range that goes from a starting temperature = 16.9 ° C and a switch-off temperature = 17.2 ° C (Figure 6.3c).

The empty space between the column and the pipe containing the heating cable (equal to 5.5 cm per side) has been completely filled with soil, representing the source of heat propagation. The thermal tests conducted on both the standard and innovative configurations involved three different configurations: 1) no-water (Figure 6.4a), 2) static water regime (Figure 6.4b) and 3) dynamic water regime (Figure 6.4c). To analyze the temperature variations, three probes were used as follows: S1 and S2 were placed to measure the inlet and outlet temperature respectively of the fluid inside the probe and S3 was placed 21 cm deep inside the ground (Figure 6.4).

Subsequently, to verify the behaviour of the cement-probe system in real conditions, an additional heat exchange element (plate heat exchanger) equipped with 2 independent circuits was considered: a primary circuit consisting of a closed loop system connected to the probe and a secondary circuit consisting of an open loop network (Figure 6.4c-d). Also, in this case the S1 and S2 probes, with the exception of S3, were used to analyse the temperature variations (Figure 6.4, Table 6.1).

*Table 6.1- Experimental data resulting from tests on the geo-exchange prototype system.*

| **Test Condition** | **Duration (min.)** | **Step (min.)** | **Configuration** | **S1 T (°C)** | **S2 T (°C)** | **S3 T (°C)** | **Configuration** | **S1 T (°C)** | **S2 T (°C)** | **S3 T (°C)** |
|---|---|---|---|---|---|---|---|---|---|---|
| | | 0 | | - | - | 14.8 | | - | - | 15.3 |
| **No Water** | 240 | 60 | | - | - | 18 | | - | - | 17.5 |
| | | 120 | | - | - | 17.7 | | - | - | 17 |
| | | 240 | | - | - | 17 | | - | - | 17.5 |
| | | 0 | | 15.9 | 15.9 | 15.9 | | 15.9 | 15.9 | 15.6 |
| | | 30 | | 15.9 | 16 | 18.7 | | 16.2 | 16.1 | 16.5 |
| **Static** | 180 | 60 | | 16 | 16.1 | 17.7 | | 16.3 | 16.2 | 17.5 |
| | | 120 | | 16.2 | 16.2 | 18.5 | | 16.7 | 16.6 | 17.1 |
| | | 180 | | 16.4 | 16.4 | 17 | | 16.9 | 16.8 | 17.1 |
| | | 0 | **Standard Prototype** | 15.3 | 15.2 | 15 | **Innovative Prototype I50** | 15.3 | 15.2 | 14.8 |
| | | 60 | | 18.5 | 17.5 | 17.4 | | 19.1 | 18.5 | 15.9 |
| **Dynamic** | 240 | 120 | | 19.8 | 18.5 | 17.7 | | 20.7 | 19.5 | 17.7 |
| | | 180 | | 20.8 | 19.1 | 18.5 | | 22.1 | 20.4 | 18.2 |
| | | 240 | | 21 | 19.3 | 18.1 | | 22.3 | 20.7 | 18.2 |
| | | 0 | | 13.6 | 11.7 | 15 | | 13.6 | 11.6 | 15 |
| **Primary/** | | 30 | | 14 | 11.9 | 17.5 | | 14.7 | 12.2 | 16.4 |
| **Secondary** | 150 | 35 | | 12.2 | 12.5 | 17.8 | | 12 | 11.7 | 16.8 |
| **System** | | 60 | | 12.6 | 12.4 | 16.9 | | 12.7 | 12.2 | 18 |
| | | 150 | | 14.6 | 12 | 17.6 | | 15.2 | 12.7 | 17.6 |

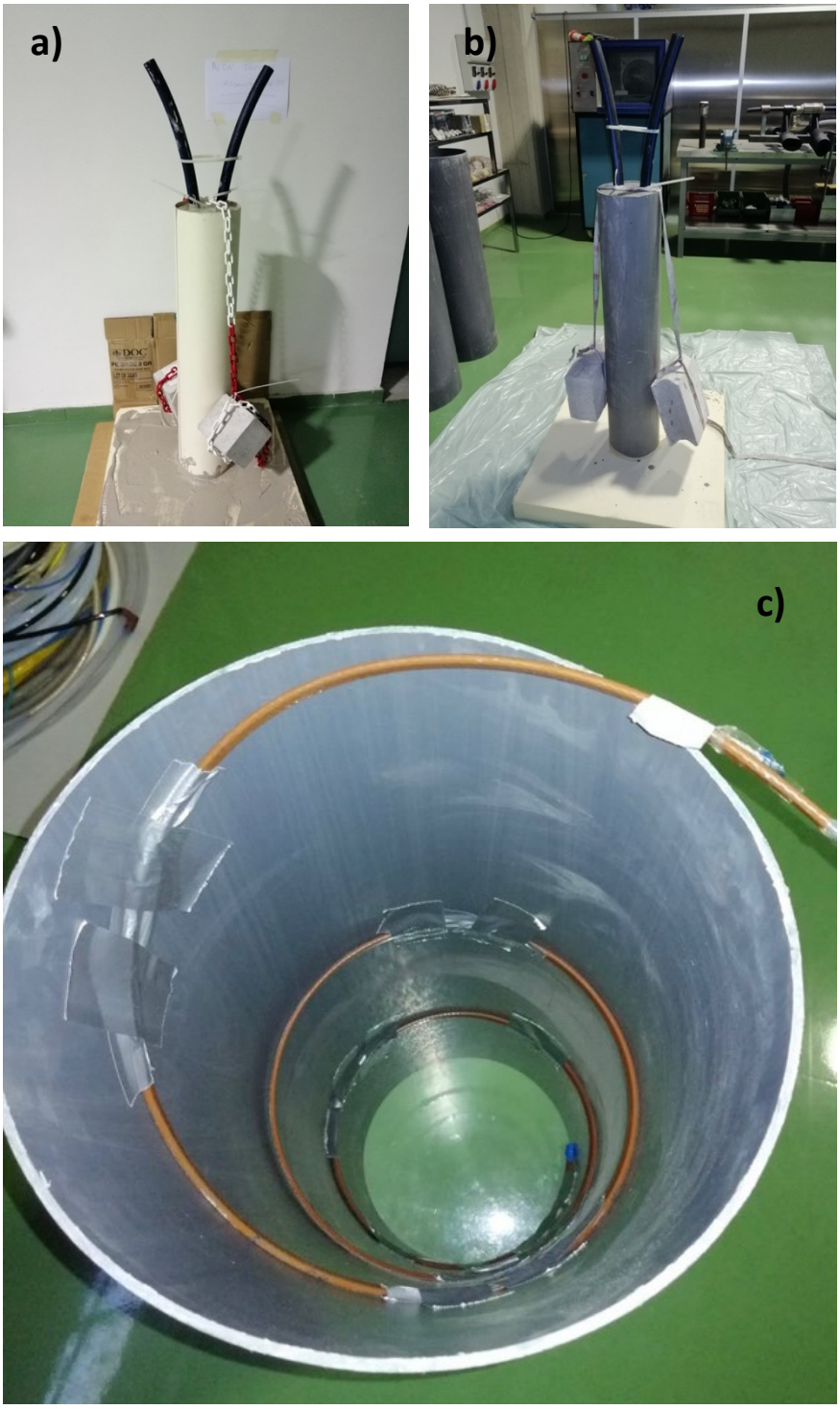


*Figure 6.3 - (a) Preparation of the standard system for the thermal response test; (b) preparation of the innovative system for the thermal response test; and (c) heating cable configuration.*

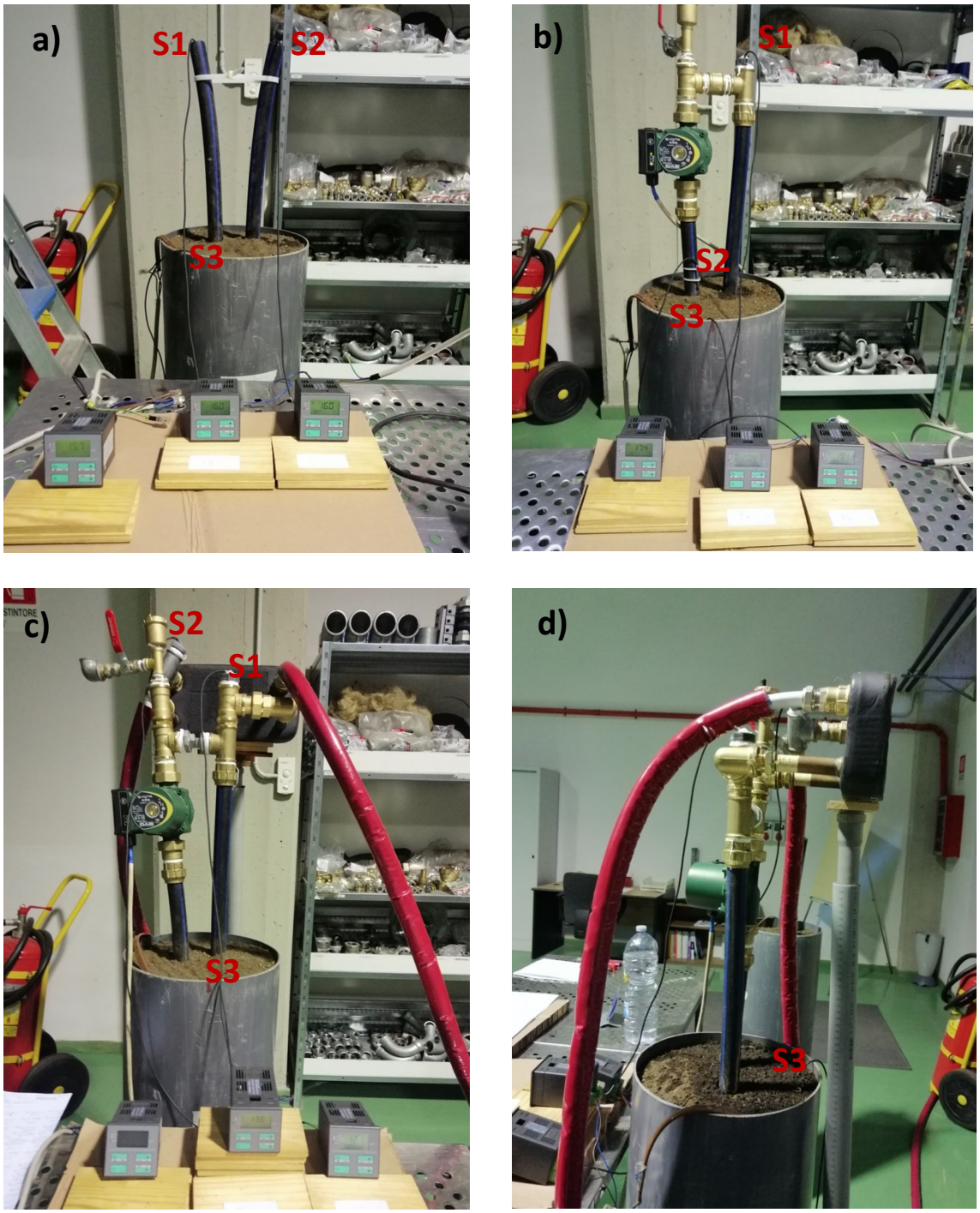


*Figure 6.4- Geo-exchange prototype configuration: (**a**) no-water and static initial condition; (**b**) dynamic regime test; (**c**) primary and secondary circuit configuration; and (**d**) details of the supplementary double circuit device.*

### *6.3.2 Developing and testing of hybrid grout*

With the aim of identifying the best grout mixing for geothermal purposes, experimental tests in the EarTherm laboratories were carried out for the determination of the mechanical and thermal characteristics of the filling grouts. The starting materials consist of standard bentonite grout already on the market with apparent density between 1.35 kg/dm³ and 1.79 kg/dm³, depending on the water/solid ratio used for the preparation of the mix. The characteristic values of the commercial mortar were determined with a high-speed mixer under laboratory conditions with a fill water/binder value of 0.44 (ratio). The fluidity declared for 1000 ml of suspension is 45 s (Marsh Cone Test with 10 mm nozzle according to the drainage regulations) (UNI 11152, 2005). The technical characteristics specified for the standard mixture report a flexural strength ~ 2 N / mm$^2$ and a uniaxial compressive strength ~ 6 N / mm$^2$ at 28 days (according to the test standard DIN 18136:2003–2011, 2011), as well as thermal conductivity ≥ 2 W / mK. To improve the thermal and mechanical properties of the standard materials, the experimental mixture has involved the addition of the carbon fiber powder composed of 60% pure carbon fiber (estimated thermal conductivity > 50 W/mK) and 40% resin (CFP) to the starting grout. Subsequently, the two different mixtures (standard and additivate one) were subjected to mechanical and thermal analysis. In detail, the tests were conducted on a pure standard grout and a standard grout with the addition of 5% CFP. The preparation of the two solutions for the subsequent tests was carried out by accredited laboratories according to the standards procedures (UNI EN 196-1:2016) (properties show in Table 6.2).

*Table 6.2- Components used for the preparation of the bentonitic grout mixtures with CFP as additive (ST% no CF powder; CFP5% mixture with 5% of CFP).*

| **component/weight** | **Pure material mixture ST%** | **Doped mixture CFP%** |
|---|---|---|
| Starting material | 1000 g | 950 g |
| CF material | 0 | 50 g |
| Water | 440 ml | 440 ml |

The tests were performed in two different steps:

1) mechanical tests (uniaxial compressive strength tests and flexural strength tests);

2) thermal conductivity measurements, according to UNI EN 196-1: 2016.

To run the mechanical tests, automatic equipment was used and based on different equations:

$$Rc = \frac{Fc}{a \cdot b} \qquad \textit{Equation 6-1}$$

where a and b fix the surface of the auxiliary plates to 1600 $mm^2$ (40 × 40 mm), while Fc is the maximum value of the load causing the collapse, for uniaxial compressive strength analysis, while the flexural strength (Rf), also called modulus of rupture, was obtained from the formula of the linear elastic regime:

$$Rf = \left(\frac{1{,}5Ff}{b^3}\right) * l \qquad \textit{Equation 6-2}$$

where l = 100 mm represents the distance between the supports; b = 40 mm coincides with the side of the section of the square prism. Ff is the maximum value of the collapse load measured during the test. 6 samples for each compound were considered for the evaluation of the uniaxial strength, while 3 samples prepared of standard material and 3 of mixed mortar were considered for the evaluation of the flexural strength. The materials response was completed 14 days and 28 days after the sample preparation (Table 6.3). The reduction of water percentages in the samples after the first (14 days) and the second step (28 days) causes significant increase in the strength of the sample.

*Table 6.3- Compressive strengths (Rc) at the fracture point obtained on the starting pure material and doped bentonitic grout (+5 % of carbon fiber). Ff is the strength applied at the center of prismatic samples.*

| **Pure starting material** | **Ff (N)** | **Rc (N/mm$^2$)** |
|---|---|---|
| 14 days | 4370 | 2.73 |
| 14 days | 4680 | 2.93 |
| 28 days | 4850 | 3.03 |
| 28 days | 4870 | 3.04 |
| 28 days | 5860 | 3.66 |
| 28 days | 5740 | 3.59 |
| **Starting material + 5% CF** | **Ff (N)** | **Rc (N/ mm$^2$)** |
| 14 days | 8350 | 5.22 |
| 14 days | 8290 | 5.18 |
| 28 days | 12640 | 7.9 |
| 28 days | 12870 | 8.04 |
| 28 days | 13130 | 8.21 |
| 28 days | 13280 | 8.3 |

The second and final analytical step involved the experimental determinations of thermal conductivity (Table 6.4). Thanks to the collaboration with the Technical Physics Laboratory of the University of Catania, the 180-second test was performed with a non-stationary hot wire method according to ASTM E 1530, 2019. During the heat transfer process from the instrument to the sample, the temperature rise is less than 20 ° C without the material properties being changed during testing (Viccaro, 2018, Fukai, et al., 2000, Lee, et al., 2012).

*Table 6.4- Thermal conductivity obtained from measures on the starting and doped (+5% of CF) bentonitic grouts.*

| | **Pure starting material** | **Starting material + 5% CF** |
|---|---|---|
| **Number of measurements** | **λ (W/m K)** | **λ (W/m K)** |
| 1 | 1.82 | 1.92 |
| 2 | 1.87 | 1.96 |
| 3 | 1.94 | 2.01 |
| 4 | 1.82 | 1.92 |
| 5 | 1.86 | 1.90 |
| 6 | 1.94 | 1.93 |

## 6.4 Results

### *6.4.1 Innovative probes (I50-I80)*

From the development and analysis conducted on the hybridized geothermal probes (section 6.3.1), the CFP rings added to a standard polyethylene probe affect not only the heat exchange but also the hydraulic properties of the final product. Starting from the hydraulic testing outputs, it is clear how the entire circuit under pressure for about 2 h did not produce any significant sign of deformation (swelling) or failure in hybridized probes. In fact, pumping gradually up to the pressure of 28 bar (in the end up to 50 bar), from the initial pressure of 5.2 bar, the circuit showed considerable resistance compared to the standard probe where permanent deformations under operating pressure of 16 bar (Badache, M., et al., 2019) would be obtained. Despite the high resistance of the CF rings, the section in between displays a considerable sausage effect. The high breaking strength of a hybridized probe is attributable to the presence of the CFP coating rings which, sufficiently spaced from each other, divided the overall length of the polyethylene pipe into shorter segments and almost doubled the operating pressure of the probe. From the observation of the thermal tests, it is possible to see significant differences in the thermal response of the standard material compared to innovative configurations (I50 and I80). The application of carbon fiber powder, in the radial direction, increased the thermal output of the probes. In particular, it was observed that the distance of the carbon fiber rings also contributes to the thermal performance dissimilarity. During the heating phase, the I80 probe shows a heat output of 1.5 ° C (+ 3.62%) higher than the standard probe, while the I50 probe shows a greater increase of 1.9 ° C (+ 4.6%) compared to polyethylene (see Figure 6.5).

During the heating/cooling testing phase, the I80 probe showed an increase of 1.7% (+0.6°C) compared to the standard probe, while the I50 probe had a thermal output higher than 5.4% (+1.9) (Figure 6.5). Finally, according to the thermal outputs of the different settings (I50-I80), I50 was considered the best configuration in terms of thermal output under multiple test conditions.

For this reason, with the aim of testing the thermal response in real conditions, a prototype geothermal well was developed considering the I50 configuration, having been later examined by several thermal tests (explained in section 6.4.2).

From the thermal response tests on the developed prototype (CFP-I50), the results show an increase in heat exchange of about 3% during the heating phase of the static water test. Considering the second step of the test (running water - dynamic condition), the heat transfer increase reaches even higher values (+ 6%) providing water at 1.3 ° C more than a standard system with a temperature increase evidenced at any point of the test (Figure 6.6).

In conclusion, the hybrid system allows a better and more effective heat exchange with the subsoil in a dynamic condition, providing a temperature increase in the water output comparing to a standard system.

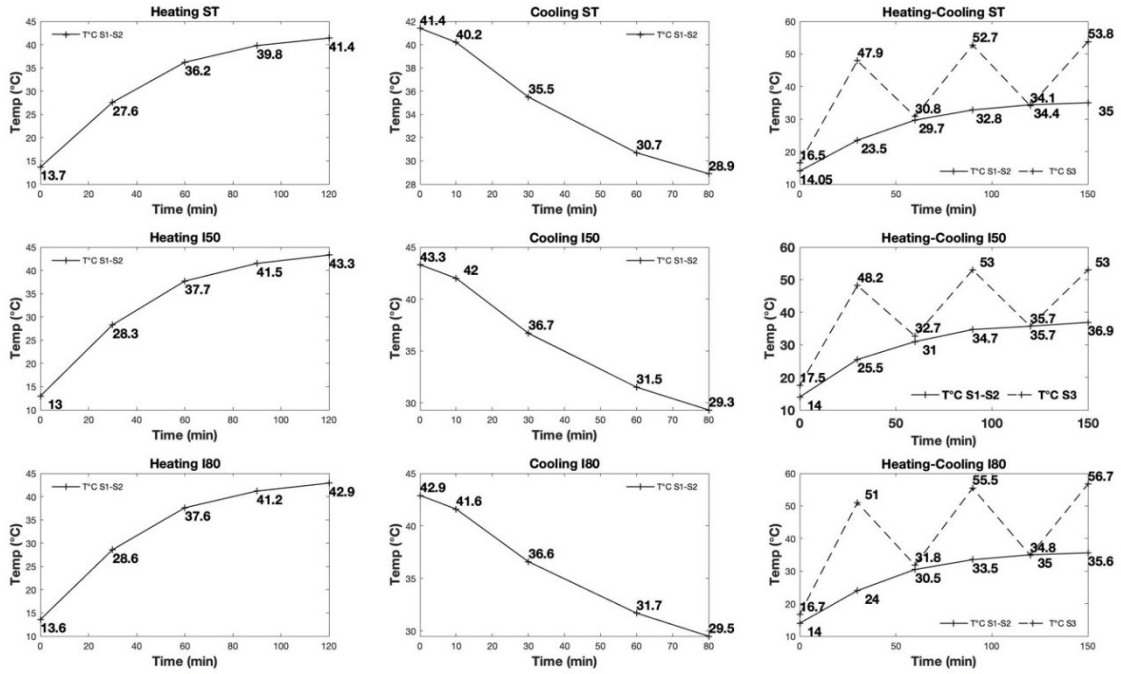


*Figure 6.5 - Results of the thermal test in standard (ST) and innovative probes (I50–I80): heating step, cooling step, heating-cooling step.*

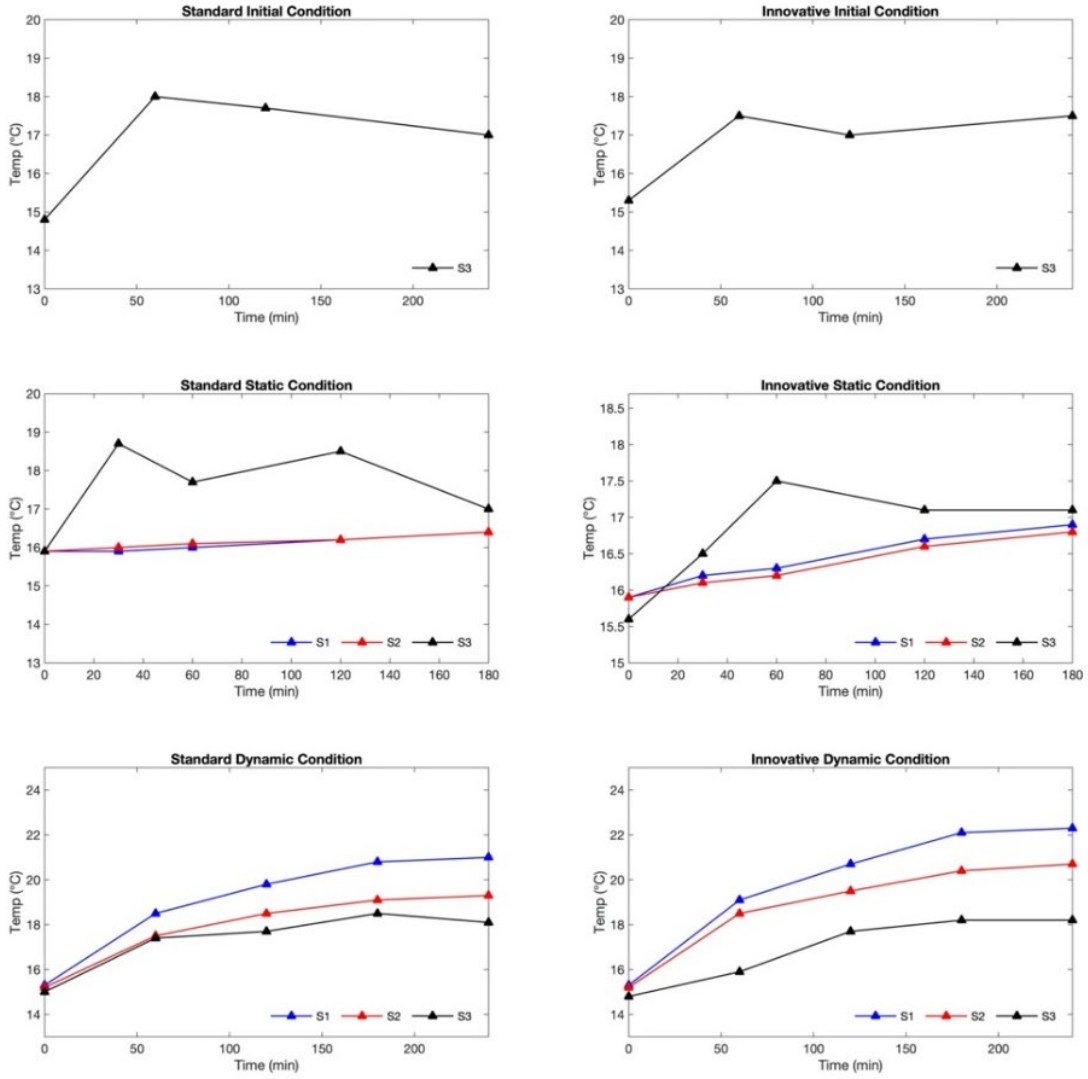


*Figure 6.6- Results of thermal test in standard (ST) and innovative geo-heat exchanger prototype (I50): standard initial condition, static condition, dynamic condition. Values were recorded every 5 min, although graphs show values at 30, 60, 120, 180, and 240 min for convenience.*

### *6.4.2 I50 prototype system*

A device made up of a plate heat exchanger has been introduced into the prototype system to assess the heat transfer process in a real configuration heat exchange system. In this regard, a secondary open circuit connected to the main water and the primary circuit, which is directly connected to the probe fluid, have both been taken into consideration (simulation of heat pump system). The essential parts of the heat exchange systems configurations (standard and innovative) are shown in Figure 6.4. The temperature variations are due to the thermal exchange between the primary and the secondary system; a significant decrease in the temperature of the heat transfer fluid and an increase in the water temperature of the secondary circuit were observed (Figure 6.7). This innovative configuration produces a higher water temperature than the regular system after the first phase of the test, although starting from the same initial value (first 30 min). Even if the heat fluid of the I50 configuration probe undergoes a higher temperature drop after the activation of the secondary circuit as a result of the introduction of cold mains water (I50 prototype = 12 °C, ST prototype = 12.2 °C), it is capable of reaching a higher temperature at the conclusion of the test (I50 prototype = 15.2 °C, ST prototype = 14.6 °C) (Figure 6.8). The outputs support the idea that in the ST system the soil does not exchange heat efficiently, since it has a tendency to store the heat and then slowly transmit it. The 15.2 °C recorded in the S1 probe demonstrate an efficient heat exchange in the hybrid system (Figure 6.8). Significantly higher temperatures result in a 4% improvement in thermal exchange compared to the standard system (ST probe plus grout).

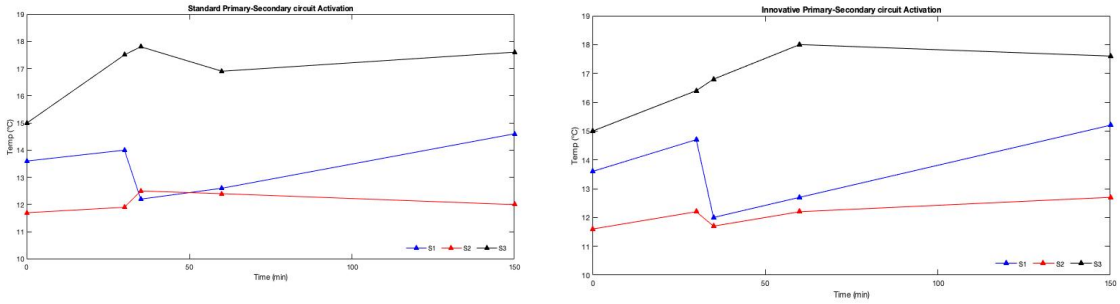


*Figure 6.7- S1, S2 and S3 measurements in standard and innovative configuration during the primary-secondary circuits tests.*

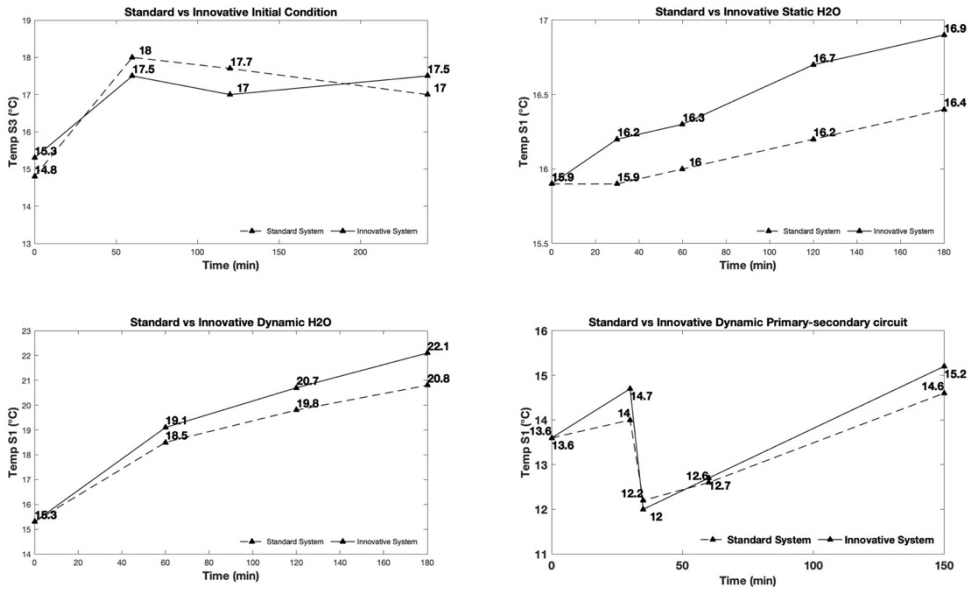


*Figure 6.8 - Standard (ST) and innovative (I) systems during the initial, static, dynamic and primary-secondary circuits tests.*

### *6.4.3 Additivate grouts*

From the analysis of the innovative grout, the re-use of CFP results in the improvement of the heat exchange efficiency in closed-loop systems. Based on the results of the implementation of CFP for the development of geothermal probes (section 6.3.1), which improves the heat exchange between probe and soil, the results on heat exchange between grout, soil and probe highlight the significant improvement of compressional and flexural strength as well the enhancement of thermal properties.

The results of the compressive strength tests performed on standard and doped materials show the significant increase in the breaking load of material with CFP (Figure 6.12a). On the sample at 14 days, we observed an increase of about 84% in uniaxial compression, namely from 2.83 N/mm$^2$ (standard material) up to the value of 5.22 N/mm$^2$ for the doped sample. On the sample at 28 days, a significant increase from 3.33 N/mm$^2$ to 8.11 N/mm$^2$ has also been observed. As for the compressive strength, a similar trend is displayed by the flexural strength with significant improvement between the standard and innovative material. In this case, the additivate sample shows an increase in the strength point from the value of 1.15 N/mm$^2$ to the value of 2.74 N/mm$^2$; at 28 days, it is possible to observe a similar adaptation and an average increase of the performed measurements from 1.24 N/mm$^2$ to 3.35 N/mm$^2$ (Figure 6.9a). As for the investigation of the mechanical property's

response, the thermal conductivity analysis has also highlighted an evident improvement in the thermal exchange characteristics (Figure 6.9b). In fact, an improvement of about 3% on average was obtained, with the only exception of the last measured values, attributable to a greater presence of pores or to the presence of greater quantities of resin that decreased the heat exchange capacity by acting as an insulator. The thermal conductivity improvement suggests that CFP, even in small percentages (5%), can enhance the heat exchange, therefore constituting a good material for the sustainability of the initial investment. Finally, the results qualify CFP as a recycling advantages material in shallow geothermal systems, since it improves the mechanical and heat exchange characteristics of the filling grouts. Other effects of adding CFP to grout used in low-enthalpy geothermal systems include the ability to obtain resistance properties useful for tolerating any stresses and ensuring excellent water resistance of the compound in order to eliminate issues related to heat transfer fluid leaks, resulting in a material that meets high environmental quality standards.

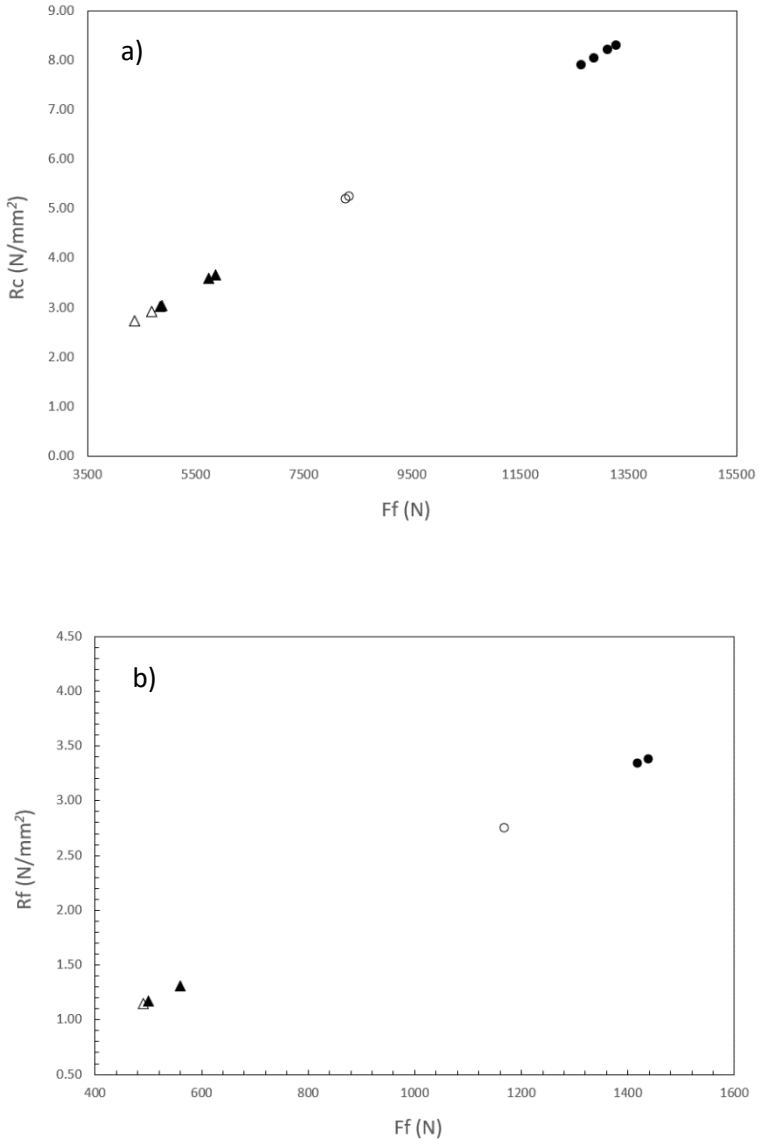


*Figure 6.9- (a) Diagram reporting the uniaxial (Rc) and (b) flexural compressive (Rf) strengths at the fracture point for the starting and doped (+ 5% of graphite powder) bentonitic grouts as a function of the load applied to the sample (Ff and Fc). Symbols are as follows: triangles for the starting grout; circles for the grout + 5% of CFP. Open symbols are for tests at 14 days, filled symbols for those at 28 days.*

### *6.4.4 The implications of using innovative compounds*

The different conductivity behaviours between the key components of a shallow geothermal system (soil-grout-probe interaction) result in a thermal output limitation. In order to investigate the total heat production, the thermal analogy between Fourier's Law and the electrical conduction of Ohm's Law can be used, assuming that the grout and probe materials are two resistors connected in series (Remund C.P., 1999; Banks D., 2009). The thermal resistances (Rb) for each element can be calculated using thermal conductivity calculations across a flat interface (values near to cylindrical surface approximation).

According to the ASHRAE (American Society of Heating, Refrigerating, and Air-Conditioning Engineers) standard normative, which was based on the studies of Ingersoll L.R. et al., 1954 and Kavanaugh, S.P. et al., 1997, the calculation of borehole length in cooling (Lc) and heating configurations (Lc) could be optimised by changing the Rb parameter regarding the thermal resistance into the following equation:

$$L_{c/h} = \frac{Q_a R_{ga} + Q_{gc/h}\left(R_b + \left(PLF_m R_{gm}\right) + R_{gd} F_{sc}\right)}{T_g - \left[\left(\frac{T_{wi} - T_{w0}}{2}\right)\right]_{c/d} - T_p} \qquad \textit{Equation 6-3}$$

where Qa is the average heat flux exchanged during 1 year (expressed in W); Rga is the equivalent thermal resistance per length unit of the ground (annual pulse, expressed in m K/W); Qg c/h is the project load at the ground side during the heating (h positive value) and cooling (c negative value) seasons (expressed in W); Rb is the equivalent thermal resistance per length unit of the heat exchanger, corresponding to the thermal exchange between the heat transfer fluid and the borehole surface (expressed in m K/W); PLFm is the monthly part load factors; Rgm is the equivalent thermal resistance per length unit of the ground (monthly pulse expressed in m K/W); Rgd is the equivalent thermal resistance per length unit of the ground (daily pulse expressed in m K/W); Fsc is the loss factor due to possible thermal short-circuits in the exchanger between input/output pipes; Tg is the ground temperature (expressed in °C) not disturbed by the exchanger; Twi and Tw0 are the input and output average temperatures (expressed in °C) of the transfer fluid during the heating and cooling seasons; Tp is the penalty temperature (expressed in °C), which evaluates the interference between exchangers. The borehole thermal resistance Rb can be calculated through several methods. One of the most popular methods was proposed

by Remund, 1999. Assuming a conventional design of the thermal exchange system (borehole and probe diameters), the results presented in this work demonstrate the effect of the changing thermal conductivity of grout in the computation of Rb for: (1) standard probe plus standard grout; (2) standard probe plus innovative grout (5% CFP); (3) innovative probes plus innovative grout (5% CFP).
Considering the equation:

$$R_b = R_p + R_{gr} \qquad \textit{Equation 6-4}$$

Where,

$$R_p = \frac{L_p}{A_p \lambda_p} \qquad \textit{Equation 6-5}$$

$$R_{gr} = \frac{1}{S_b \lambda_{gr}} \qquad \textit{Equation 6-6}$$

where Lp refers to the thickness of probe, Ap refers to the area perpendicular to heat flow (expressed in $m^2$) for the probe, and it is obtained from the relation 2prh, where r is the probe radius (m), h is the depth (m), lp is the thermal conductivity of the probe (expressed in W/mK), Sb is the short-circuit factor and lgr is the thermal conductivity of the sealing grout (expressed in W/mK).
Concerning the short-circuit factor (Sb), it can be calculated as follows:

$$S_b = \beta_0 \left( \frac{d_b}{D_{po}} \right)^{\beta_1} \qquad \textit{Equation 6-7}$$

where $\beta_0$ and $\beta_1$ are coefficients depending on the geometry of input/output pipes into the borehole (Remund, 1999), whereas $d_b$ and $D_{po}$ are the borehole (expressed in m) and the pipe (i.e., the probe diameter) diameter (expressed in m). In changing the $\lambda_{gr}$ parameters, the impacts on the total sizing of the low-enthalpy geothermal installation can be therefore

assessed in terms of borehole length (equation 6-4). Indeed, even small variations of the thermal conductivity of the sealing material affect the total heat exchange between the subsoil heat and the geothermal system.

In line with the analysis, the final Rgr can be reduced from 0.08 m K/W down to 0.07 m K/W by changing the $\lambda_{gr}$ from 1.82 W/m K (standard grout) to 2.01 W/m K (innovative CFP grout), fixing the geometry of the probe pipes, borehole and probe dimensions, and generating a homogenous subsurface (Table 6.5). Although Rb parameter adjustments were not significant, the Lc/h calculation (equation 6-3) shows that they do have an important impact on the overall borehole length. According to equation 6-4, adopting the innovative configuration (innovation CFP grout plus innovative CFP probe) comparing to the conventional setting resulted in a reduction of 38.5% of the overall Rb resistance. The setup of the GHPS system is significantly impacted by the equivalent thermal Rb resistance, decreasing because of an increase in thermal exchange. In fact, using the equation 6-3 as a reference, a simple computation to determine Lc/h was performed by comparing the different configurations. For example, a vertical geothermal field for a residential building complex that required heating and free cooling was examined. The field comprises of two double U-tube boreholes of 100 metres in length and having a pipe diameter of 32 millimetres.

*Table 6.5 - Calculated thermal resistance (Rb) for a 250 m borehole filled with standard and innovative grout.*

| | $\lambda_{grout}$ [W/m K] | $\lambda_{probe}$ [W/m K] | $R_{grout}$ [m K/ W] | $R_{probe}$ [m K/ W] | $R_{b\_tot}$ [m K/ W] |
|---|---|---|---|---|---|
| ST | 1,82 | 0,45 | 0,08 | 0,05 | 0,13 |
| CFP $5\%_{gr}$ | 2,01 | 0,45 | 0,07 | 0,05 | 0,12 |
| CFP_innovative | 2,01 | 1,30 | 0,07 | 0,01 | 0,08 |

The thermal conductivity of 2 W/mK was taken into consideration for the soil. All the variables utilised to determine the ideal geothermal system sizing are displayed in Table 6.6. Based on the ASHRAE methodology, the use of the innovative CF grout and probe system allows a reduction of the boreholes number (from 42 BHEs to 36 BHEs—Table 6.7) resulting in a total decrease of 600 linear metres. This suggests a greater economic benefit in terms of drilling cost or the number of installed probes. Thus, the rise in thermal

conductivity improves the overall heat exchange, allowing a shorter geothermal vertical probes system for the same heat output.

*Table 6.6- Parameters for the geothermal field model following the ASHRAE approach.*

| | **ST** | **CFP 5%$_{gr}$** | **CFP_innovative** |
|---|---|---|---|
| Qa (W) | 4340 | 4340 | 4340 |
| Qh (W) | 158000 | 158000 | 158000 |
| Rb (mK/W) | 0,13 | 0,08 | 0,07 |
| PLFm | 0,60 | 0,60 | 0,60 |
| Fsc | 1.04 | 1.04 | 1.04 |
| Tg (°C) | 14 | 14 | 14 |
| Tm (°C) | 4 | 4 | 4 |

*Table 6.7- Dimensioning of the geothermal field (probes of 100 m length).*

| | **N° Vertical probes** | **Linear meters** |
|---|---|---|
| ST system | 42 | 4200 |
| ST$_{probe}$ + CF 5%$_{gr}$ | 40 | 4000 |
| CFP innovative system | 36 | 3600 |

## 6.5 End of Waste and economic implication on Geothermal Applications

Considering the "End of Waste" concept and the contextual circular economy perspectives, it is crucial to assess how Carbon fiber powder (CFP) waste derived from industrial processes may be reuses in the geothermal industry by enhancing the qualities of the geothermal plant's elements. By enhancing the physical properties and significantly improving the heat exchange, CFP novel probes and grout enables benefits in both mechanical and thermal characteristics. In addition, the subsequent economic saving for low enthalpy geothermal systems (the decrease in costs also includes the amount related to the reduction of linear meters of perforation) is one of the most important aspects of the reutilization of CFP in geothermal applications.

The reuse of material, which is considered only a waste for many industrial processes, enables CFP to return to the market as a raw material. Additionally, taking into account

the high disposal cost of CFP, the reuse results in cost savings. Considering, for example, the geothermal field case study described in section 6.4.4, an amount of 5 Kg of CFP for each geothermal well could be considered; therefore, a total amount of 171 Kg is necessary for the geothermal field of the case study.

Considering also the disposal cost of industries for CFP as waste material, a significant saving for the total disposal price is obtained (Table 6.8). Since the businesses involved could re-market CFP as a raw material, such savings would lead to profits. The cost of CFP is still low when compared to the market price of grout material, which will allow commercial grout material producers to save money.

Even if currently there are no common pricing lists for the CFP, 0.10 cents/kg has been proposed as possible price. Table 6.8 illustrates the differences in terms of economic impact for the construction of both standard and innovative geothermal plant solutions. After analysing the overall economic impact (costs and savings for the stakeholders in charge of the production chain) and the real economic cost for the realisation of the geothermal heat pump system, a cost saving of 10% is noticeable for the realisation of a geothermal field probe with the innovative system. Due to the wide variation and lack of official pricing lists of the cost of waste disposal among the European countries, an average value of the Italian cost for waste disposal procedures based on input from multiple specialised Italian businesses, as well as administrative local fixed fees, has been considered. In order to maintain geographic conformity on prices for the materials used in the experiments, therefore, 0.50 Euro/Kg has been considered for the waste material and about 300 Euros of administrative costs. By assuming an average value of 50 Euros per linear meter for perforation (geothermal field of about 40 probes), a cost reduction of about 35,000 Euros from the standard to the innovative solution could be envisaged. In addition, Table 6.8 shows a simple and indicative analysis of the economic savings obtained by using CFP composite materials applied to the example defined above.
Therefore, the efficiency of geo probe systems exponentially increases with the optimization of the probes' setting and grout mixture for low enthalpy geothermal systems. The achieved results show that there are both financial and ecological benefits. The realisation of a geothermal field probe with the innovative system once again clearly shows the entire economic impact and the real economic cost for the geothermal system (cost saving of around 10%). In this light, the establishment of a supply chain for raw materials offers both an innovative management strategy for the realization of a circular

business model in the industrial CF manufacturing processes, as well as innovative management for the achievement of the "End of Waste" model promoted by EU policies.

*Table 6.8- Global economy impact by using CFP composite materials in geothermal systems.*

| | **ST system (Euro)** | **CF innovative system (Euro)** |
|---|---|---|
| CFP disposal cost | 400 | 0 |
| CFP cost | 0 | 18 |
| Commercial Grout cost | 1302 | 1060 |
| Cost of commercial Probe | 40173 | 0 |
| Cost of innovative Probe (PE – 100) | 0 | 46486 |
| Cost of geothermal perforation | 210000 | 180000 |
| Total amount | 251875 | 227564 |

# Conclusions and future perspectives

The methods explored in this thesis aimed at characterizing the geothermal configuration of the Sicilian subsurface in order to lay the foundations of the geothermal energy's exploitation perspectives in Sicily. A new approach for the geothermal characterization, based on the validation of the geological model by means of gravity calibration and subsequently a thermal numerical simulation stage, has been developed. To achieve this, the gravity validated 3D structural model has been used to investigate the steady-state thermal response of the lithospheric context. According to multiple boundary conditions and considering the input of heat from the bottom, the steady-state thermal field has been obtained. It is important to note how the resulting steady-state thermal field relies on the first geological modelling stage; thus, the configuration of the used major density contrasts require more specific dataset to improve the resolution of the regional outputs. This approach becomes useful not only for geothermal purposes, but also in geodynamic implications on a lithospheric scale. In fact, the analysis on the conversion of Vs tomographies for the lithospheric mantle will be useful to constraint the physical parameters of the deeper crust.

From the numerical thermal modelling of the region, Sicily displays several areas suitable for the exploitation of high-enthalpy geothermal resources, especially associated with carbonate lithologies. Areas such as the Pantelleria Isle, the Aeolian arc and the western domain show above-average geothermal gradients exploitable as medium-to-high enthalpy resources. Future research should include transient thermal numerical simulations on a regional context, as well as rheological models coupled with convective heat transport, in order to obtain a more realistic approach for the thermal response. Based on these assumptions, it would be necessary to increase the resolution of the investigation in these areas, trying to integrate additional datasets on heat flow rates.

Although the regional context shows suitable areas for the production of electricity, the identification of favourable areas to the exploitation of medium-to-low temperature gradients has been achieved. In this regard, in order to provide an example of a high-resolution geothermal investigation, a detailed thermal simulation was carried out in a case study in the south-eastern sector of Sicily. Starting from a validated geological model, by means of a new gravimetric dataset, the thermal conditions have been studied. According to the same workflow used for the regional investigation, the thermal analysis

of the local domain has been carried out. In addition, it was possible to investigate how the implementation of fluid and tectonic components affects the heat transfer in the shallow Meso-Cenozoic carbonate sediments. The detailed analysis of the thermal field defines the most suitable areas for possible exploitation through an open-loop system. The numerical simulation in this sense, considering the transient conditions over a period of 10 years, suggests the sustainability of the plant operations over time, providing a starting point for the implementation of similar applications in the area. In this regard, future analysis on the reuse of existing hydrocarbons wells in the area could be the new frontier.

With the aim of making the results of the research useful for their remote interrogation, the outputs have been integrated and implemented in a web portal. This approach results in a useful tool for academics and industry experts and provides a wide coverage of the geothermal information in Sicily. Consequently, the idea of a "Geothermal Micro-zonation" through the implementation of new and more detailed thermal models has been proposed. Nevertheless, implementing other high-resolution thermal models in the portal is necessary, as new information regarding geothermal resources becomes available. Similarly, further geothermal parameters and potentiality of geothermal energy in terms of specific power outputs (Kw) should be integrated to better constrain the geothermal potential of the explored domain.

Together with the definition of thermal fields, the performance of a low enthalpy geothermal system generally depends on the ground-heat exchanger. In this regard, new solutions have been provided by the research program. Probes and Borehole space fills often use pure materials that influence the heat transfer efficiency. However, standard products often do not provide optimal heat exchange properties, and for this reason, new carbon fibre mixtures have been designed in order to guarantee the optimal thermal exchange and energy efficiency of the entire geothermal system. The enhanced products (both probes and grout) result in a highly eligible elements into low enthalpy installations. The optimization leads to an exponential increase in the efficiency of geo-probe systems, and subsequent environmental/financial benefits have been demonstrated too. The subsequent development of a supply chain of new materials mirrors the objectives of sustainable growth and represents a circular business model in the industrial production processes, as well as an innovative management strategy for the achievement of the "End of Waste" process promoted by EU policies.

The innovation supported by the research can potentially contribute to the improvement of the coverage of the regional geothermal information, which currently lacks accuracy. In addition, the investigation introduces a very solid workflow for the geothermal characterization, which is transferable to other geologically complex areas worldwide and explores new solutions for the optimization of geothermal application systems. The combination of these aspects makes Sicily a sort of pilot region for geothermal exploration and for the potential sustainable use of this renewable energy resource.

This are relevant results, especially if we consider the actual socio-political context and the current energy market dynamics. Therefore, the outputs of the research can only accelerate the transition towards a more sustainable use of renewable energy resources such as subsoil stored heat.

# Appendix

**A_2**

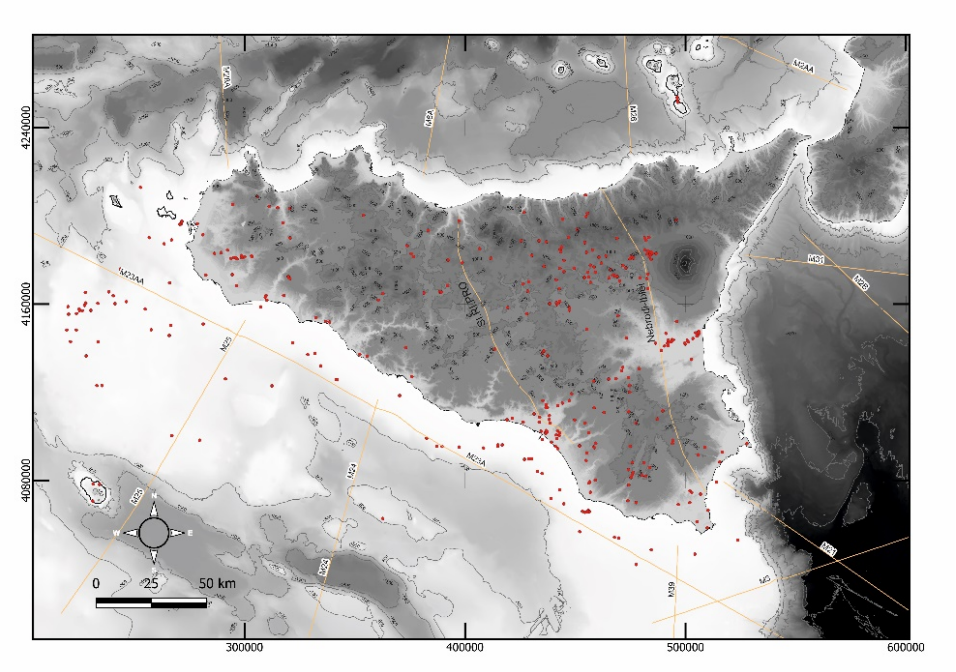


Geological and Geoseismic section used for the implementation of the starting geological model

- M23A-M23AA from Catalano et al. 2000;
- M3-M21 from Catalano 2000;
- M25-M26-M28-M39 from Chironi 2000.

Geological interpretation western domain from Catalano et al. 2000.

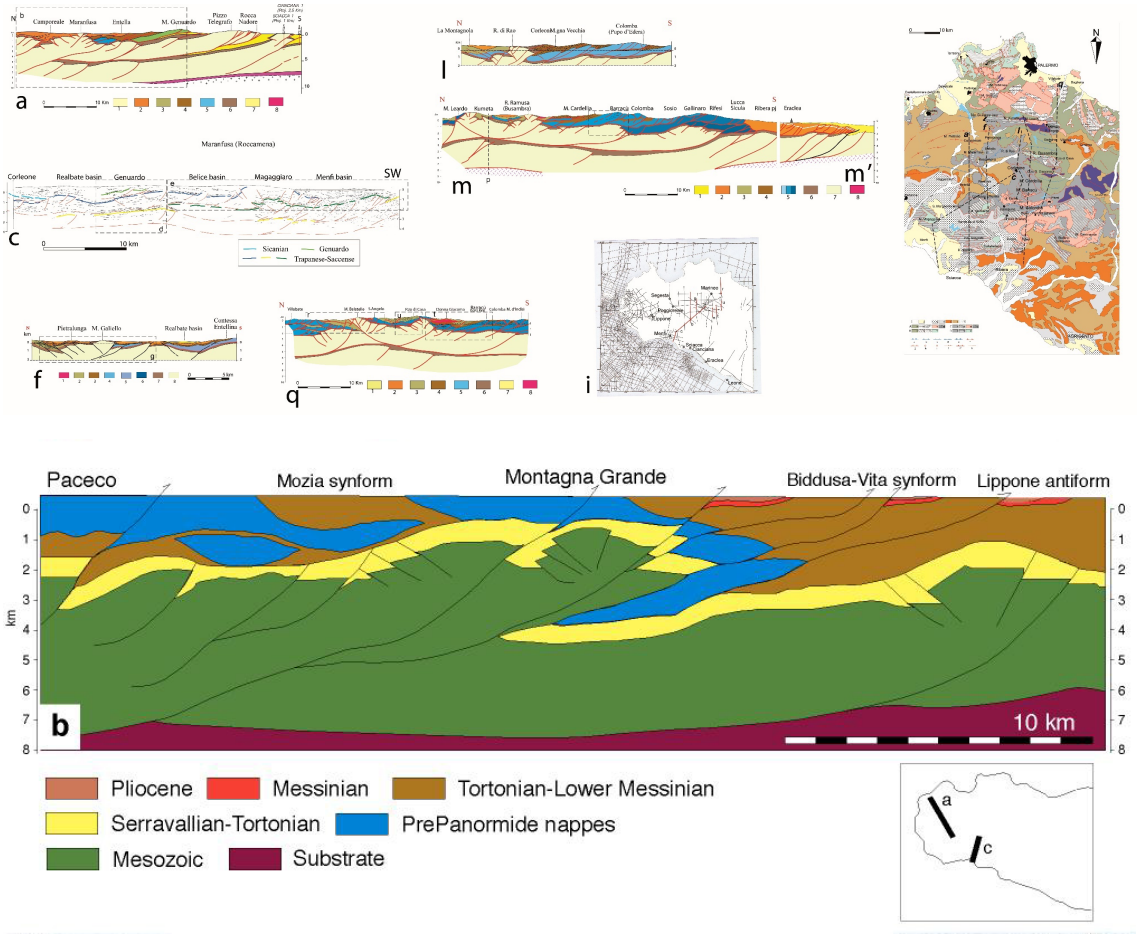

Geo-seismic line **M23** (Catalano et al., 2000)

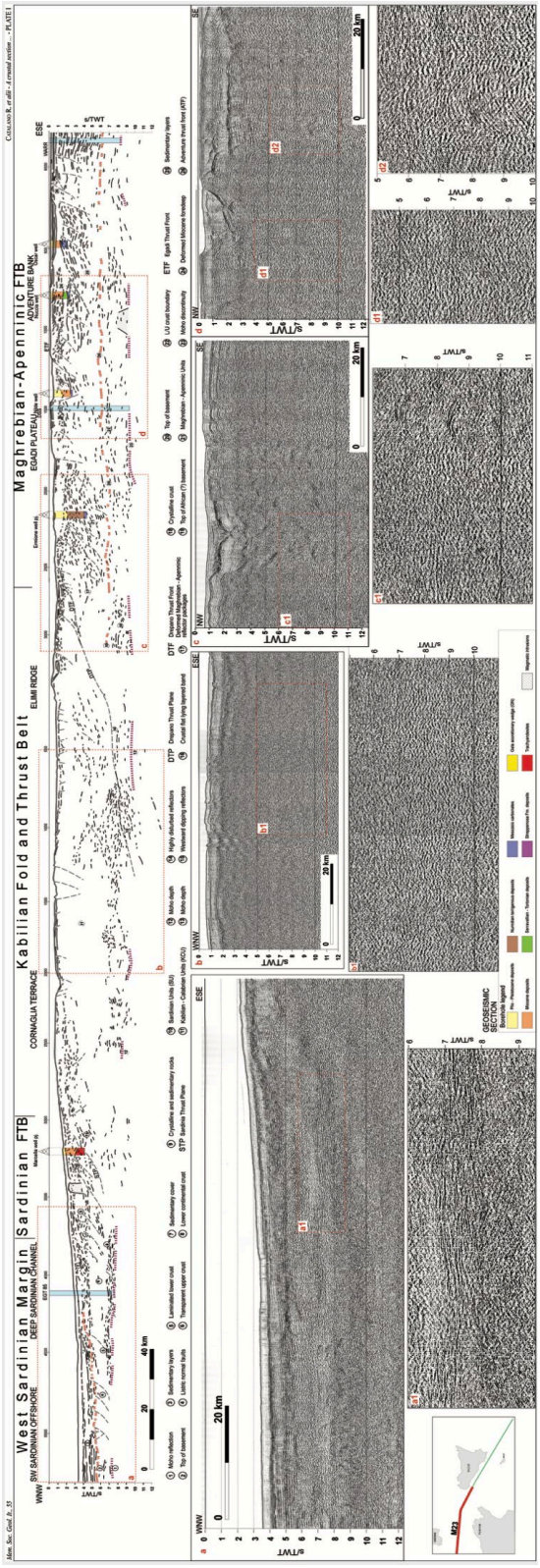

Simplified geological cross-section from Hyblean-Malta shelf to the Ionian abyssal plain (Catalano et al. 2000). **M23**

Velocity model and geological interpretation for **M25** CROP line (Chironi 2000).

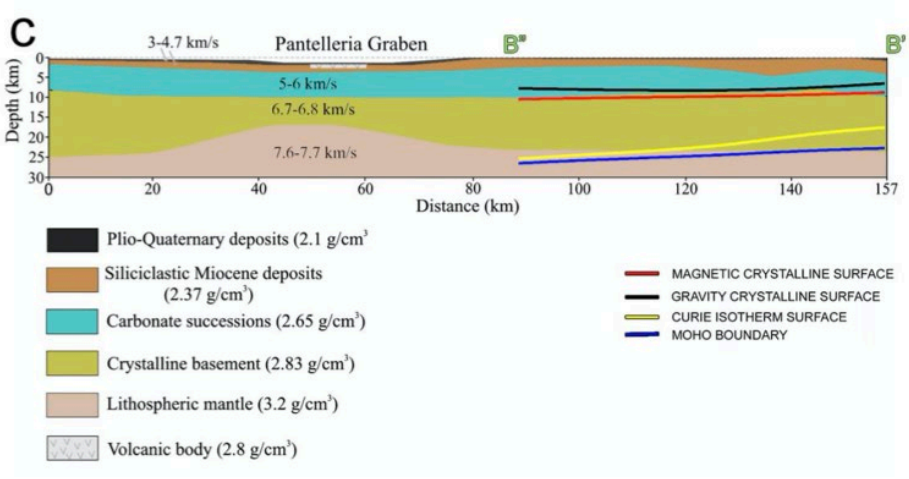


Geo-seismic section of ionian slab subduction **M2** (Catalano, Sulli et al., 2006)

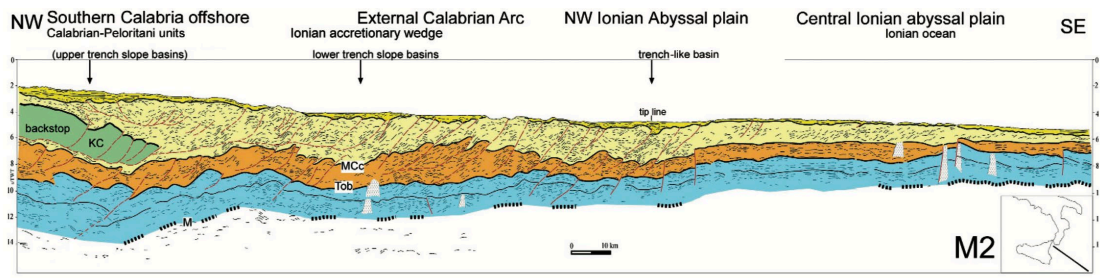


Fig. 9 - Geoseismic section showing the NW deepening oceanic crust and the SE verging Ionian accretionary wedge that is formed by slices of oceanic crust and its sedimentary cover. KC: Kabilian-Calabrian units; MCc: top of the Meso-Cenozoic Ionian sedimentary units; TOB: top of the Ionian oceanic crust; M: Moho.

Semplified geological interpretation used for the geological 3D modelling (from Catalano, 2000)

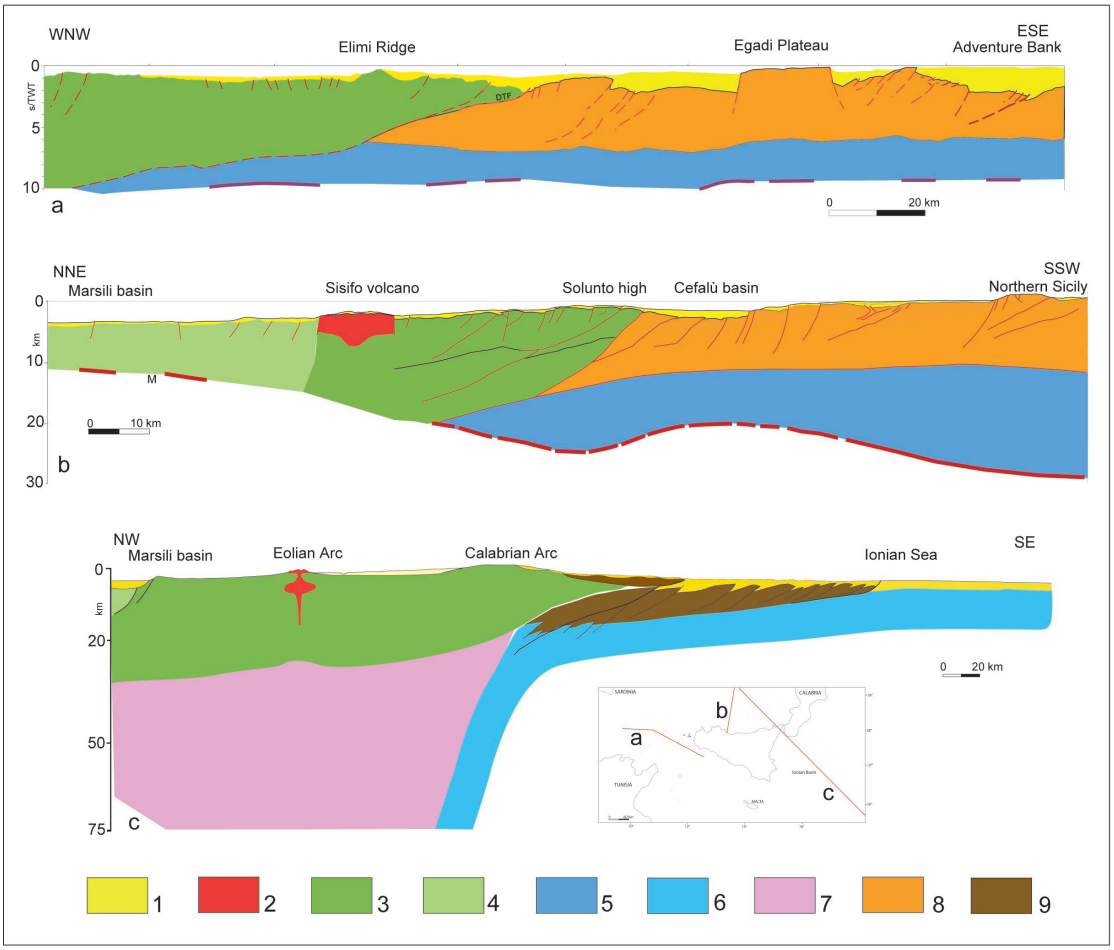

**SI.RI.PRO** Catalano et al., 2013.

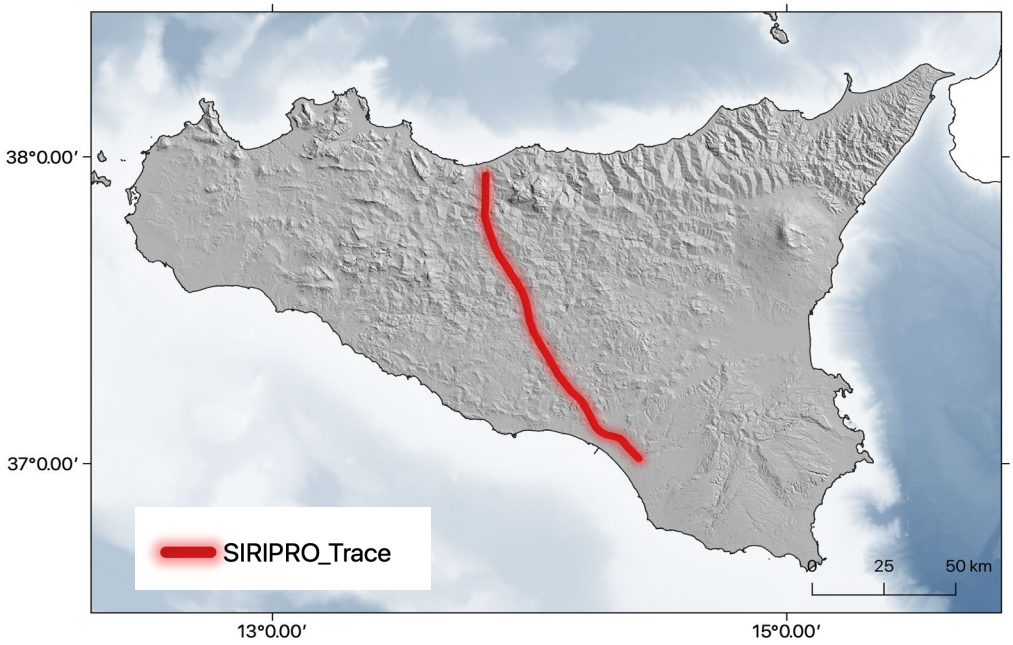


Interpretation of the seismic stack section of the **SI.RI.PRO** profile (Catalano et al., 2013)

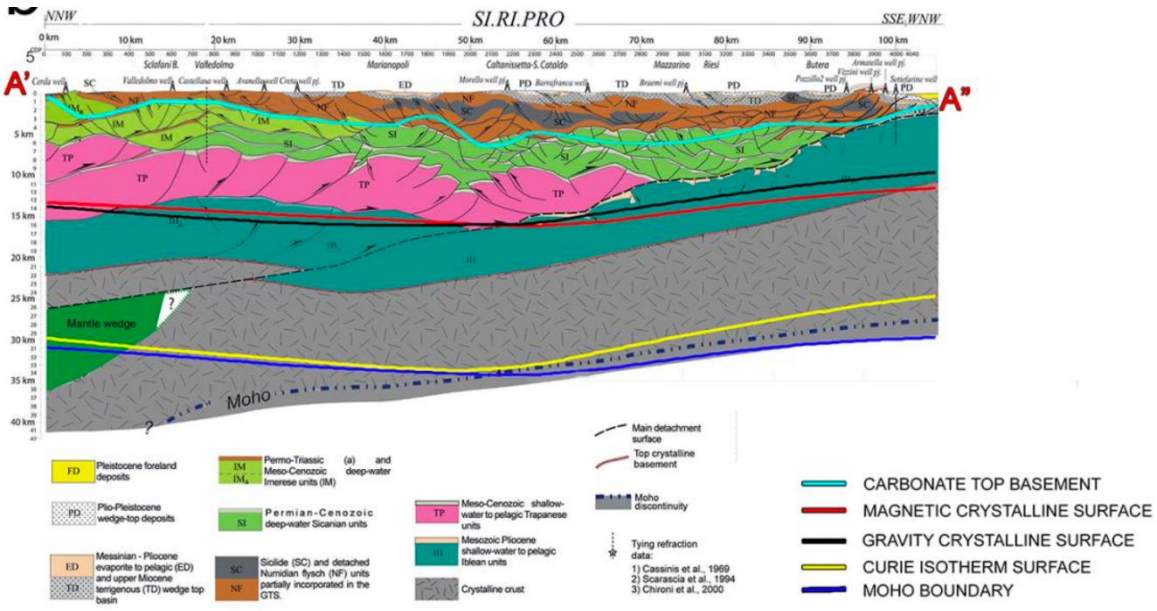

Nebrodi-Iblei Bianchi et al., 1987.

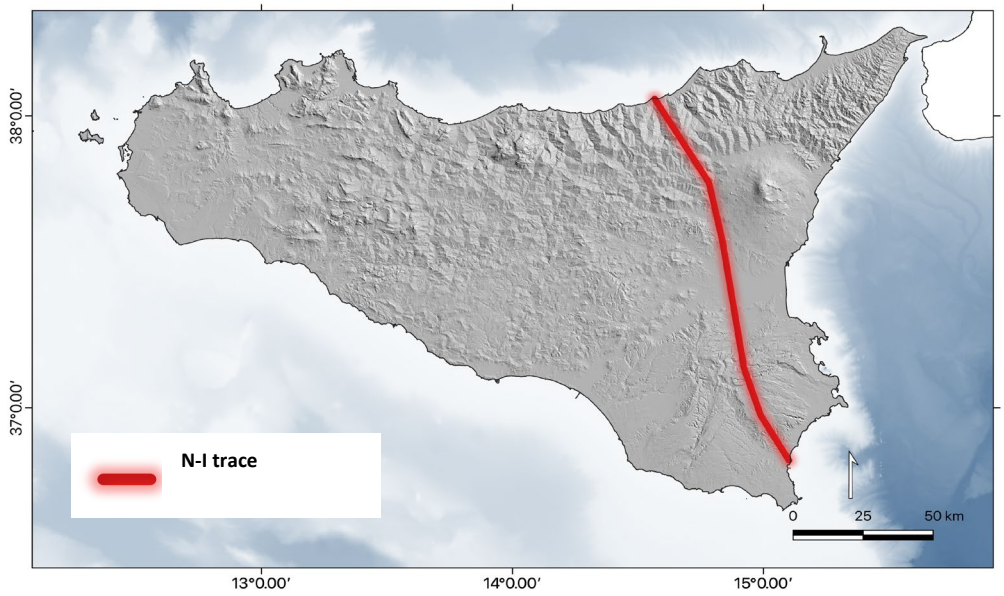


Geological interpretation of the Nebrodi-Iblei section

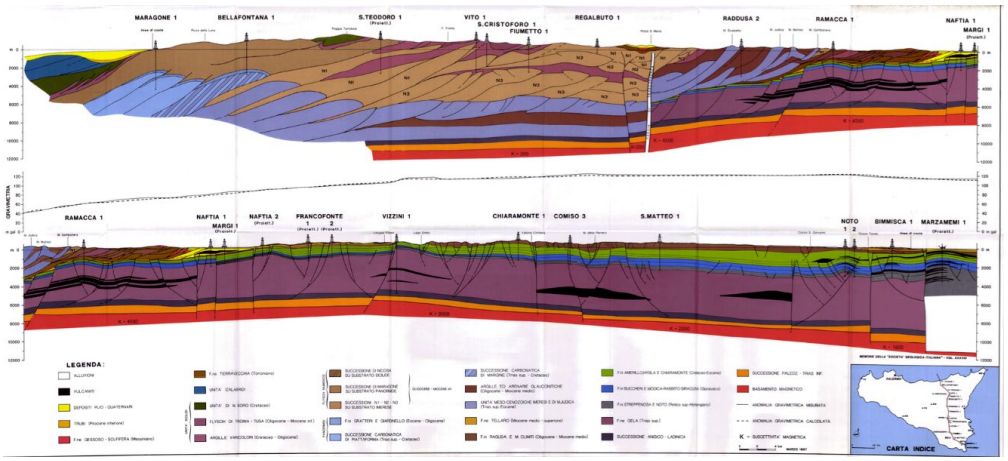

1D Velocity model (Sgroi et al., 2012)

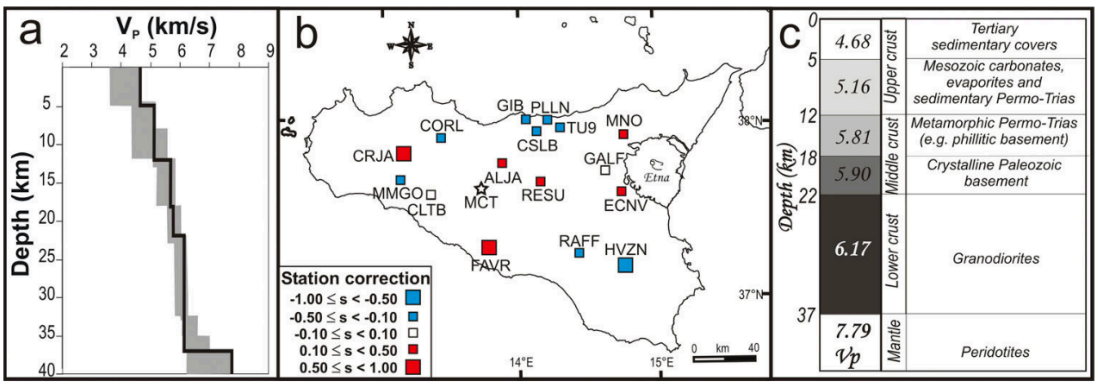

**A_3**

3D model and calculated vs measured bouger anomaly dataset

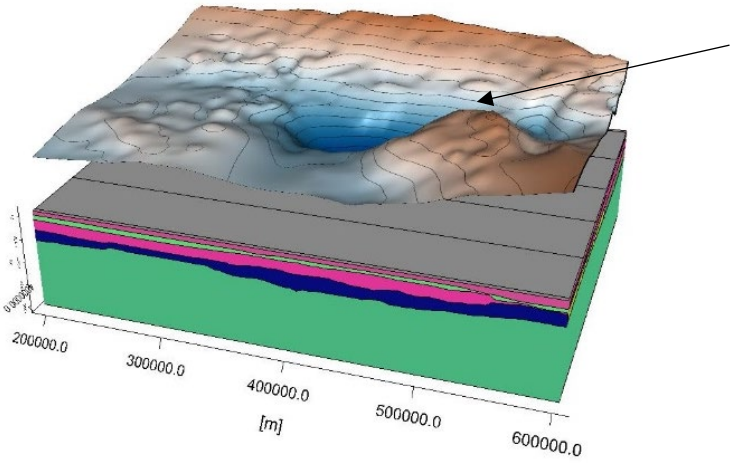


**Measured Bouger anomaly from (Cartografia Gravimetrica Digitale d'Italia alla scala 1:250.000)**

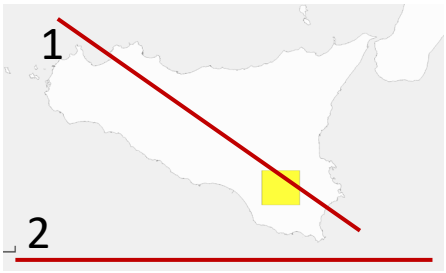


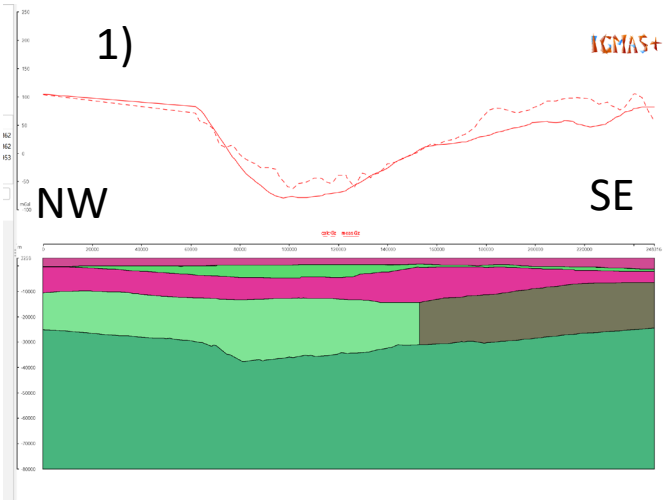


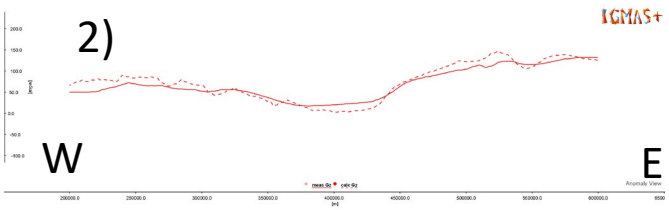


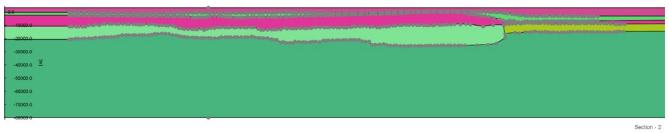

Example of computed dataset for the tomographies conversion

# Temperature output

# Input file: ./2_csem_europe_Sicily_UTM33N.dat

# Velocity scale factor: 1.0

# Mantle composition:

# cpx_di - 0.168

# gnt - 0.0

# ol - 0.518

# opx_en - 0.279

# sp - 0.035

# XFe - 0.126

# Pressure calculation: AK135

# Wave frequency (Omega) / Hz: 0.02

# Anelasticity parameters: Sobolev et al. (1996)

# Alpha depending on: Nothing

# Columns:

# 1 - X

# 2 - Y

# 3 - Z / masl

# 4 - V_S / m/s

# 5 - T_syn / degC

# 6 - Rho / kg/m3

139398.301660 3991354.133080 -50000.000000 4352.13 939.6 3316.0

184492.198291 3989616.832850 -50000.000000 4289.40 988.4 3311.7

229578.629941 3988111.962420 -50000.000000 4305.37 976.7 3312.7

274658.656783 3986839.183060 -50000.000000 4315.44 969.1 3313.4

319733.341875 3985798.208340 -50000.000000 4405.40 890.9 3320.4

364803.750681 3984988.804060 -50000.000000 4510.86 761.2 3332.0

409870.950590 3984410.788150 -50000.000000 4427.58 867.9 3322.4

454936.010432 3984064.030600 -50000.000000 4463.63 826.3 3326.1

**A_4**

Lithological sequence and measured/calculated parameters from Margherita_1 well:

| depth (m) | unit | thickness | Δt WELL LOG (μs/ft) | ρ(g/cm³) | V (m/s) |
|---|---|---|---|---|---|
| 55m -94m | RAGUSA | 39m | 105 | 2.27 | 2902 |
| 94m-182m | | 88m | 90 | 2.36 | 3386 |
| 182m-225m | | 43m | 95 | 2.33 | 3208 |
| 225m-305m | | 80m | 90 | 2.36 | 3386 |
| 305m-320m | | 15m | 110 | 2.24 | 2771 |
| 320m-350m | AMERILLO | 30m | 75 | 2.47 | 4064 |
| 350m-494m | | 144m | 80 | 2.43 | 3810 |
| 494m-563m | | 69m | 75 | 2.47 | 4064 |
| 563m-573m | | 10m | 85 | 2.39 | 3586 |
| 573m-637m | | 64m | 75 | 2.47 | 4064 |
| 637m-652m | | 15m | 85 | 2.39 | 3586 |
| 652m-679m | | 27m | 75 | 2.47 | 4064 |
| 679m-710m | | 29m | 80 | 2.43 | 3810 |
| 710m-719m | HYBLA | 9m | 85 | 2.39 | 3586 |
| 719m-731m | | 12m | 90 | 2.36 | 3386 |
| 731m-746m | | 15m | 95 | 2.33 | 3208 |
| 746m-762m | | 16m | 120 | 2.2 | 2540 |
| 762m-792m | | 30m | 80 | 2.43 | 3810 |
| 792m-883m | | 91m | 100 | 2.3 | 3048 |
| 883m-905m | | 22m | 80 | 2.43 | 3810 |
| 905m-950m | | 45m | 85 | 2.39 | 3586 |
| 950m-975m | CHIARAMONTE | 25m | 70 | 2.51 | 4354 |
| 975m-1009m | | 34m | 75 | 2.47 | 4064 |
| 1009m-1121m | | 112m | 70 | 2.51 | 4354 |
| 1121m-1210m | | 90m | 65 | 2.56 | 4689 |
| 1210m-1219m | BUCCHERI | 9m | 80 | 2.43 | 3810 |
| 1219m-1234m | | 15m | 65 | 2.56 | 4689 |
| 1234m-1301m | | 67m | 90 | 2.36 | 3386 |
| 1301m-1335m | | 34m | 65 | 2.56 | 4689 |
| 1335m-1356m | | 21m | 80 | 2.43 | 3810 |
| 1356m-1411m | | 55m | 95 | 2.33 | 3208 |
| 1411m-1423m | | 12m | 110 | 2.24 | 2771 |
| 1423m-1472m | | 49m | 75 | 2.47 | 4064 |
| 1472m-1493m | | 21m | 65 | 2.56 | 4689 |
| 1493m-1520m | | 27m | 80 | 2.43 | 3810 |
| 1520m-1575m | | 55m | 75 | 2.47 | 4064 |
| 1575m-1584m | STREPPENOSA | 9m | 95 | 2.33 | 3208 |
| 1584m-1597m | | 13m | 75 | 2.47 | 4064 |
| 1597m-1627m | NOTO | 30m | 85 | 2.39 | 3586 |
| 1627m-1645m | | 18m | 75 | 2.47 | 4064 |
| 1645m-1661m | | 16m | 80 | 2.43 | 3810 |
| 1661m-1694m | | 33m | 65 | 2.56 | 4689 |
| 1694m-1701m | | 7m | 80 | 2.43 | 3810 |
| 1701m-1706m | | 5m | 65 | 2.56 | 4689 |
| 1706m-1725m | | 19m | 95 | 2.33 | 3208 |
| 1725m-1740m | GELA | 15m | 55 | 2.67 | 5542 |

Relationship by Schlumberger for the calculation of velocity from Transit Time (ΔT):

$$\text{Velocity (ft/s)} = 1/\ \Delta T 10^{-6}$$

$$\text{Velocity (m/s)} = \text{Velocity ()}$$

Empirical relationship by Gardner et al. (1974) used for density computation:

$$\rho(g/cm^3) = 1.74 Vp(km/s)^{0.25}$$

**A_5**

3D visualization of the thermal model domains

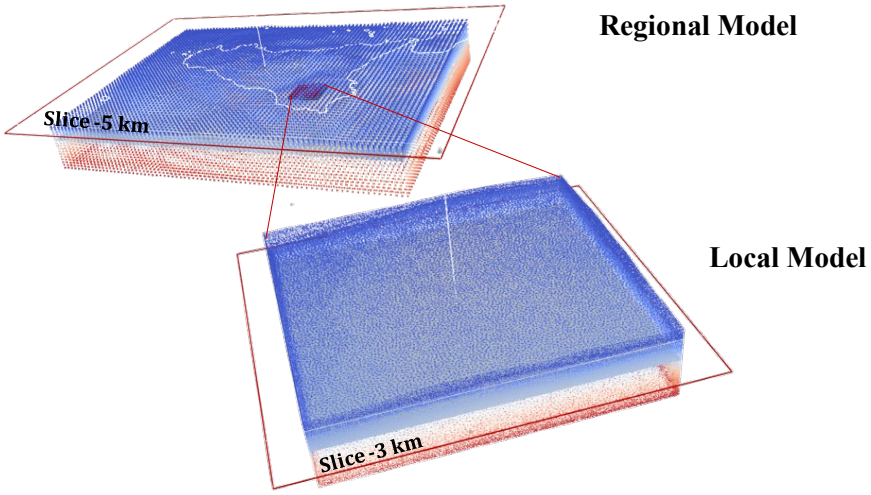


Example of regional dataset

Block Name,Point ID,Points_0,Points_1,Points_2,Points_Magnitude,ids,temperature

basement,19708,394759,4.09295e+06,-15738.4,4.11197e+06,74693,498.297

basement,19709,399759,4.09295e+06,-15666.1,4.11246e+06,74694,494.696

basement,19710,404759,4.09295e+06,-15846.3,4.11295e+06,74695,496.07

basement,19711,409759,4.09295e+06,-15907.9,4.11344e+06,74696,494.064

basement,19712,414759,4.09295e+06,-16351.3,4.11394e+06,74697,500.432

basement,19713,419759,4.09295e+06,-17227.7,4.11446e+06,74698,516.719

basement,19714,424759,4.09295e+06,-17670.5,4.11497e+06,74699,524.529

….

….

# References

Aate, S., Angelino, A., Balasco, M., Botteghi, S., Bruno, P., Caielli, G., Caputi, A., Cardellicchio, N., Catalano, R., Contino, A., 2014. VIGOR: Sviluppo geotermico nella regione Sicilia – Studi di fattibilità a Mazara del Vallo e Termini Imerese, Valutazione geotermica con geofisica elitrasportata. https://doi.org/10.13140/RG.2.1.4496.7449

Abesser, C., 2010. Open-Loop Ground Source Heat Pumps and the Groundwater Systems: A Literature Review of Current Applications, Regulations and Problems, British Geological Survey Nottingham: Nottingham, UK.

Afonso, J.C., Zlotnik, S., 2011. The Subductability of Continental Lithosphere: The Before and After Story. In: Arc-Continent Collision, Frontiers in Earth Sciences book series, 53-86 pp. Springer, Berlin, Heidelberg. https://doi.org/10.1007/978-3-540-88558-0_3

Aureli, A., 1993.Caratteristiche e vulnerabilità delle falde idriche presenti nel settore sud-orientale ibleo. 1° convegno nazionale sulla protezione e gestione delle acque sotterranee: metodologie, tecnologie e obiettivi.

Anon, O.H., 1979. Classification of rocks and soils for engineering geological mapping. Part 1: rock and soil materials. Bull Int Assoc Eng Geol, 19(1), pp.364-437.

Badache, M., Eslami-Nejad, P., Bastani, A., Aidoun, Z., Nguyen, A., 2019. Theoretical and experimental analysis of a vertical direct expansion geothermal evaporator using CO2 as refrigerant. Sci. Technol. Built Environ., 25, 1081–1094. https://doi.org/10.1080/23744731.2019.1648131

Badenes, B., Sanner, B., Mateo Pla, M.Á., Cuevas, J.M., Bartoli, F., Ciardelli, F., González, R.M., Ghafar, A.N., Fontana, P., Lemus Zuñiga, L., et al., 2020. Development of advanced materials guided by numerical simulations to improve performance and cost-efficiency of borehole heat exchangers (BHEs). Energy, 201.

Ball, D.A., Fischer, R., Talbert, S.G., Hodgtt, D., Aurer, F., 1983. State-of-the-art survey of existing knowledge for the design of ground-source heat pump system. NASA STI/Recon Technical Report N, 84, 16504. https://doi.org/ 10.3390/en15072685

Banks, D., 2009. An introduction to “thermogeology” and the exploitation of ground source heat. Q. J. Eng. Geol. Hydrogeol., 42, 283–293.

Basilici, M., Mazzoli, S., Megna, A., Santini, S., Tavani, S., 2019. Geothermal Model of the Shallow Crustal Structure across the "Mountain Front Fault" in Western Lurestan, Zagros Thrust Belt, Iran. Geosciences 9, 301. https://doi.org/10.3390/geosciences9070301

Basilici, M., Mazzoli, S., Megna, A., Santini, S., Tavani, S., 2020. 3-D Geothermal Model of the Lurestan Sector of the Zagros Thrust Belt, Iran. Energies 13, 2140. https://doi.org/10.3390/en13092140

Bhatt, P., Goe, A., 2017. Carbon Fibres: Production, Properties and Potential Use. Mater. Sci. Res. India, 14, 52–57. http://dx.doi.org/10.13005/msri/140109

Bianca M., Monaco, C., Tortorici, L., Cernobori, L., 1999. Quaternary normal faulting in southeastern Sicily (Italy): A seismic source for the 1693 large earthquake, Geophys. J. Int., vol. 139, no. 2, pp. 370–394.

Bianchini, G., Yoshikawa, M., Sapienza, G.T., 2010. Comparative study of ultramafic xenoliths and associated lavas from South-Eastern Sicily: Nature of the lithospheric mantle and insights on magma genesis. Mineralogy and Petrology 98, 111–121.https://doi.org/10.1007/s00710-009-0056-3

Blázquez, C.S., Martín, A.F., Nieto, I.M., García, P.C., Sánchez Pérez, L.S., González-Aguilera, D., 2017. Analysis and study of different grouting materials in vertical geothermal closed-loop systems. Renew. Energy, 114, 1189–1200. https://10.1016/j.renene.2017.08.011

Burollet P. F. Mugniot J. M., and Sweeney P., 1978. 'The Geology of the Pelagian Block: The Margins and Basins off Southern Tunisia and Tripolitania', in The Ocean Basins and Margins, A. E. M. Nairn, W. H. Kanes, and F. G. Stehli, Eds. Boston, MA: Springer US, pp. 331–359.

Buonasorte g., Rizzi F., Passaleva G., 2010. Direct Uses of Geothermal Energy in Italy 2005-2009: Update Report and Perspectives. Proceedings World Geothermal Congress Bali, Indonesia, 25-29 April 2010.

Giorgio Buonasorte(1), Francesco Rizzi(2), Giancarlo Passaleva(1)

Cacace, M., Jacquey, A.B., 2017. Flexible parallel implicit modelling of coupled thermal–hydraulic–mechanical processes in fractured rocks. Solid Earth 8, 921–941. https://doi.org/10.5194/se-8-921-2017

Calcagnile, G., D'Ingeo, F., Farrugia, P., Panza, G.F., 1982. The lithosphere in the central-eastern Mediterranean area. Pure and Applied Geophysics 120, 389–406. https://doi.org/10.1007/BF00877044

Calò, M., Dorbath, C., Luzio, D., Rotolo, S.G., D'Anna, G., 2012. Seismic velocity structures of southern Italy from tomographic imaging of the Ionian slab and petrological inferences. Geophysical Journal International 191, 751–764. https://doi.org/10.1111/j.1365-246X.2012.05647.x

Caracausi, A., Favara, R., Italiano, F., Nuccio, P.M., Paonita, A., Rizzo, A., 2005. Active geodynamics of the central Mediterranean Sea: Tensional tectonic evidences in western Sicily from mantle-derived helium. Geophysical Research Letters 32, 1–5. https://doi.org/10.1029/2004GL021608

Carbone, S., Grasso, M., Lentini, F., Pedley, H.M., 1987. The distribution and palaeoenvironment of early Miocene phosphorites of southeast Sicily and their relationships with the Maltese phosphorites. Palaeogeography, Palaeoclimatology,

Palaeoecology 58, 35–53. https://doi.org/https://doi.org/10.1016/0031-0182(87)90004-6

Cassinis, R., Scarascia, S., Lozej, A., 2003. The deep crustal structure of Italy and surrounding areas from seismic refraction data; new synthesis. Italian Journal of Geosciences 122 (3), 365–376.

Catalano, R., Lo Cicero, G. and Sulli, A., 2002. Geology of Sicily: an introduction. General Field Trip Guidebook, 6th International Symposium on the Jurassic System (pp. 12-22).

Catalano, R., Valenti, V., Albanese, C., Sulli, A., Morticelli G., Accaino, F., Tinivella, U., Giustiniani, M., Zanolla, C., Avellone, G., Basilone, L., 2012. Crustal structures of the Sicily orogene along the SIRIPRO seismic profile. Rendiconti Online della Società Geologica Italiana 21, 67–68.

Catalano, R., Franchino, A., Merlini, S., Sulli, A., 2000. A crustal section from the Eastern Algeria basin to the Ionian Ocean (Central Mediterranean). Memorie della Società Geologica Italiana 55, 71–85.

Cataldi, R., Mongelli, F., Squarci, P., Taffi, L., Zito, G., Calore, C., 1995. Geothermal ranking of Italian territory. Geothermics 24, 115–129. https://doi.org/10.1016/0375-6505(94)00026-9

Chierici, R., Grassi, S., La Rosa, N., Nannini R., Squarci P., Zurlo, 1995. Geothermal Exploration in Pantelleria Island (Sicily Channel): First results. World Geothermal Congress 1995, Florence, Italy.

Ciardi, M., Cataldi, R., 2005. Il calore della terra – Contributo alla storia della geotermia in Italia, Pisa, Edizioni ETS.

Ciliberto, E., Crisafulli, C., Manuella, F.C., Samperi, F., Scirè, S., Scribano, V., Viccaro, M., Viscuso E., 2009. Aliphatic hydrocarbons in metasomatized gabbroic xenoliths from Hyblean diatremes (Sicily): genesis in a serpentinite hydrothermal system. Chemical Geology 258, 258-268. https://doi.org/10.1016/j.chemgeo.2008.10.029.

Clauser, C., Huenges, E., 1995. Thermal Conductivity of Rocks and Minerals. Rock Physics & Phase Relations. American Geophysical Union (AGU), pp. 105–126. https://doi.org/10.1029/RF003p0105

Connolly, J., 2009. The geodynamic equation of state: What and how. Geochemistry, Geophysics, Geosystems 10. https://doi.org/10.1029/2009GC002540

Connolly, J., 2005. Computation of phase equilibria by linear programming: A tool for geodynamic modeling and its application to subduction zone decarbonation. Earth and Planetary Science Letters 236, 524–54. https://doi.org/https://doi.org/10.1016/j.epsl.2005.04.033

Correale, A., Martelli, M., Paonita, A., Rizzo, A., Brusca, L., Scribano, V., 2012. New evidence of mantle heterogeneity beneath the Hyblean Plateau (southeast Sicily, Italy)

as inferred from noble gases and geochemistry of ultramafic xenoliths. Lithos 132–133, 70–81. https://doi.org/10.1016/j.lithos.2011.11.007

Cristofolini, R., Ghisetti, F., Scarpa, R., Vezzani, L., 1985. Character of the stress field in the Calabrian Arc and Southern Apennines (Italy) as deduced by geological, seismological and volcanological information. Tectonophysics 117, 39-58.

Degen, D., Spooner, C., Scheck-Wenderoth, M., Cacace, M., 2021. How biased are our models? – a case study of the alpine region. Geoscientific Model Development 14, 7133–7153. https://doi.org/10.5194/gmd-14-7133-2021

Della Vedova, B., Bellani, S., Pellis, G., Squarci, P., 2001. Anatomy of an Orogen: the Apennines and Adjacent Mediterranean Basins, Vai, G.B., Martini, I.P. (Eds.), Springer book Archive. https://doi.org/10.1007/978-94-015-9829-3

Di Sipio, E., Galgaro, A., Destro, E., Giaretta, A., Chiesa, S., Team, V., 2013. Thermal conductivity of rocks and regional mapping. Proceedings of European Geothermal Conference 2013.

Di Stefano, R., Bianchi, I., Ciaccio, M.G., Carrara, G., Kissling, E., 2011. Three-dimensional Moho topography in Italy: New constraints from receiver functions and controlled source seismology. Geochemistry, Geophysics, Geosystems 12, 1–15. https://doi.org/10.1029/2011GC003649

Doukas H. and Nikas A., 2022. Europe's energy crisis — climate community must speak up. Nature 608, 472. https://doi.org/10.1038/d41586-022-02199-5

El-Hage, Y., Hind, S., Robitaille, F., 2018. Thermal conductivity of textile reinforcements for composites. J. Text. Fibrous Mater., 1. https://doi.org/10.1177/2515221117751154

Eurostat, 2020. Energy Data – 2020. Luxembourg: Publications Office of the European Union. https://doi.org /10.2785/68334

European Geothermal Energy Council, 2020a. Geothermal Market Report 2019 Key Findings 14. https://www.egec.org/media-publications/egec-geothermal-market-report-2019/

European Geothermal Energy Council, 2020b. The geothermal energy market grows exponentially, but needs the right market conditions to thrive 2019, 2018–2019. https://www.egec.org/the-geothermal-energy-market-grows-exponentially-but-needs-the-right-market-conditions-to-thrive/

European Geothermal Energy Council, 2019. EGEC Geothermal Market Report, 2018 20. https://www.egec.org/media-publications/egec-geothermal-market-report-2018/

Favara, R., Grassa, F., Inguaggiato, S., D'Amore, F. 1998. Geochemical and hydrogeological characterization of thermal springs in Western Sicily, Italy. Journal of Volcanology and Geothermal Research 84, 125–141

Favara, R., Grassa, F., Inguaggiato, S., Valenza, M., 2001. Hydrogeochemistry and stable isotopes of thermal springs: earthquake-related chemical changes along Belice Fault (Western Sicily). Applied Geochemistry 16, 1±17.

Fetting, C., 2020. "The European Green Deal", ESDN Report, ESDN Office: Vienna, Austria.

Fichtner, A., Van Herwaarden, D.P., Afanasiev, M., Simutė, S., Krischer, L., Çubuk-Sabuncu, Y., Taymaz, T., Colli, L., Saygin, E., Villaseñor, A., Trampert, J., Cupillard, P., Bunge, H.P., Igel, H., 2018. The Collaborative Seismic Earth Model: Generation 1. Geophysical Research Letters 45, 4007–4016. https://doi.org/10.1029/2018GL077338

Finetti, I.R., Lentini, F., Carbone, S., Ben, A., Di Stefano, A., Forlin, E., Guarnieri, P., Pipan, M., Prizzon, A., 2005. Geological outline of Sicily and lithospheric tectono-dynamics of its Tyrrhenian margin from new CROP seismic data. CROP Project: deep seismic exploration of the Central Mediterranean and Italy. Atlases in Geoscience 1, 75-155.

Fukai, J., Kanou, M., Kodama, Y., Miyatake, O., 2000. Thermal conductivity enhancement of energy storage media using carbon fibers. Energy Convers. Manag., 41, 1543–1556.

Galgaro, A., Di Sipio, E., Destro, E., Chiesa, S., Uricchio, V., Bruno, D., Masciale, R., Lopez, N., Iaquinta, P., Teza, G., Iovine, G., Montanari, D., Manzella, A., Soleri, S., Greco, R., di Bella, G., Monteleone, S., Sabatino, M., Iorio, M., Petruccione, E., Giaretta, A., Tranchida, G., Trumpy, E., Gola, G., D'Arpa, S., 2012. Methodological approach for evaluating the geo-exchange potential: VIGOR Project. Acque Sotterranee - Italian Journal of Groundwater 1, 43–53. https://doi.org/10.7343/as-014-12-0029

Gardner, G.H.F., Gardner, L.W., Gregory, A.R., 1974. Formation velocity and density; the diagnostic basics for stratigraphic traps. Geophysics 39 (6), 770–780. https://doi.org/10.1190/1.1440465

Gola, G., Manzella, A., Trumpy, E., Montanari, D., van Wees, J.D., 2013. Deep-seated Geothermal Resource Assessment of the VIGOR Project Regions, Italy. European Geothermal Congress 3–7.

Hatta, I., Yamane, T., Katayama, S., Todoki, M., 2000. The Measurements of Thermal Conductivity of Carbon Fibers. J.Wide Bandgap Mater., 7, 294–305.

Henriquet, M., Dominguez, S., Barreca, G., Malavieille, J., Cadio, C., Monaco, C., 2019. Deep Origin of the Dome-Shaped Hyblean Plateau, Southeastern Sicily: A New Tectono-Magmatic Model. Tectonics, 38, 12, 4488-4515. https://doi.org/10.1029/2019TC005548

Huttrer, G.W., 2020. Geothermal Power Generation in the World 2015-2020 Update Report. Proceedings World Geothermal Congress 2020 1–17.

Inagaki, M., 2000. (Ed.) Chapter 4 - Carbon Fibers. In New Carbons—Control of Structure and Functions, Elsevier Science: Oxford, UK, pp. 82–123, ISBN 978-0-08-043713-2.

Indacoechea-Vega, I., Pascual-Muñoz, P., Castro-Fresno, D., Calzada-Pérez, M.A., 2015. Experimental Characterization and Performance Evaluation of Geothermal Grouting Materials Subjected to Heating-Cooling Cycles. Constr. Build. Mater., 98, 583–592.

Ingersoll, L.R., Zobel, O.J., Ingersoll, A.C., 1954. Heat Conduction with Engineering, Geological, and Other Applications, University of Wisconsin Press: Madison, WI, USA.

ISPRA, ENI, OGS, 2009. Cartografia Gravimetrica Digitale d'Italia alla scala 1:250.000.

Karaipekli, A., Sari, A., Kaygusuz, K., 2007. Thermal Conductivity Improvement of Stearic Acid Using Expanded Graphite and Carbon Fiber for Energy Storage Applications. Renew. Energy, 32, 2201–2210.

Karlsson, C., Silander, D., Pircher, B., 2019. Smart, Sustainable and Inclusive Growth: Political Entrepreneurship for a Prosperous Europe, Edward Elgar Publishing: Cheltenham, UK, ISBN 9781788974080.

Katzman, H.A., Adams, P.M., Le, T.D., Hemminger, C.S., 1994. Characterization of low thermal conductivity pan-based carbon fibers. Carbon, 32, 379–391. https://doi.org/10.1016/0008-6223(94)90158-9

Kavanaugh, S.P., Rafferty, K., 1997. Ground-Source Heat Pumps, Design of Geothermal Systems for Commercial and Institutional Buildings, ASHRAE: Atlanta, GA, USA.

Kim, J., Im, U.-S., Lee, B., Peck, D.-H., Yoon, S.-H., Jung, D.-H., 2016. Pitch-based carbon fibers from coal tar or petroleum residue under the same processing condition. Carbon Lett., 19, 72–78.

Kumar, A., 2022. V2RhoT. Zenodo. https://doi.org/10.5281/ZENODO.6538257

Lavecchia, G., Frerrarini, F., d Nardis, R., Visini, F., Barbano, M.S., 2007. Active thrustingas a possible seismogenic source in Sicily (Southern Italy): some insights fromintegrated structural–kinematic and seismological data. Tectonophysics 445,145–167.http://dx.doi.org/10.1016/j.tecto.2007.07.007.

Langsdorf, S., 2011. EU Energy Policy: From the ECSC to the Energy Roadmap 2050, Green European Foundation: Brussels, Belgium.

Lee, C., Park, M., Nguyen, T.B., Sohn, B., Choi, J.M., Choi, H., 2012. Performance Evaluation of Closed-Loop Vertical Ground Heat Exchangers by Conducting in-Situ Thermal Response Tests. Renew. Energy, 42, 77–83.

Lentini, F., Carbone, S., 2014. Introduzione-Geologia della Sicilia. Memorie descrittive della carta Geologica d'Italia 95, 7–30.

Limberger, J., Boxem, T., Pluymaekers, M., Bruhn, D., Manzella, A., Calcagno, P., Beekman, F., Cloetingh, S., van Wees, J.D., 2018. Geothermal energy in deep aquifers:

A global assessment of the resource base for direct heat utilization. Renewable and Sustainable Energy Reviews 82, 961-975. https://doi.org/10.1016/j.rser.2017.09.084

Lund, H., 2007. Renewable energy strategies for sustainable development. Energy 32, 912–919. https://doi.org/10.1016/j.energy.2006.10.017

Lund, J.W., Toth, A.N., 2021. Direct Utilization of Geothermal Energy 2020 Worldwide Review. Geothermics, 90, 101915.

Ma, H., Xu, F., Zhou, Z., Xu,W., Ren, F., 2018. Polymer Composites with Enhanced Thermal Conductivity and Mechanical Properties for Geothermal Heat Pump Pipes. Polym. Polym. Compos., 26, 251–258.

Macias, J.D., Bante-Guerra, J., Cervantes-Alvarez, F., Rodrìguez-Gattorno, G., Arés-Muzio, O., Romero-Paredes, H., Arancibia-Bulnes, C., Ramos-Sánchez, V., Villafán-Vidales, H.I., Ordonez-Miranda, J., et al., 2019. Thermal Characterization of Carbon Fiber-Reinforced Carbon (C/C). Appl. Compos. Mater., 26, 321–337.

Mahmoud, M., Ramadan, M., Pullen, K., Abdelkareem, M.A., Wilberforce, T., Olabi, A.G., Naher, S., 2021. A Review of Grout Materials in Geothermal Energy Applications. Int. J. Thermofluids, 10, 100070.

Manuella F.C, Brancato A., Carbone S., Gresta S., 2013. A crustal–upper mantle model for south eastern Sicily (Italy) from the integration of petrologic and geophysical data. Journal of Geodynamics, Volume 66, Pages 92-102. http://dx.doi.org/10.1016/j.jog.2013.02.006

Manzella A., Bonciani R., Allansdottir A., Botteghi S., Donato A., Giamberini S., Lenzi A., Paci M., Pellizzone A., Scrocca D., 2018. Environmental and social aspects of geothermal energy in Italy. Geothermics, Volume 72, Pages 232-248, ISSN 0375-6505. https://doi.org/10.1016/j.geothermics.2017.11.015

McCray, K., 1997. Guidelines for the Construction of Vertical Boreholes for Closed Loop Heat Pump Systems, National GroundWater Association: Westerville, OH, USA.

Meeßen, C., Sippel, J., Scheck-Wenderoth, M., Heine, C., Strecker, M.R., 2018. Crustal Structure of the Andean Foreland in Northern Argentina: Results From Data-Integrative Three-Dimensional Density Modeling. Journal of Geophysical Research: Solid Earth 123, 1875–1903. https://doi.org/10.1002/2017JB014296

Mendrinos, D., Katsantonis, S., Karytsas, C., 2016. Pipe materials for borehole heat exchangers. In Proceedings of the European Geothermal Congress, Strasbourg, France, 19–24 September 2016, pp. 19–24.

Mendrinos, D., Katsantonis, S., Karytsas, C., 2017. Review of Alternative Pipe Materials for Exploiting Shallow Geothermal Energy. Innov. Corros. Mater. Sci., 7, 13–29. https://doi.org/10.2174/2352094907666170327163227

Milano, M., Kelemework, Y., la Manna, M., Fedi, M., Montanari, D., Iorio, M., 2020. Crustal structure of Sicily from modelling of gravity and magnetic anomalies. Scientific Reports 10, 1–18. https://doi.org/10.1038/s41598-020-72849-z

Midttømme, K., Banks, D., 2008. Ground-source heat pumps and underground thermal energy storage: Energy for the future. NGU Spec. Publ., 11, 93–98.

Moeck, I. 2014. Catalog of geothermal play types based on geologic controls. Renewable and Sustainable Energy Reviews 37, 867–882, https://doi.org/10.1016/j.rser.2014.05.032

Montanari, D., Albanese, C., Catalano, R., Contino, A., Fedi, M., Gola, G., Iorio, M., la Manna, M., Monteleone, S., Trumpy, E., Valenti, V., Manzella, A., 2015. Contour map of the top of the regional geothermal reservoir of Sicily (Italy). Journal of Maps 11, 13–24. https://doi.org/10.1080/17445647.2014.935503

Montanari, D., Minissale, A., Doveri, M., Gola, G., Trumpy, E., Santilano, A., Manzella, A., 2017. Geothermal resources within carbonate reservoirs in western Sicily (Italy): A review. Earth-Science Reviews 169, 180–201. https://doi.org/10.1016/j.earscirev.2017.04.016

Morelli, C., 2007. Confirmations and apparent contradictions from the new geophysical deep constraints in the southern Apennines. Bollettino della Società Geologica Italiana, Supplemento 7, 3–12.

Morelli, C., 2003. An historical perspective to the CROP Project. Memorie descrittive della Carta Geologica d'Italia 62, 1–7.

Naslain, R., 2000. Carbon Fibers From Pan and Pitch. In Advanced Inorganic Fibers: Process—Structure—Properties—Applications, Wallenberger, F.T., Naslain, R., Macchesney, J.B., Ackler, H.D., Wallenberger, F.T., Eds., Springer: Boston, MA, USA, pp. 233–264, ISBN 978-1-4419-8722-8.

Patacca E., Scandone P., Giunta G., and Liguori V., 1979. Mesozoic paleotectonic evolution of the Ragusa zone (southeastern Sicily), Geologica Romana, vol. 18. pp. 331–369.

Punturo, R., Kern, H., Cirrincione, R., Mazzoleni, P., Pezzino, A., 2005. P- and S-wave velocities and densities in silicate and calcite rocks from the Peloritani Mountains, Sicily (Italy): The effect of pressure, temperature and the direction of wave propagation. Tectonophysics 409, 55–72. https://doi.org/10.1016/j.tecto.2005.08.006

Punturo R., Kern H., Scribano V., Atzori P., 2000. Petrophysical and petrological characteristics of deepseated xenoliths from Hyblean Plateau, south-eastern Sicily, Italy: suggestions for a lithospheric model. Mineral Petrogr Acta 43, 1-20.

Remund, C.P., 1999. Borehole thermal resistance: Laboratory and field studies. ASHRAE Trans., 105, 439.

Riahi, A., Damjanac, B., Moncarz, P., 2017. Innovative Closed-Loop GeothermalWell Designs UsingWater and Super Critical Carbon Dioxide as Working Fluids. In Proceedings of the Forty-Second Workshop on Geothermal Reservoir Engineering, Stanford, CA, USA, 13–15 February 2017.

Rodriguez Piceda, C., Scheck-Wenderoth, M., Bott, J., Gomez Dacal, M. L, Cacace, M., Pons, M. Prezzi, C.B. Strecker, M. R., 2022. Controls of the Lithospheric Thermal Field of an Ocean-Continent Subduction Zone: The Southern Central Andes. Lithosphere 1, 2237272. https://doi.org/10.2113/2022/2237272

Romagnoli, G., Catalano, S., Pavano, F., Tortorici, G., 2015. Geological map of the Tellaro River Valley (Hyblean Foreland, southeastern Sicily, Italy), J. Maps, vol. 11, no. 1, pp. 66–74.

Roumeli, E., Markoulis, A., Kyratsi, T., Bikiaris, D., Chrissafis, K., 2014. Carbon nanotube-reinforced crosslinked polyethylene pipes for geothermal applications: From synthesis to decomposition using analytical pyrolysis-GC/MS and thermogravimetric analysis. Polym. Degrad. Stab., 100, 42–53.

Ruggieri, R., 1990. Assetto idrogeologico e intrusione delle acque marine nell'entroterra costiero ibleo. Atti del I Convegno Naz. di Idrogeol. Modena.

Rybach, L., 2010. CO2 Emission Mitigation by Geothermal Development-Especially with Geothermal Heat Pumps. In Proceedings of the World Geothermal Congress, Bali, Indonesia, 25–29 April 2010.

Sanner, B., 2017. Ground Source Heat Pumps – history, development, current status, and future prospects. 12th IEA Heat Pump Conference 2017 1–14.

Santilano, A., Donato, A., Galgaro, A., Montanari, D., Menghini, A., Viezzoli, A., Di Sipio, E., Destro, E., Manzella, A., 2016. An integrated 3D approach to assess the geothermal heat-exchange potential: The case study of western Sicily (southern Italy). Renewable Energy 97, 611–624. https://doi.org/10.1016/j.renene.2016.05.072

Santini, S., Basilici, M., Invernizzi, C., Mazzoli, S., Megna, A., Pierantoni, P.P., Spina, V., Teloni, S., 2020. Thermal Structure of the Northern Outer Albanides and Adjacent Adriatic Crustal Sector, and Implications for Geothermal Energy Systems. Energies 13, 6028. https://doi.org/10.3390/en13226028

Santini, S., Basilici, M., Invernizzi, C., Jablonska, D., Mazzoli, S., Megna, A., Pierantoni, P.P., 2021. Controls of Radiogenic Heat and Moho Geometry on the Thermal Setting of the Marche Region (Central Italy): An Analytical 3D Geothermal Model. Energies, 14, 6511. https://doi.org/10.3390/en14206511

Sapienza G., Scribano V., 2000. Distribution and representative whole-rock chemistry of deep-seated xenoliths from the Iblean Plateau, south-eastern Sicily, Italy. Periodico di Mineralogia, Volume 69, 2.

Scarfì, L., Barberi, G., Barreca, G., Cannavò, F., Koulakov, I., Patanè, D., 2018. Slab narrowing in the Central Mediterranean: The Calabro-Ionian subduction zone as imaged

by high resolution seismic tomography. Scientific Reports 8, 1–12. https://doi.org/10.1038/s41598-018-23543-8

Scheck-Wenderoth, M., Cacace, M., Maystrenko, Y. P., Cherubini, Y., Noack, V., Kaiser, B.O., Sippel, J., Björn, L., 2021. Models of heat transport in the Central European Basin System: effective mechanisms at different scales. Marine and Petroleum Geology 55, 315-331. https://doi.org/10.1016/j.marpetgeo.2014.03.009

Schiano, P., Clocchiatti, R., Ottolini, L., Busà, T., 2001. Transition of Mount Etna lavas from a mantle-plume to an island-arc magmatic source. Nature, vol. 412, no. 6850, pp. 900–904

Schmidt, S., Anikiev, D., Götze, H.-J., Gomez Garcia, À., Gomez Dacal, M.L., Meeßen, C., Plonka, C., Rodriguez Piceda, C., Spooner, C., Scheck-Wenderoth, M., 2020. IGMAS+ – a tool for interdisciplinary 3D potential field modelling of complex geological structures. EGU General Assembly, EGU2020-8383.

Schmincke, U., Behncke, B., Grasso M, and Raffi S., 1997. Evolution of the northwestern Iblean Mountains, Sicily: uplift, Plicocene / Pleistocene sea-level changes, paleoenvironment, and volcanism, pp. 637–669.

Scribano, V., Viccaro, M., Cristofolini, R., Ottolini, L., 2009. Metasomatic events recorded in ultramafic xenoliths from the Hyblean area (Southeastern Sicily, Italy). Mineralogy and Petrology 95, 235-250. https://doi.org/10.1007/s00710-008-0031-4.

Scribano, V., Sapienza, G., Braga, R. Morten, L. 2006. Gabbroic xenoliths in tuff-breccia pipes from the Hyblean Plateau: Insights into the nature and composition of the lower crust underneath South-eastern Sicily, Italy. Mineralogy and Petrology (2006) 86: 63–88. https://doi.org/10.1007/s00710-005-0092-6.

Sgroi, T., de Nardis, R., Lavecchia, G., 2012. Crustal structure and seismotectonics of central Sicily (southern Italy): New constraints from instrumental seismicity. Geophysical Journal International 189, 1237–1252. https://doi.org/10.1111/j.1365-246X.2012.05392.x

Sippel, J., Meeßen, C., Cacace, M., Mechie, J., Fishwick, S., Heine, C., Scheck-Wenderoth, M., Strecker, M.R., 2017. The Kenya rift revisited: insights into lithospheric strength through data-driven 3-D gravity and thermal modelling. Solid Earth 8, 45-81. https://doi.org/10.5194/se-8-45-2017

Sommaruga, C., 1984. Le ricerche geotermiche svolte a Vulcano negli anni ’50. Rendiconti della Società Geologica Italiana di Mineralogia e Petrologia, 39, 355-366.

Spooner, C., Scheck-Wenderoth, M., Cacace, M., Götze, H.-J., Luijendijk, E., 2020. The 3D thermal field across the Alpine orogen and its forelands and the relation to seismicity. Global and Planetary Change 193, 103-288. https://doi.org/10.1016/j.gloplacha.2020.103288

Stober, I., Bucher, K., 2013. Geothermal Probes. In Geothermal Energy: From Theoretical Models to Exploration and Development, Springer: Berlin/Heidelberg,

Germany, pp. 65–113. ISBN 978-3-642-13352-7. https://doi.org/10.1007/978-3-642-13352-7

Tonarini, S., D'Orazio, M., Armienti, P., Innocenti, F., Scribano, V., 1996. Geochemical features of eastern Sicily lithosphere as probed by Hyblean xenoliths and lavas. European Journal of Mineralogy 8, 1153–1174. https://doi.org/10.1127/ejm/8/5/1153

Trumpy, E., Botteghi, S., Caiozzi, F., Donato, A., Gola, G., Montanari, D., Pluymaekers, M., Santilano, A., Van Wees, J., Manzella, A., 2016. Geothermal potential assessment for a low carbon strategy: A new systematic approach applied in southern Italy. Energy 103, 167–181. https://doi.org/10.1016/j.energy.2016.02.144

Trumpy, E., Donato, A., Gianelli, G., Gola, G., Minissale, A., Montanari, D., Santilano, A., Manzella, A., 2015. Data integration and favourability maps for exploring geothermal systems in Sicily, southern Italy. Geothermics 56, 1–16. https://doi.org/10.1016/j.geothermics.2015.03.004

Trumpy, E., Manzella, A., 2017. Geothopica and the interactive analysis and visualization of the updated Italian National Geothermal Database. International Journal of Applied Earth Observation and Geoinformation 54, 28–37. https://doi.org/10.1016/j.jag.2016.09.004

UGI (Unione Geotermica Italiana), November 2007. Geothermal Energy – Yesterday, Today, Tomorrow. Special Issue of UGI's Newsletter, Second edition, revised and updated.

Uieda, L., Vanderlei C., Ferreira, A., Santos, H., Caparica, J., Markall, G., Bentley, M., Almeida, V., Kass, M., Kurnik, P., Silva, R., Soler, S. 2016. Fatiando a Terra v0.5: Modeling and inversion in geophysics. Zenodo. https://doi.org/10.5281/zenodo.157746

Vasile, C., Pascu, M., 2005. Practical Guide to Polyethylene, Smithers Rapra Publishing: Shawbury, UK.

Verdoya, M., Pasquale, V., Chiozzi, P. 2005. Thermo-mechanical evolution and rheology of the northern sector of the Tyrrhenian–Apennines system. Journal of Volcanology and Geothermal Research 148 (2005) 20 – 30.

Viccaro, M., Zuccarello, F., 2017. Mantle ingredients for making the fingerprint of Etna alkaline magmas: implications for shallow partial melting within the complex geodynamic framework of Eastern Sicily. Journal of Geodynamics 109, 10–23. https://doi.org/10.1016/j.jog.2017.06.002

Viccaro, M., 2018. Doped bentonitic grouts for implementing performances of low-enthalpy geothermal systems. Geotherm. Energy, 6. https://doi.org/10.1186/s40517-018-0090-7

Vilà, M., Fernández, M., Jiménez-Munt, I., 2010. Radiogenic heat production variability of some common lithological groups and its significance to lithospheric thermal modeling. Tectonophysics 490, 152–164. https://doi.org/10.1016/j.tecto.2010.05.003

Waples, D.W., 2001. A New Model for Heat Flow in Extensional Basins: Radiogenic Heat, Asthenospheric Heat, and the McKenzie Model. Natural Resources Research 10, 227–238. https://doi.org/10.1023/A:1012521309181

Yang, K.S., Choi, Y.O., Kim, Y.M., Park, S.H., Yang, C.M., Kim, Y.J., Soh, S.Y., 2000. Preparations of carbon fibers from precursor pitches synthesized with coal tar or petroleum residue oil. Fibers Polym., 1, 97–102.

Zhang, X., Fujiwara, S., Fujii, M., 2000. Measurements of Thermal Conductivity and Electrical Conductivity of a Single Carbon Fiber. Int. J. Thermophys., 21, 965–980.

Zhu, H., Bozdăg, E., Tromp, J., 2015. Seismic structure of the European upper mantle based on adjoint tomography. Geophysical Journal International 201, 18–52. https://doi.org/10.1093/gji/ggu492

**Report and technical legislation**

American Society of Heating, Refrigerating and Air-Conditioning Engineers 2007. ASHRAE Handbook: Heating, Ventilating, and Air-Conditioning Applications, Tullie Circle, N.E., Ed., ASHRAE: Atlanta, GA, USA, ISBN 9781933742144.

ASTM E 1530, 2019. Standard Test Method for Evaluating the Resistance to Thermal Transmission by the Guarded Heat Flow Meter Technique. ASTM International: West Conshohocken, PA, USA.

DIN 1164-11, 2003. Special Cement—Part 11: Composition, Specification and Conformity Evaluation for Cement with Short Setting Time. European Standards s.r.o.: Pilsen, Czech Republic.

DIN 18136:2003–2011, Soil—Investigation and Testing—Unconfined Compression Test. European Standards s.r.o.: Pilsen, Czech Republic.

European Commission. The European Green Deal. Communication from the Commission to the European, The European Council, The Council, The European and Social Committee of the Regions, European Commission: Brussels, Belgium, 2011. European Commission. An EU Strategy on Heating and Cooling. Communication from the Commission to the European, The European Council, The Council, The European and Social Committee of the Regions, European Commission: Brussels, Belgium, 2016.

European Geothermal Energy Council. EGEC Geothermal Market Report, 2018, 8th ed., EGEC: Brussels, Belgium, 2019, ISBN 9788578110796.

European Geothermal Energy Council. EGEC Geothermal Market Report, 2019, 9th ed., EGEC: Brussels, Belgium, 2020.

European Commission. Changing How We Produce and Consume: New Circular Economy Action Plan Shows the Way to a Climate- Neutral, Competitive Economy of Empowered Consumers: Brussels, Belgium, 2020.

Ground Source Heat Pump Association, 2011. Closed-Loop Vertical Borehole Design, Installation & Materials Standards, Ground Source Heat Pump Association: Milton Keynes, UK, pp. 1–45.

International Ground Source Heat Pump Association. Standards Committee Closed-Loop/Geothermal Heat Pump Systems. In Design and Installation Standards, International Ground Source Heat Pump Association: Stillwater, OK, USA, 2016.

UNI 11152, Aqueous Suspensions for Injections of Hydraulic Binders—Characteristics and Test Methods. Ente Nazionale Italiano di Unificazione (UNI): Milan, Italy, 2005. (In Italian)

UNI EN 196-1:2016, Methods for Test of Cements—Part 1: Determination of Mechanical Strengths. Ente Nazionale Italiano di Unificazione (UNI): Milan, Italy.

***on-line portal***

VIGOR project

http://www.vigor-geotermia.it/

VIDEPI project

https://www.videpi.com/videpi/videpi.asp

GEOTHOPICA database

http://geothopica.igg.cnr.it/

***Software***

QGIS

https://www.qgis.org/it/site/

ArcGIS Pro

https://www.esri.com/en-us/arcgis/products/arcgis-pro/overview

PETREL

https://www.software.slb.com/products/petrel

IGMAS+

https://www.gfz-potsdam.de/en/software/3d-modelling-of-potential-fields-igmas

FATIANDO A TERRA

https://www.fatiando.org/

MeshIt

https://www.gfz-potsdam.de/en/software/meshing-reservoirs-meshit

MOOSE

https://mooseframework.inl.gov/

GOLEM

https://www.gfz-potsdam.de/en/software/moose-modelling-application-golem

PARAVIEW

https://www.paraview.org/